A LOCAL MINIMAX METHOD USING THE GENERALIZED NEHARI MANIFOLD FOR FINDING DIFFERENTIAL SADDLES

A Dissertation

by

BINGBING JI

Submitted to the Office of Graduate and Professional Studies of
Texas A&M University
in partial fulfillment of the requirements for the degree of

DOCTOR OF PHILOSOPHY

Chair of Committee,	Jianxin Zhou
Committee Members,	Joseph Pasciak
	Bojan Popov
	Akhil Datta-Gupta
Head of Department,	Emil Straube

December 2017

Major Subject: Mathematics

ABSTRACT

In order to find the first few unconstrained saddles of functionals with different types of variational structures, a new local minimax method (LMM), based on a dynamics of points on virtual geometric objects such as curves, surfaces, etc., is developed. Algorithm stability and convergence are mathematically verified. The new algorithm is tested on several benchmark examples commonly used in the literature to show its stability and efficiency, then it is applied to numerically compute saddles of a semilinear elliptic PDE of both M-type (focusing) and W-type (defocusing). The Newton's method will also be investigated and used to accelerate the local convergence and increase the accuracy.

The Nehari manifold is used in the algorithm to satisfy a crucial condition for convergence. The numerical computation is also accelerated and a comparison of computation speed between using the Nehari manifold and quadratic geometric objects on the same semilinear elliptic PDEs is given, then a mixed M and W type case is solved by the LMM with the Nehari manifold.

To solve the indefinite M-type problems, the generalized Nehari manifold is introduced in detail, and a generalized dynamic system of points on it is given. The corresponding LMM with a correction technique is also justified and a convergence analysis is presented, then it is tested on an indefinite M-type case. A numerical investigation of bifurcation for an indefinite problem will be given to provide numerical evidence for PDE analysts for future study.

DEDICATION

In memory of my grandfather, and my grandmother, who gave me lots of love and joy in my childhood.

ACKNOWLEDGMENTS

Firstly, I would like to express my sincere gratitude to my Ph.D. advisor, Dr. Jianxin Zhou, for his encouragement during my graduate study, his guidance to my research and writing of this dissertation, and his constructive suggestion to my life and career.

My sincere gratitude also goes to the members of my advisory committee, Dr. Joseph Pasciak, Dr. Bojan Popov and Dr. Akhil Datta-Gupta for their prompt response to my questions and their insightful comments to my research.

I would like to thank Ms. Monique Stewart, for her patience, professionalism and incredible knowledge with university and department administration. I am also grateful to the fellow students in the Department of Mathematics, Shubin Fu, Meiqin Li, Sam Scholze, Guchao Zeng and Sheng Zhang for the deep friendship.

Last but not the least, I would like to thank my parents and my wife for their emotional support and care during my Ph.D. study. Ph.D. study is a long and tough journey. My parents always stand by my side and fight with me. My wife is the greatest gift I have ever received.

CONTRIBUTORS AND FUNDING SOURCES

Contributors

This work was supervised by a dissertation committee consisting of Dr. Jianxin Zhou, Dr. Joseph Pasciak and Dr. Bojan Popov of the Department of Mathematics and Dr. Akhil Datta-Gupta of the Department of Petroleum Engineering.

The Numerical Examples in Section 2 were conducted in part and in cooperation with Dr. Jianxin Zhou of the Department of Mathematics at Texas A&M University and Professor Zhaoxiang Li of the Department of Mathematics at Shanghai Normal University and were submitted in 2016 in an article listed in the references.

All other work conducted for the dissertation was completed by the student independently under the guidance of the dissertation advisor, Dr. Jianxin Zhou.

Funding Sources

Graduate study was supported by the graduate teaching assistantship from the Department of Mathematics at Texas A&M University.

NOMENCLATURE

LMM	Local Minimax Method
PDE	Partial Differential Equation
NLSE	Nonlinear Schrödinger Equation
MI	Morse Index
$L^p(\Omega)$	Space of p-Lebesgue-integrable functions $u(x)$ on Ω, i.e., $\int_\Omega \|u(x)\|^p dx < \infty$
$W^{k,p}(\Omega)$	Space of functions $u(x)$ in $L^p(\Omega)$ s.t. $\forall \|\alpha\| \leq k, D^\alpha u \in L^p(\Omega)$
$H_0^1(\Omega)$	Space of functions in $H^1(\Omega) = W^{1,2}$ that vanish at the boundary of Ω
$\mathrm{N_{It}}$	Iteration number in the algorithm
$\mathcal{N}$	Nehari manifold
$\mathcal{M}$	Generalized Nehari manifold
$\mathbb{N}^+$	Set of positive integers
$\mathbb{R}^+$	Set of non-negative real numbers

TABLE OF CONTENTS

Page

LIST OF FIGURES

FIGURE Page

LIST OF TABLES

TABLE Page

1. INTRODUCTION AND MAIN PROBLEM

1.1 Introduction

Let H be a Hilbert space with its inner product $\langle \cdot, \cdot \rangle$ and norm $\| \cdot \|$ and $J : H \to \mathbb{R}$ be a $\mathcal{C}^1$ functional, called a generic energy functional. Let $u^* \in H$ be a solution of $J'(u) = 0$, where J' is the Fréchet derivative of J, then u^* is called a critical point of J. For a critical point u^*, the number $c = J(u^*) \in \mathbb{R}$ is called a critical value. For a critical value c, the set $J^{-1}(c)$ is called a critical level. The most well-studied critical points are the local extrema of J, and the classical calculus of variations and numerical methods focus on finding such stable solutions. Critical points u^* which are not local extrema are unstable and called saddles, i.e., in any neighborhood $N(u^*)$ of u^*, there exists two points $v, w \in N(u^*)$ s.t. $J(v) < J(u^*) < J(w)$. A k-saddle is a critical point which is a local maximum of J in a k-dimensional subspace and a local minimum of J in the corresponding k-co-dimensional subspace. Morse index (MI) is introduced to measure the instability of saddles. Assume $J''(u^*)$ is a self-adjoint Fredholm operator, then H has an orthogonal spectral decomposition as $H = H^- \oplus H^0 \oplus H^+$ where H^-, H^0, H^+ are respectively the maximum negative, null and maximum positive subspaces of the linear operator $J''(u^*)$ in H with $\dim(H^0) < \infty$. If $H^0 = \{0\}$, u^* is said to be *non-degenerate* otherwise it is said to be *degenerate*. By the Morse theory, the dimension of H^- is defined as the Morse index of u^*, denoted by MI(u^*). In particular, a non-degenerate critical point u^* is a local minimizer and a stable solution if MI$(u^*) = 0$. If MI$(u^*) = k > 0$, u^* is an unstable k-saddle and a min-max type.

Excited states in a system, as unstable local equilibria, with various configurations and performance indices at different energy levels exist in many excitation/reaction/transition processes in physics, chemistry, biology, etc. Nowadays new (synchrotronic, laser, etc.)

technologies can be developed to induce, reach or control some of those excited states so that they become long-lived as to be stable for practical purposes. Such excited states are called *metastable*. The phenomenon of metastability exists in many excitation, reaction and transition process in physics, chemistry and biology, etc. For instance, in quantum mechanics, various states are found in aggregated systems of subatomic particles. Some of them are excited states. Among those excited states, some ones have lifetimes lasting 10^2 to 10^3 times longer than some short states, thus they are metastable. Although all the excited states will decay to the stable state, metastable states are long-lived. Another example about metastability is in optical vector solitons which arise in condensed matter physics, the dynamics of biomolecules, and nonlinear optics, etc. [1], where a new type of optical vector soliton was found in [2, 3], and called a dipole-mode vector soliton. Compared to the previously found vortex-mode solitons, dipole-mode vector solitons are much more stable and robust even though both of them are unstable. According to the numerical results, unstable modes of a dipole vector soliton are very rare and hard to excite, and "they have a typical lifetime of several hundred diffraction lengths and survive a wide range of perturbations." [2]

Critical points correspond to local equilibrium states in a physical process. Physically, a local minimum point is a ground state as a stable local equilibrium. Most conventional numerical algorithms focus on finding such stable solutions. Saddles correspond to excited states, and metastable states may exist among the first few saddles. The physical nature of saddles is complicated since their instability behavior can be very different [4]. Comparing to the local minimum computation, numerical search for saddles is much more challenging due to their instability and multiplicity. Note that we are going to find multiple unstable solutions instead of a single stable solution, as usual results presented in the literature. Numerical methods for finding single stable solution and for finding multiple unstable solutions are very different in functionality and complexity. For the latter, we need to use

the information obtained from previously found solutions to find a new solution at the next critical level.

Many algorithms were proposed to find 1-saddles in computational physics,chemistry, and biology [5–10]. However, most of them are lack of proper mathematical justifications, including analysis on algorithm stability and convergence result. While in the mathematical area, a huge literature can be found on the mathematical analysis of multiple solution problems. Most of them basically focus on the existence issue. Typically a minimax type critical point is characterized by the Ljusternik-Schnirelman principle (LSP) [11]

$$\min_{A\in\mathcal{A}} \max_{u\in A} J(u), \tag{1.1}$$

where $\mathcal{A}$ is a collection of certain compact sets A. Note that the min and max in 1.1 are taken in the global sense. It is too expensive to do the numerical implementation, so new approaches are needed. The Mountain Pass Lemma proven in 1973 by Ambrosetti-Rabinowitz [12] sets a milestone in critical point analysis. Motivated by the Mountain Pass Lemma, Choi-McKenna proposed the mountain pass algorithm in 1993 [13] for finding 1-saddles. In 1999, Ding-Costa-Chen developed a numerical high linking method to find 2-saddles. Global max and a local min in LSP were used in their methods, but there is a gap between their methods and LSP since LSP is a two-level global optimization problem. Then the mathematical justification of their methods could be too difficult to establish, as the theories in LSP are not applicable to them. Inspired by the numerical works above, Li-Zhou developed a local minimax method (LMM) in 2001 [14]. In their work, a critical point is characterized by a solution to a two-level local minimax problem. Besides, a stronger energy dissipation law for algorithm stability and a convergence result were established [15]. Their work does not only opens a new door for solving the multiple solution problem numerically in the local sense, but also lays a mathematical foundation

for the local minimax method. Motivated by their LMM, this research is to develop a new LMM to numerically compute multiple saddles in a stable way. Our new LMM unifies the methods for solving M-type and W-type problems, which will be introduced below.

1.2 Main Problem

To motivate our research, let us consider one of the canonical models in physics, the nonlinear Schrödinger equation (NLSE) of the form:

$$i\frac{\partial w(x,t)}{\partial t} = -\Delta w(x,t) + V(x)w(x,t) + \kappa f(x,|w(x,t)|)w(x,t), \tag{1.2}$$

where $V(x)$ is the potential function, κ is a physical constant and f is a nonlinear function satisfying certain regularity/growth condition. To study the solution pattern, instability and other properties, soliton solutions of the form $w(x,t) = u(x)e^{-i\lambda t}$ are investigated, where λ is the wave frequency and u is the wave amplitude function. For simplicity we assume $V(x) = 0$, then by the localized property, it leads to solving a non-autonomous nonlinear elliptic PDE which is the main problem in the research:

$$-\Delta u(x) - \lambda u(x) + \kappa f(x,u(x)) = 0 \tag{1.3}$$

in $H = H_0^1(\Omega) = W_0^{1,2}(\Omega)$, where $\Omega \subset \mathbb{R}^N$ is an open bounded domain and the notation of $f(x,\xi) = f(x,|\xi|)\xi$ is abused. Let

$$F(x,u) = \int_0^u f(x,s)ds, \tag{1.4}$$

then we list the following assumptions **AS** for the main problem (1.3):

(**AS.1**) The function $f : \Omega \times \mathbb{R} \mapsto \mathbb{R}$ is a Carathéodory function, $f(x,u)$ is $\mathcal{C}^1$ in u and

$$|f(x,u)| \leq C(1+|u|^p)$$

for some $C > 0$ and $p \in (1, 2^*)$, where $2^* = (N+2)(N-2)^{-1}$ if $N \geq 3$ and $2^* = \infty$ if $N = 1$ or 2;

(**AS.2**) $f(x,u) = o(u)$ uniformly in x as $|u| \to 0$;

(**AS.3**) $F(x,u)/u^2 \to \infty$ uniformly in x as $|u| \to \infty$;

(**AS.4**) $u \mapsto f(x,u)/|u|$ is strictly increasing on $(-\infty, 0)$ and $(0, \infty)$;

(**AS.5**) There exists $\eta > 2$ such that

$$0 < \eta F(x,u) \leq f(x,u)u$$

for every $u \neq 0$;

(**AS.6**) There exists $\theta \in (0,1)$ such that

$$0 < u^{-1} f(x,u) \leq \theta f'_u(x,u)$$

for every $u \neq 0$ and f'_u is a Carathéodory function with

$$|f'_u(x,u)| \leq C(1+|u|^{p-1})$$

for some $C > 0$ and $p \in (1, 2^*)$;

The assumption (**AS.5**) is actually the standard Ambrosetti-Rabinowitz superlinear condition and it implies (**AS.3**) and (**AS.4**) [16, 17], while the assumption (**AS.6**) is stronger

than the Ambrosetti-Rabinowitz superlinear condition (**AS.5**) [18], so only (**AS.1**), (**AS.2**) and (**AS.6**) are sufficient for our research. However, we still use all these assumptions in the research as some of them can lead to the expected results directly when we prove our claims.

In most numerical examples of our research, we take

$$f(x,u) = |x|^r |u(x)|^{p-1} u(x) \text{ and } F(x,u) = \int_0^u f(x,s)ds = \frac{1}{p+1} |x|^r |u(x)|^{p+1}, \tag{1.5}$$

where $p \in (1, 2^*)$ and r is a prescribed parameter. It is known that the nonlinear term f is used in the Hénon equation modeling spherical stellar systems and $2^* + 1$ is the Sobolev critical exponent for Sobolev embedding. [19–21] We can easily check that f satisfies all the assumptions **AS**.

We obtain the model problem in the research which is a non-autonomous semilinear elliptic PDE:

$$-\Delta u - \lambda(x)u + \kappa |x|^r |u(x)|^{p-1} u(x) = 0, \tag{1.6}$$

The corresponding energy functional for the model problem is

$$J(u) = \int_\Omega \left[\frac{1}{2} |\nabla u(x)|^2 - \frac{1}{2}\lambda(x)u^2(x) + \frac{\kappa}{p+1} |x|^r |u(x)|^{p+1} \right] dx. \tag{1.7}$$

The critical points of (1.7) are the solutions of our model problem (1.6) and our objective is to find the first few saddles of J.

Let $0 < \lambda_1 < \lambda_2 < \dots$ be the eigenvalues of $-\Delta$ satisfying zero Dirichlet boundary condition and $\{e_1, e_2, \dots\}$ be their corresponding eigenfunctions. The sign of the physical constant κ is significant since it gives us two physically and mathematically very different cases. The system (1.6) is called *focusing* (M-type) if $\kappa < 0$ and $\lambda_k < \lambda < \lambda_{k+1}$ ($k = 0, 1, 2, \dots, \lambda_0 = -\infty$) and *defocusing* (W-type) if $\kappa > 0$ and $\lambda_k < \lambda < \lambda_{k+1}$ ($k =$

$1, 2, \ldots,$). In addition, for M-type problems, if $k = 0$, i.e., $\lambda < \lambda_1$, they are called definite problems in the literature. If $\lambda > \lambda_1$, they are called indefinite problems. The profiles of these two types of functions are given in Figure 1.1. The shapes of these two types look like upside-down to each other, but are actually not since they have a significant difference in space dimensions, so they are very different not only in physical nature but also in mathematical structure. If we consider the Morse indices for the non-trivial solutions, we only have the ones with MI larger than k for M-type cases and smaller than k for W-type cases. In particular, for the M-type with $\lambda < \lambda_1$, J has a mountain pass structure and 0 is the only local minimum so the mountain pass/linking type approaches or methods can be applied. However, for the W-type with $k \geq 1$, J has two local minima but has no mountain pass structure, thus the mountain pass/linking type approach or algorithms are not applicable. In the literature, two very different types of variational methods were used to treat those two cases respectively. While in our research, we will develop numerical methods and their related theory for finding saddles for both the focusing and defocusing problems.

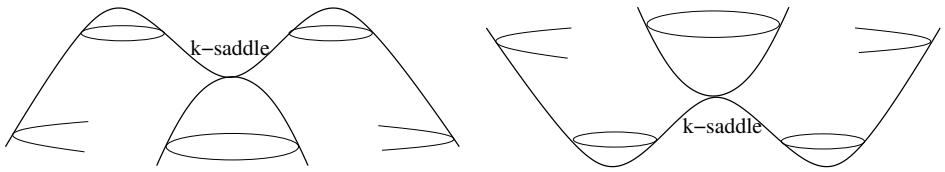

Figure 1.1: Function profiles of M-type (left) where $\cap$-shape in $[e_1, \ldots, e_k]$, M-shape in $[e_1, \ldots, e_k]^\perp$ vs. W-type (right) where $\cup$-shape in $[e_1, \ldots, e_k]^\perp$, W-shape in $[e_1, \ldots, e_k]$.

Even though the Newton-type or other local convergence based methods can be used to converge very fast, an initial guess sufficiently close to a target solution is still needed.

Thus these methods alone are not suitable for solving the problem, since it is known that for an unknown target solution, finding such an initial guess can be very hard for an infinite-dimensional highly nonlinear multiple solution problem. Thus we will not discuss more about Newton-type or other locally convergent methods in our research. On the other hand, they can be used after an approximating solution is computed as a proper initial guess to speed up the convergence. Instead we focus on developing a new general stable local min-max algorithm (LMM) for finding k-saddles using only J' in a Hilbert space, which includes several very different types of variational methods in the literature as special cases. It is known that energy dissipation law is crucial for an algorithm related dynamics to be stable, but it alone is not enough for the algorithm to be convergent in an infinite-dimensional space. In fact, we need the stepsize rule, a stronger energy dissipation law. In our research, we will establish LMM's mathematical justification including a solution characterization, a stepsize rule and a convergence result. As for numerical examples, the algorithms will be implemented and tested on our model problem with two very different W-type and M-type variational structures. Virtual geometric objects will be used in our algorithm, and we will show how easily they can be defined without knowing their explicit expressions. This feature gives us a great flexibility to choose some particular geometric objects to speed up algorithm convergence. Since all the nontrivial critical points stay on the Nehari manifold, we use it as an auxiliary equation (a void constraint) to define the geometric objects used in the algorithm to speed up the numerical computation. Such an expectation is verified by the numerical results. Then this idea is modified and then implemented on finding saddles of a mixed M and W type problem, which is hard to handle with the methods in the literature. For the indefinite M-type problems, the generalized Nehari manifold will be used since a crucial condition for establishing the algorithm convergence result can be verified on it. It is discussed in detail, including its properties, a minimax characterization, a stepsize rule and a convergence analysis. Then a numerical example is

presented to illustrate the algorithm and its related theory.

In the M-type model problem (1.6), the term $|x|^r$ plays a significant role in the property of the solution and r is usually called a bifurcation parameter. In detail, for the definite problem with a convex domain Ω which is symmetric about the origin, when r is not greater than certain value, the ground state solution is positive, symmetric and has one peak centered at the origin. Bifurcation occurs when r goes beyond certain value. Then the ground state solution bifurcates to multiple asymmetric positive solutions and the peak moves further away from the origin as r increases if λ is a constant. Bifurcation for definite problems has been investigated by many researchers, such as the discussion in [22]. In this research, we will study the bifurcation of indefinite problems, where the phenomena are more complicated.

2. LOCAL MINIMAX METHOD WITH VIRTUAL GEOMETRIC OBJECTS

2.1 A Local Minimax Characterization of 1-saddle Based on Virtual Curves

Let $P(t,s)$ be a t-parametrized family of smooth curves in variable s connecting u_r to u_{p_t} where u_r is a local minimum of J and u_{p_t} can be another local minimum u_p or a fixed or moving point with $J(u_{p_t}) \leq J(u_r)$ and $\|u_r - u_{p_t}\| > \delta > 0$. Thus for each $t \geq 0$, $P(t,s)$ is a smooth curve in the variable s. We may assume $0 \leq s \leq 1$ with $P(t,0) = u_r$ and $P(t,1) = u_{p_t}$. Let $s(t) \in (0,1)$ be the first local maximum of $J(P(t,s))$ in s for each $t \geq 0$. Since u_r is a local minimum of $J(P(t,s))$ in s and $J(u_{p_t}) \leq J(u_r)$, such an $s(t)$ always exists with $0 < \delta < s(t) < 1$ for some $\delta > 0$ if u_r is nondegenerate. We have

$$\frac{dJ(P(t,s))}{ds}|_{s=s(t)} = J'(P(t,s(t)))P_s'(t,s(t)) = 0. \tag{2.1}$$

Once the value $s(t)$ and the direction $P_s'(t,s(t))$ are specified as in (2.1), for the t-parametrized family of curves $P(t,s)$ to evolve in t in a regular way or to avoid a sliding, we need to assign a moving direction. Let H_t be the hyperplane normal to $P_s'(t,s(t))$ at $P(t,s(t))$ and called the normal plane of the curve $P(t,s)$ at $P(t,s(t))$. Since $P_t'(t,s(t))$ defines the direction of the t-parametrized family of curves $P(t,s)$ moving away locally from the point $P(t,s(t))$, for this evolution in t to be regular or to avoid a sliding, the moving direction should be on H_t. By (2.1), $J'(P(t,s(t))) \in H_t$. Thus we set $P_t'(t,s(t)) = -J'(P(t,s(t)))/C_t$, where $C_t = \max\{\|J'(P(t,s(t)))\|, 1\}$ and a negative sign is used since we hope that the curves $P(t,s)$ evolves in t along certain negative gradient flow so that the value of $J(P(t,s(t))$ will be strictly decreasing (or obey the energy dissipation law), and the scalar C_t is introduced to enhance the stability of this evolution

in search for an unstable 1-saddle. We propose a 1-saddle search system:

$$\langle J'(P(t,s(t))), P_s'(t,s(t))\rangle = 0, \tag{2.2}$$

$$P_t'(t,s(t)) = -J'(P(t,s(t)))/C_t, \tag{2.3}$$

starting from an initial point $P(0,s(0))$ on a given initial smooth curve $P(0,s)$.

For the dynamic system (2.2) - (2.3), we would like to give some important notes here:

(1) The system (2.2) - (2.3) is actually not a dynamics of t-parametrized family of smooth curves $P(t,s)$. In fact, it is a dynamics of t-parametrized points $P(t,s(t))$ starting from an initial point $P(0,s(0))$. Thus we will concentrate on the evolution of the points $P(t,s(t))$;

(2) There are infinitely many smooth curves satisfying the dynamic system (2.2) - (2.3) and we do not have to know their explicit expressions, so we call these curves $P(t,s)$ *virtual*. This feature gives us a great flexibility to choose preferred smooth curves for different purposes or to satisfy certain constraints if exist. For instance, the Nehari manifold will be used in our research to speed up the numerical computation and enable us to easily extend the method for finding k-saddles. The method of the Nehari manifold will be discussed in Section 3;

(3) We assume that the scalar function $s(t)$ is locally Lipschitz continuous. Since for each $t \geq 0$, (2.2) can be used to solve for $s(t)$, a local maximum of $J(P(t,s)))$ in s, by using the implicit function theorem, a condition can always be proposed to achieve this. The locally Lipschitz continuity of s will be used in the convergence analysis.

Note that (2.2) is achieved by taking a local maximum of J along the curve $P(t,s)$ in s and (2.3) indicates that this system follows a negative gradient flow and leads to a local minimum of $J(P(t,s(t)))$ in t. Thus the system (2.2) - (2.3) is a new local minimax principle for a 1-saddle. Modifications of the system (2.2) - (2.3) can be developed for

other purposes. Different discrete realizations of the system in t may lead to different numerical algorithms. Since a 1-saddle is unstable, we do not want to go too fast to lose the algorithm stability in the search. The energy dissipation law is good for stability but only itself is not enough, thus we need a stepsize rule, a stronger version of the energy dissipation law.

Lemma 2.1.1. *(Stepsize Rule) If $P(t_0, s(t_0))$ is not a critical point, then there exists $s_0 > 0$ s.t. when $0 < t' < s_0$, we have a stepsize rule*

$$J(P(t_0 + t', s(t_0 + t'))) - J(P(t_0, s(t_0))) < \frac{-t'}{4}\|J'(P(t_0, s(t_0)))\|^2/C_{t_0}.$$

Furthermore, if $P(t_k, s(t_k)) \to P(t_0, s(t_0))$ as $t_k \to t_0$, then there exists $N > 0$ s.t. when $0 < t' < s_0/2, k > N$, we have a uniform stepsize rule

$$J(P(t_k + t', s(t_k + t'))) - J(P(t_k, s(t_k))) < \frac{-t'}{4}\|J'(P(t_k, s(t_k)))\|^2/C_{t_k}.$$

Proof. We first note that

$$\begin{aligned}
&P(t_0 + t', s(t_0 + t')) - P(t_0, s(t_0)) \\
=&P'_t(t_0, s(t_0))t' + P'_s(t_0, s(t_0))(s(t_0 + t') - s(t_0)) + o(t' + |s(t_0 + t') - s(t_0)|) \\
=&- J'(P(t_0, s(t_0)))t'/C_{t_0} + P'_s(t_0, s(t_0))(s(t_0 + t') - s(t_0)) \\
&+ o(t' + |s(t_0 + t') - s(t_0)|).
\end{aligned}$$

Then we assume that $s(t)$ is locally Lipschitz continuous, i.e., $|s(t_0 + t') - s(t_0)| \leq \ell_0 t'$.

It follows that $o(\|P(t_0+t', s(t_0+t')) - P(t_0, s(t_0))\|) = o(|t'|)$ and we have

$$\begin{aligned}
&J(P(t_0+t', s(t_0+t'))) - J(P(t_0, s(t_0))) \\
=&\langle J'(P(t_0, s(t_0))), P(t_0+t', s(t_0+t')) - P(t_0, s(t_0))\rangle \\
&+ o(\|P(t_0+t', s(t_0+t')) - P(t_0, s(t_0))\|) \\
=&\langle J'(P(t_0, s(t_0))), P'_t(t_0, s(t_0))t' + P'_s(t_0, s(t_0))(s(t_0+t') - s(t_0))\rangle + o(|t'|) \\
=&-t'\|J'(p(t_0, s(t_0)))\|^2/C_{t_0} + o(|t'|) \text{ (by (2.2) and (2.3)).}
\end{aligned}$$

Then it is easy to see there exist $s_0 > 0$ such that when $0 < t' < s_0$,

$$J(P(t_0+t', s(t_0+t'))) - J(P(t_0, s(t_0))) < \frac{-t'}{4}\|J'(P(t_0, s(t_0)))\|^2/C_{t_0}. \tag{2.4}$$

Since J and J' both are continuous, the second conclusion follows directly from $P(t_k, s(t_k)) \to P(t_0, s(t_0))$ as $t_k \to t_0$ and the stepsize rule in the first part. □

Theorem 2.1.2. *(Local Minimax Characterization) If* $t_0 = \arg\text{loc-}\min_{t>0} J(P(t, s(t)))$. *Then* $P(t_0, s(t_0))$ *is a saddle point.*

Proof. Arguing by contradiction, suppose $P(t_0, s(t_0))$ is not a saddle point, since it is a local maximum of J along the smooth curve $P(t_0, s)$ in s, it cannot be a local minimum of J either. Then by Lemma 2.1.1, there exists $s_0 > 0$ s.t. when $0 < t' < s_0$, we have

$$J(P(t_0+t', s(t_0+t'))) - J(P(t_0, s(t_0))) < \frac{-t'}{4}\|J'(P(t_0, s(t_0)))\|^2/C_{t_0}, \tag{2.5}$$

which yields a contradiction to $t_0 = \arg\text{loc-}\min_{t>0} J(P(t, s(t)))$. □

Remark 2.1.1. When the local minimum in Theorem 2.1.2 is numerically approximated, it leads to a local minimax method (LMM) for a 1-saddle. It is also interesting to indicate

the significant differences between LMM (2.2)-(2.3) and the well-known minimax method characterized by the mountain pass lemma [12]. In the latter, $u_{p_t} = u_p$ is fixed in an assumed mountain pass structure and the minimum and maximum are all in the global sense, in particular, the minimum must be taken over all possible continuous paths connecting u_r and u_p. Numerically this is impossible. While in our LMM, u_{p_t} is flexible, it does not assume a mountain pass structure, the minimum and maximum are all in the local sense, and the paths $P(t, s)$ can be any one-parameter family of smooth curves connecting u_r and u_{p_t}. Thus LMM (2.2)-(2.3) has clear advantages in numerical algorithm design and implementation. We present the following flowchart of the new local minimax method (LMM).

2.2 Flowchart of the New LMM

Assume that u_r is a local minimum of J and u_{p_0} is either another fixed local minimum of J or any point with $J(u_{p_0}) \leq J(u_r)$. Given λ, ϵ, $\tau_k > 0$ with $\tau_k \to 0$ as $k \to \infty$, $\sum_{k=0}^{\infty} \tau_k = +\infty$.

Step 1: Let $P(0, s)$ be the straight line or a given smooth curve such that $P(0, 0) = u_r$, $P(0, 1) = u_{p_0}$ and $s(0)$ be the first local maximum of $J(P(0, s))$, namely, $s(0) = \text{argmax}_{s>0} J(P(0, s))$. Set $k = 0$, $t_0 = 0$, $u_k = P(t_k, s(t_k))$;

Step 2: Evaluate $d_k = J'(u_k)$. If $\|d_k\| < \epsilon$, then output u_k and stop, otherwise continue;

Step 3: For $t' = \frac{\lambda}{2^m}$, $m = 1, 2, \ldots$, let $u_k(t') = P(t_k, s(t_k)) - t' d_k \,/\, C_k$. Let $u_{p_k,t'}$ be a local minimum of J or chosen in a continuous way in t' such that $J(u_{p_k,t'}) \leq J(u_r)$. Construct a smooth curve $P(t_k + t', s)$ passing through u_r, $u_k(t')$, $u_{p_k,t'}$. Use $s(t_k)$ as an initial guess to solve for $s(t_k + t') = \arg\max_{s>0} J(P(t_k + t', s))$. Denote

$$t'_k = \max\{t' = \frac{\lambda}{2^m} \leq \tau_k \mid m \in \mathbb{N}^+, J(P(t_k + t', s)) - J(u_k) \leq -\frac{t'}{4}\|d_k\|^2 \,/\, C_{t_k}\},$$

$t_{k+1} = t_k + t'_k$ and $u_{k+1} = P(t_{k+1}, s(t_{k+1}))$;

Step 4: Set $k = k + 1$ and go to Step 2.

Remark 2.2.1. (1) In Step 3, the first line is a discrete version of the condition (2.3), namely, a finite difference in t-variable $P(t + t', s(t)) \approx P(t, s(t)) - t'J'(t, s(t))$ is used to approximate the condition (2.3)
$-J'(P(t, s(t))/C_t = P'_t(t, s(t)) = \lim_{t'\to 0} \frac{P(t+t',s(t))-P(t,s(t))}{t'}$. Thus for algorithm stability, we choose the approximation

$$u(t') = P(t + t', s(t)) \approx P(t, s(t)) - t'J'(t, s(t))/C_t.$$

The condition (2.2) is always satisfied at a local maximum $J(P(t_k + t', s))$ in s. Since along a smooth path $J(P(t, s))$, there can be multiple selections of local maxima of J in s. Each one is called a peak selection. An oscillation among different peak selections will destroy the continuity of P in s. Our strategy is in Step 3 we use the previous peak selection $s(t_k)$ as the initial guess to consistently trace a peak selection. Doing so will help us avoid the unnecessary oscillation and hold the continuity of $P(t, s(t))$ in t. On the other hand, in Step 1, by starting with $s > 0$ small, we intend to choose the peak selection which is closest to the local minimum u_r;

(2) In an extreme case, just like a negative gradient flow may be stuck at a saddle not necessarily a local minimum (0-saddle), LMM may be stuck at a k-saddle u^* ($k > 1$) not necessarily a 1-saddle. In this rare case, we check $J''(u^*)$. It will have at least two negative eigenvalues. We may use their eigenfunctions, two decreasing directions of J at u^*, to construct a decreasing direction v^- orthogonal to $P'_s(t^*, s(t^*))$, then move along $u^* + t'v^-$ to stay away from u^* and continue the algorithm iteration to search for a 1-saddle. Since the algorithm is descending, it will not come back to u^*.

2.3 Convergence Analysis

The following Palais-Smale (PS) condition is introduced before we prove the convergence of the algorithm.

Definition 2.3.1. *A functional $J \in \mathcal{C}^1(H, \mathbb{R})$ is said to satisfy the Palais-Smale (PS) condition if any sequence $\{u_k\} \subset H$ with $\{J(u_k)\}$ bounded and $J'(u_k) \to 0$ has a convergent subsequence.*

Theorem 2.3.1. *Let $t_{k+1} = t_k + t'_k$ where $0 < t'_k \leq \tau_k, \tau_k \to 0, \sum_{k=0}^{\infty} \tau_k = +\infty$ and $u_k = P(t_k, s(t_k))$ be the sequence generated by the algorithm with $\varepsilon = 0$. Then*

*(**a**) $\lim_{k\to\infty} t'_k J'(u_k)/C_{t_k} = 0$; Furthermore if J satisfies the PS condition, then*

*(**b**) there is a subsequence $u_{k_j} \to u^*$, a saddle of J;*

Denote $K = \{u \in H : J'(u) = 0, J(u) = J(u^*)\}$, then

*(**c**) any convergent subsequence of $\{u_k\}$ converges to a point of K;*

*(**d**) Let $\overline{\{u_k\}}$ be all the limiting points of $\{u_k\}$. If in addition, $\|P'_s(t_k, s(t_k))\|$ is bounded and the scalar function $s(t)$ is Lipschitz continuous, then $\overline{\{u_k\}} \cap K \neq \emptyset$ is connected and dis$(u_k, K) \to 0$ as $k \to \infty$.*

Proof. Since $J(u_r) < J(u_{k+1}) < J(u_k)$ by the stepsize rule, $\lim_{k\to\infty} J(u_k)$ exists and

$$J(u_r) - J(u_0) \leq \lim_{k\to\infty} J(u_k) - J(u_0) = \sum_{k=0}^{\infty} (J(u_{k+1}) - J(u_k)) < -\frac{1}{4} \sum_{k=0}^{\infty} t'_k \|J'(u_k)\|^2 / C_{t_k},$$

where $C_{t_k} = \max\{1, \|J'(u_k)\|\}$. Thus $t'_k \|J'(u_k)\|^2 / C_{t_k} \to 0$ and then $t'_k J'(u_k)/C_{t_k} \to 0$ since $0 < t'_k < \tau_k \to 0$. So (a) is verified.

To prove (b), there are totally two Cases for $\{u_k\}$, (1) there is $\eta > 0$ s.t. $\|J'(u_k)\| > \eta, k = 1, 2, ...$, or (2) there is a subsequence $J'(u_{k_i}) \to 0$.

If Case (1) holds, we may assume $\eta < \frac{1}{2}$. Thus $-\|J'(u_k)\| < -\eta < -\eta^2$ and

$$J(u_r) - J(u_0) < -\frac{1}{4}\sum_{k=0}^{\infty} t'_k \|J'(u_k)\|^2 / C_{t_k} \leq -\frac{\eta^2}{4}\sum_{k=0}^{\infty} t'_k = -\frac{\eta^2}{4}\sum_{k=0}^{\infty} |t_{k+1} - t_k|. \quad (2.6)$$

That is, $\{t_k\}$ is a Cauchy sequence. We obtain $t_k \to t^*$. By the continuity, we have $u_k = P(t_k, s(t_k)) \to u^* = P(t^*, s(t^*))$ and $\|J'(P(t^*, s(t^*)))\| \geq \eta$, i.e., u^* is not a critical point. Then Lemma 2.1.1 states that there exist $s_0 > 0, N > 0$ s.t. when $k > N$, we have $\frac{s_0}{2} \leq t'_k < \tau_k \to 0$, a contradiction. Thus Case (2) must hold true. Since $\{J(u_k)\}$ is bounded and $J'(u_{k_j}) \to 0$, by the PS condition, (b) is proven.

To establish (c), let $\{u_{k_j}\} \subset \{u_k\}$ be any convergent subsequence with $u_{k_j} \to u'$. If $J'(u') \neq 0$, we can pass to a subsequence if necessary, then $t'_k J'(u_k)/C_{t_k} \to 0$ and $\|J'(u_{k_j})\| > \eta > 0$ lead to $t'_{k_j} \to 0$, a contradiction to Lemma 2.1.1 under $u_{k_j} \to u'$. Thus $J'(u') = 0$ must hold. Since $J(u_k)$ is monotonically decreasing, we have $J(u') = J(u^*)$, i.e., $u' \in K$.

To prove (d), we have

$$\begin{aligned} u_{k+1} - u_k &= P(t_{k+1}, s(t_{k+1})) - P(t_k, s(t_k)) \\ &= P'_t(t_k, s(t_k))t'_k + P'_s(t_k, s(t_k))(s(t_{k+1}) - s(t_k)) \\ &+ o(|t'_k| + |s(t_{k+1}) - s(t_k)|) \\ &= -J'(u_k)t'_k/C_{t_k} + P'_s(t_k, s(t_k))(s(t_{k+1}) - s(t_k)) \\ &+ o(|t'_k| + |s(t_{k+1}) - s(t_k)|). \end{aligned}$$

Note that the scalar function $s(t)$ is Lipschitz continuous, as $k \to \infty$ we have $0 < t'_k \leq \tau_k \to 0$,

$$\|J'(u_k)/C_{t_k}\| \leq 1, \|P'_s(t_k, s(t_k))\| \leq M, \ |s(t_{k+1}) - s(t_k))| \leq \ell(t'_k) \to 0.$$

Thus there is an $\ell_1 > 0$ s.t.

$$\|u_{k+1} - u_k\| = \|P(t_{k+1}, s(t_{k+1})) - P(t_k, s(t_k))\| \leq \ell_1(t'_k) \to 0 \ \text{ as } \ k \to \infty. \tag{2.7}$$

From (b), we have $u^* \in K \neq \emptyset$. Let $I \subset \mathbb{N}^+ = \{1, 2, ...\}$ and call $\sum_{i\in I} \|u_{i+1} - u_i\|$ the total distance traveled by the subsequence $\{u_i\}_{i\in I}$. For any given $\eta > 0$, let $i \in I \subset \mathbb{N}^+$ denote the whole index set in $\mathbb{N}^+$ with $\|J'(u_i)\| > \eta$. Since $J(u_r) < J(u_{k+1}) < J(u_k)$, similar to (2.6), we have

$$\begin{aligned} -\infty \ &< \ J(u_r) - J(u_0) \leq \sum_{k=1}^{\infty}[J(u_{k+1}) - J(u_k)] \leq \sum_{i\in I}[J(u_{i+1}) - J(u_i)] \\ &< \ -\frac{1}{4}\sum_{i\in I} t'_i \|J'(u_i)\|^2 / C_{t_i} \leq -\frac{\eta^2}{4}\sum_{i\in I} t'_i. \end{aligned} \tag{2.8}$$

By (2.7), it leads to

$$\sum_{i\in I} \|u_{i+1} - u_i\| \leq \ell_1 \sum_{i\in I} t'_i < +\infty, \tag{2.9}$$

i.e., the total distance traveled by $\{u_i\}_{i\in I}$ is finite.

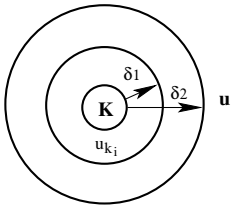

Figure 2.1: Three regions around K.

Suppose there is $\delta_2 > 0$ s.t. there are infinitely many points u in $\{u_k\}$ with dis$(u, K) > \delta_2$. By the inequality (2.7), for any $0 < \delta_1 < \delta_2$, there is $M > 0$ s.t. when $k > M$, $\|u_{k+1} - u_k\| < \frac{1}{4}(\delta_2 - \delta_1)$. Without loss of generality we may simply assume such $M = 1$.

It is clear from (b) that $u^* \in \overline{\{u_k\}} \cap K \neq \emptyset$. Then $\{u_k\}$ has to go into each one of the three regions for infinitely many times, see Figure 2.1. There should be infinitely many points $\{u_{k_i}\} \subset \{u_k\}$ satisfying $u_{k_i} \in \mathcal{R} = \{u \in H : \delta_1 < \text{dis}(u, K) < \delta_2\}$. Thus every time the subsequence $\{u_{k_i}\}$ enters the region $\mathcal{R}$ from one region, it has to travel for at least $\frac{1}{2}(\delta_2 - \delta_1)$ distance to pass the region $\mathcal{R}$ into another region. Therefore the total distance traveled by $\{u_{k_i}\}$ is infinite. However by (2.9), for any $\eta > 0$, the total distance traveled by all the points $u \in \{u_i\}$ with $\|J'(u)\| > \eta$ is finite. Thus there must be a subsequence $\{u_{k_{i'}}\} \subset \{u_{k_i}\}$ s.t. $J'(u_{k_{i'}}) \to 0$ and $J(u_{k_{i'}}) \to J(u^*)$. By the PS condition, there is a subsequence, denoted by $\{u_{k_{i'}}\}$ again, s.t. $u_{k_{i'}} \to u'$ with $J'(u') = 0$ and $J(u') = J(u^*)$. Thus $u' \in K$ and $\delta_1 \leq \text{dis}(u', K) \leq \delta_2$. It leads to a contradiction. Thus for any $\delta_2 > 0$, there are at most a finite number of points $u \in \{u_k\}$ s.t. $\text{dis}(u, K) > \delta_2$, i.e., $\text{dis}(u_k, K) \to 0$ as $k \to \infty$.

Next we let u^* be any limit point of $\{u_k\}$ by (b) or (c) and $\bar{u}$ be another limiting point of $\{u_k\}$ if exists. Then $u^*, \bar{u} \in K$. For any $0 < \delta_2 < \|u^* - \bar{u}\|$, there are infinitely many points $u \in \{u_k\}$ s.t. $\delta_2 < \|u^* - u\|$. Replacing K by u^* and repeating the above proof after (2.7), we obtain $u' \in K$ s.t. $\delta_1 \leq \|u^* - u'\| \leq \delta_2$. Since $0 < \delta_1 < \delta_2$ can be any such numbers, $\overline{\{u_k\}} \cap K$ must be connected. Finally (d) is verified. □

Remark 2.3.1. To obtain a sequence convergence (d) from a subsequence convergence (b) in Theorem 2.3.1, it is reasonable to assume the bounded scalar function $s(t)$ to be Lipschitz continuous. Observe that if $s(t) \in (0, 1)$ is only continuous with unbounded $|s'(t_k)|$, it must oscillate infinitely many times. Then there could be subsequences of $\{s(t_k)\}$ converging to different points in $[0, 1]$. Consequently we can have only the subsequence convergence (b) but not the sequence convergence (d). The boundedness of $\|P'_s(t_k, s(t_k))\|$ will also be checked when we discuss about the numerical implementations. Conclusion (d) implies $u_k \to u^*$ if u^* is isolated. It is clear that this convergent result can be easily

extended for k-saddles and actually covers several different variational methods since the algorithm setting is general.

The above LMM can be easily extended to numerically find 2-saddles or saddles with higher MI if they are interested. The convergence results for them can be easily proven in a similar way.

2.4 Finding 2-saddles with Virtual Surfaces

Let $P(t, s_1, s_2)$ be a t-parametrized family of smooth 2D-surfaces in variables s_1, s_2 connecting u_r, u_{p_t}, u_s where u_r, u_{p_t} are the same as before and u_s is a previously found proper 1-saddle of J but it is not a local maximum of J on $P(t, s_1, s_2)$. Such a structure is necessary for a 2-saddle to exist and to be numerically computable. We may assume $P(t, 0, 0) = u_r, P(t, 1, 0) = u_{p_t}, P(t, 0, 1) = u_s$. Denote $s = (s_1, s_2)$ and $P(t, s(t)) = P(t, s_1(t), s_2(t))$ where $s(t) = (s_1(t), s_2(t))$ is a local maximum point of J on the surface $P(t, s)$ closest to u_s. By the chain rule, we have

$$J'(P(t, s_1(t), s_2(t)))P'_{s_1}(t, s(t)) = 0,\ J'(P(t, s_1(t), s_2(t)))P'_{s_2}(t, s(t)) = 0. \tag{2.10}$$

Let H_t be the normal space of the surface $P(t, s)$ at $P(t, s(t))$, i.e., $H_t = \{v \in H : v \perp P'_{s_1}(t, s(t)), v \perp P'_{s_2}(t, s(t))\}$. Since $P'_t(t, s(t))$ is the direction of this t-parametrized family of surfaces moving away locally from the point $P(t, s(t))$ and we want this evolution to be nonsliding and also to follow a negative gradient flow, we choose $P'_t(t, s(t)) = -J'(P(t, s(t)))/C_t \in H_t$. Thus we propose the following 2-saddle search system

$$\begin{aligned} J'(P(t, s(t)))P'_{s_1}(t, s(t)) &= 0,\ J'(P(t, s(t)))P'_{s_2}(t, s(t)) = 0, & (2.11)\\ P'_t(t, s(t)) &= -J'(P(t, s(t)))/C_t & (2.12) \end{aligned}$$

starting from an initial point $P(0, s(0))$ on an initial surface $P(0, s)$. Again the system (2.12)-(2.12) is not a system of surfaces $P(t, s)$ but a system of points $P(t, s(t))$. There are infinitely many surfaces satisfying the system and we do not have to know their expressions. For this reason, we call those surfaces *virtual*. We denote $P'_s(t, s(t)) = (P'_{s_1}(t, s(t)), P'_{s_2}(t, s(t)))$ and assume $s(t)$ to be locally Lipschitz continuous in t, since for each $t \geq 0$, the equations in (2.11) can be used to solve for $s(t)$. By the implicit function theorem, conditions can always be proposed so that $s(t)$ is locally $\mathcal{C}^1$.

We give a similar result of stepsize rule and minimax characterization in the following but omit the proofs of them which can be proven in the same way as the ones for Lemma 2.1.1 and Theorem 2.1.2.

Lemma 2.4.1. *(Stepsize Rule) If $P(t_0, s(t_0))$ is not a critical point of J, then there exists $s_0 > 0$ s.t. when $0 < t' < s_0$, we have*

$$J(P(t_0 + t', s(t_0 + t'))) - J(P(t_0, s(t_0))) < \frac{-t'}{4} \|J'(P(t_0, s(t_0)))\|^2 / C_{t_0}.$$

Furthermore, if $P(t_k, s(t_k)) \to P(t_0, s(t_0))$, then there exists $s_0 > 0$ and $N > 0$ s.t. when $0 < t' < s_0, k > N$, we have the uniform stepsize rule

$$J(P(t_k + t', s(t_k + t'_k))) - J(P(t_k, s(t_k))) < \frac{-t'}{4} \|J'(P(t_k, s(t_k)))\|^2 / C_{t_k}.$$

Proof. Similar to that of Lemma 2.1.1. □

Theorem 2.4.2. *(Index-2 Saddle Characterization). Let $t_0 = \arg \operatorname{loc\text{-}min}_{t \geq 0} J(P(t, s(t)))$. Then $P(t_0, s(t_0))$ is a saddle point.*

Proof. By Lemma 2.4.1 and follow a proof similar to that of Theorem 2.1.2. □

A convergence result similar to Theorem 2.3.1 can be proven.

LMM for finding 2-saddles. Let u_s be a previously found 1-saddle, following the algorithm described in Section 2.2: In Step 1, let $P(0,s)$ where $s=(s_1,s_2)$, be a preferred initial smooth surface s.t. $P(0,(0,0))=u_r, P(0,(0,1))=u_{p_0}, P(0,(1,0))=u_s$. Find a local maximum $P(0,s(0))$ of J on $P(t,s)$ closest to u_s; In Step 3, $u(t')$ is the same. Instead of using $u_r, u_k(t')$ and $u_{p_k,t'}$ to construct a new preferred smooth curve, this time we use $u_r, u_s, u_k(t')$ and $u_{p_k,t'}$ to construct a new preferred surface. Then use $s(t_k)$ as an initial guess to solve for $s(t_k+t')$..... Other parts in LMM remain the same.

LMM can be further modified to find higher index saddles in a similar way if needed.

2.5 Numerical Implementation

Since those geometric objects are virtual, there are infinitely many ways to implement the new LMM.

2.5.1 Using lines and planes for M-type problems

For the M-type functional (1.7) with $\lambda<\lambda_1$, there is only one local minimum at $u_r=0$ with $J(0)=0$. However due to its M-type structure $\lim_{s\to\infty}J(su_t)=-\infty$ along each direction u_t, we always have $J(s_tu_t)<J(0)=0$ when $s_t>0$ is large. So to find a 1-saddle, instead of using $u_{p_t}=s_tu_t$, we can use a straight line $P(t,s)=su_t$ where $\|P'_s(t,s(t))\|=\|u_t\|=1$ is bounded and find the first local maximum $s(t)>0$ of $J(su_t)$ in s. Once a 1-saddle u_s is found, to find a 2-saddle, for each direction $u_t\perp u_s$, we can use the three points u_r, u_s and u_t to construct a plane $P(t,s_1,s_2)$ where $\|P'_s(t,s(t))\|^2=\|(P'_{s_1}(t,s(t)),P'_{s_2}(t,s(t)))\|^2=\|u_s\|^2+\|u_t\|^2=\|u_s\|^2+1$ is bounded, and find a local maximum of J on this plane closest to u_s. Due to the M-type structure, a point $u_{p_t}=s_tu_t$ on the plane $P(t,s_1,s_2)$ with $J(u_{p_t})<J(u_r)$ can always be easily found. But such an information is already contained in the plane $P(t,s_1,s_2)$ on which we find a local maximum closest to u_s. Such a strategy using straight lines and planes, etc., leads to the local minimax method successfully developed for finding saddles of many M-type

problems [13, 23, 24]. Also since the term $P'_s(t, s(t))$ is always bounded in this case, the convergence result Theorem 2.3.1 can be applied.

2.5.2 Using quadratic curves or surfaces

2.5.2.1 Using quadratic curves for 1-saddles

To use quadratic curves for finding 1-saddles, in Step 3 of the algorithm, we let

$$L(t_k, t', x, y) = u_r + x(u_k(t') - u_r) + y(u_{pk,t'} - u_r) \tag{2.13}$$

be an xy-plane passing through the points $u_r, u_k(t'), u_{pk,t'}$ and then let $x = c_1(s), y = c_2(s)$ be the parametrized equations of a quadratic curve in the xy-plane s.t. $(c_1(0), c_2(0)) = (0, 0), (c_1(1), c_2(1)) = (0, 1)$ and $(c_1(s), c_2(s)) = (1, 0)$ for some $0 \leq s \leq 1$. There are many ways to do so, e.g., in our numerical computation, we take

$$(x - \frac{1}{2})^2 + (y - \frac{1}{2})^2 = \frac{1}{2}, \tag{2.14}$$

which leads to

$$c_1(s) = \frac{1}{\sqrt{2}} \cos(\frac{3\pi}{4}(2s - 1)) + \frac{1}{2},\ c_2(s) = \frac{1}{\sqrt{2}} \sin(\frac{3\pi}{4}(2s - 1)) + \frac{1}{2} \tag{2.15}$$

and we obtain an explicit expression for the curve

$$P(t_k + t', s) = u_r + c_1(s)(u_k(t') - u_r) + c_2(s)(u_{p_k,t'} - u_r). \tag{2.16}$$

Thus the term $P'_s(t_k + t', s) = c'_1(s)(u_k(t') - u_r) + c'_2(s)(u_{p_k,t'} - u_r)$ is bounded if the two terms $u_k(t'), u_{p_k,t'}$ are bounded. The term $u_{p_k,t'}$ can be selected bounded while the term $u_k(t') = P(t_k, s(t_k)) - t'd_k/C_k$, where $t'd_k/C_k$ is always bounded. Thus the term

$P'_s(t, s(t))$ is bounded if and only $P(t_k, s(t_k))$ is bounded. By LMM, we have the property $J(u_r) < J(P(t_k, s(t_k))) < J(P(t_0, s(t_0)))$ which for many problems implies that $P(t_k, s(t_k))$ is bounded, e.g., let $J(u) = \frac{1}{2}\|u\|^2_{H_0^1} - \frac{\lambda}{2}\|u\|^2_{L^2} + \frac{1}{p+1}\|u\|^{p+1}_{L^{p+1}}$, $(p > 1)$ be a W-type functional. For $\|u\|_{H_0^1} = 1$ and $-M = J(u_r) < J(tu) < 0, t > 0$, we have

$$\frac{\lambda}{2}\|u\|^2_{L^2} - Mt^{-2} < \frac{1}{2} + \frac{t^{p-1}}{p+1}\|u\|^{p+1}_{L^{p+1}} < \frac{\lambda}{2}\|u\|^2_{L^2} < \frac{\lambda}{2}\lambda_1^{-1},$$

where the last inequality is due to the Poincare inequality and λ_1 is the minimal positive eigenvalue of $-\Delta$ in the space $H_0^1(\Omega)$. It implies that such t must be bounded since $\|u\|_{L^2} \leq |\Omega|^{\frac{1}{2}-\frac{1}{p+1}}\|u\|_{L^{p+1}}$ by the Hölder's inequality. It is interesting to note that $(c_1(0), c_2(0)) = (0, 0), (c_1(\frac{1}{3}), c_2(\frac{1}{3})) = (1, 0)$, $(c_1(1), c_2(1)) = (0, 1)$, i.e., (2.15) remains the same for different points $u_r, u_k(t'), u_{p_k,t'}$. A local maximum of the function $g(s) = J(P(t_k + t', s))$ for $0 \leq s \leq 1$ can be easily computed by many 1-D optimization methods, e.g., in our numerical computation, it is done by calling the Matlab subroutine "fminunc" with the initial guess $s = \frac{1}{3}$. To consistently trace the local maxima of such g, we should always use the s-value $s(t_k)$ stored from the previous iteration as an initial guess to find a local maximum of a new g.

2.5.2.2 Using quadratic surfaces for 2-saddles

To use quadratic surfaces for finding 2-saddles, in Step 3 of LMM, we let

$$L(t_k, t', x, y, z) = u_r + x(u_k(t') - u_r) + y(u_{p_k,t'} - u_r) + z(u_s - u_r) \tag{2.17}$$

be a xyz-space passing through the points $u_r, u_k(t'), u_{p_k,t'}, u_s$ and then let $s = (s_1, s_2), x = c_1(s), y = c_2(s), z = c_3(s)$ be the parametrized equations of a quadratic surface in xyz-space passing through the four points $(0, 0, 0), (1, 0, 0), (0, 1, 0)$ and $(0, 0, 1)$. There are

many ways to do so, e.g., in our numerical computation, we take

$$(x-\frac{1}{2})^2+(y-\frac{1}{2})^2+(z-\frac{1}{2})^2=\frac{3}{4}, \tag{2.18}$$

which leads to spherical coordinates

$$c_1(s)=\frac{1}{2}+\frac{\sqrt{3}}{2}\sin(s_1)\cos(s_2),\ c_2(s)=\frac{1}{2}+\frac{\sqrt{3}}{2}\sin(s_1)\sin(s_2),\ c_3(s)=\frac{1}{2}+\frac{\sqrt{3}}{2}\cos(s_1) \tag{2.19}$$

passing through the four points $(0,0,0),(1,0,0),(0,1,0),(0,0,1)$ and we obtain an explicit expression for the surface

$$P(t_k+t',s)=u_r+c_1(s)(u_k(t')-u_r)+c_2(s)(u_{p_k,t'}-u_r)+c_3(s)(u_s-u_r). \tag{2.20}$$

Note that (2.19) remains the same for different points $u_r, u_{p_k,t'}, u_k(t'), u_s$. A local maximum of $g(s)=J(P(t_k+t',s))$ in $s=(s_1,s_2)$ can be easily computed by many finite-dimensional unconstrained optimization methods, e.g., in our numerical computation, it is done by calling the Matlab subroutine "fminunc" with the initial guess $s=(s_1,s_2)=(\cos^{-1}(\frac{-\sqrt{3}}{3}),\frac{-\pi}{4})$. To consistently trace local maxima of such g, we should always use the s-value $s(t_k)$ saved from the previous iteration as an initial guess to find a local maximum of a new g.

2.6 Numerical Examples

2.6.1 Tests on finite-dimensional benchmark problems

We now test LMM on some benchmark problems that are commonly used by finite-dimensional algorithms in the literature.

Example 2.6.1. Consider finding 1-saddles of a W-type function

$$J(x, y) = (1 - x^2 - y^2)^2 + y^2/(x^2 + y^2), \tag{2.21}$$

with two local minima $u_r = (-1, 0)$ and $u_p = (1, 0)$, two 1-saddles $(0, 1)$ and $(0, -1)$, and a local maximum $(0, 0)$. We choose an initial guess (x_0, y_0) with $-1 < x_0 < 1$ and construct a quadratic curve $P(0, s)$ connecting $u_r, (x_0, y_0), u_p$. Since J is symmetric about the y-axis, $P(0, s(0)) = (0, y_0^*)$ for some y_0^*. If $y_0 > 0$ is selected, LMM finds the 1-saddle $(0, 1)$ and if $y_0 < 0$ is selected, LMM yields another 1-saddle $(0, -1)$. See Figure 2.2 and Table 2.1, where and below $\mathrm{N_{It}}$ denotes the iteration number.

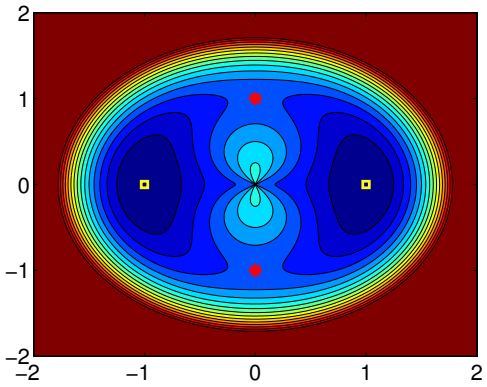

Figure 2.2: Contours of the function (2.21) with two local minima (□) at $(-1, 0), (1, 0)$, two 1-saddles (*) at $(0, -1), (0, 1)$ and one local maximum (O) at $(0, 0)$.

Example 2.6.2. Find 1-saddles of a W-type function with a triple-well potential function

$$J(x, y) = 3e^{-x^2-(y-\frac{1}{3})^2} - 3e^{-x^2-(y-\frac{5}{3})^2} - 5e^{-(x-1)^2-y^2} - 5e^{-(x+1)^2-y^2} + 0.2x^4 + 0.2(y - \frac{1}{3})^4. \tag{2.22}$$

N_{It}	Saddle	$\|J'(\cdot)\|$
1	(1.2104e-07,0.718750000000)	1.389770507813
2	(8.101e-08,0.968750000000)	0.238403320313
3	(-2.603e-08,0.998550415039)	0.011571476313
4	(-2.603e-08,0.999996849578)	2.520325611e-05
5	(-2.603e-08,0.999999999985)	5.207054057e-09

Table 2.1: Numerical results on (2.21) by LMM in the nth iteration.

J has three minima at $(1.048054984, -0.0420936582)$, $(-1.0480549862, -0.0420936637)$, $(-6.0e\text{-}08, 1.5370819624)$, a local maximum at $(-4.94e\text{-}07, 0.5191867341)$, and three 1-saddles as shown in Figure 2.3 (left) and Table 2.2.

	Numerical Solution	$\|J'(\cdot)\|$	ε	N_{It}
1-Saddle 1	(0.000000016,-0.315828508)	9.623269e-06	1e-05	36
1-Saddle 2	(0.617273601,1.1027353229)	9.555707e-06	1e-05	27
1-Saddle 3	(-0.6172852268,1.1027945717)	3.630596e-04	4e-04	18

Table 2.2: Numerical results of (2.22) by LMM with the stepsize $s = 0.05$.

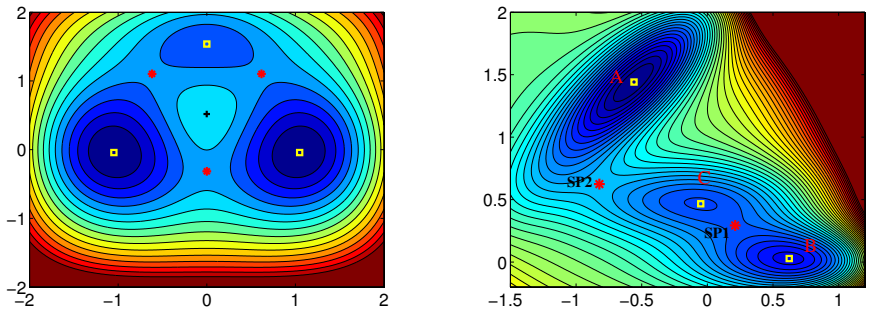

(a) (b)

Figure 2.3: (left) Contours of the function (2.22) with three local minima (□), a local maximum (+) and three 1-saddles (∗) and (right) contours of the Muller potential (2.23) with three local minima A, B, C and two 1-saddles SP1 and SP2.

Example 2.6.3. We compute 1-saddles of the Muller function

$$J(x,y) = \sum_{i=1}^{4} K_i e^{[a_i(x-x_i^0)^2 + b_i(x-x_i^0)(y-y_i^0) + c_i(y-y_i^0)^2]} \tag{2.23}$$

where the vectors $K = (-200, -100, -170, 15)$, $a = (-1, -1, -6.5, 0.7)$,

$b = (0, 0, 11, 0.6)$, $c = (-10, -10, -6.5, 0.7)$, $x^0 = (1, 0, -0.5, -1)$, $y^0 = (0, 0.5, 1.5, 1)$.

Three local minima $A = (-0.55822363677964, 1.44172582715450)$,

$B = (0.62349936799644, 0.02803774112374)$,

$C = (-0.05001028122511, 0.46669409222955)$ are found by the Matlab subroutine "fminunc" and then two 1-saddles $SP1 = (0.212486571139517, 0.292988327843969)$ and $SP2 = (-0.822001541054890, 0.624312898567439)$ are found by LMM in 12 and 432 iterations, respectively, with $\|J'(\cdot)\| < 10^{-4}$ as shown in Figure 2.3 (right).

Remark 2.6.1. In our numerical computation, if $u_r = B$ and $u_p = C$ are used, LMM produces the 1-saddle SP1; if $u_r = A$ and $u_p = C$ are assigned, then LMM yields the 1-saddle SP2. However, if we set $u_r = A$ and $u_p = B$, LMM may find the 1-saddle

SP1 or SP2 depending on the initial guess selected. By comparison, it is much harder to find 1-saddles of the Muller function than other benchmark problems. Except the rough solutions in [25], we have not seen any more precise results in the literature.

Example 2.6.4. As the last benchmark test, we consider finding 1-saddles and 2-saddles of a 3D M-type function for given $r \neq 0$,

$$J(x_1, x_2, x_3) = x_1^2 + 2x_2^2 + 3x_3^2 - r^2(x_1^2 + x_2^2 + x_3^2 - 1)^2. \tag{2.24}$$

By a direct computation, J has a local minimum at $A = (0, 0, 0)$, two local maxima at $B = (0, 0, (\frac{3}{2r^2} + 1)^{1/2})$, $C = (0, 0, -(\frac{3}{2r^2} + 1)^{1/2})$, two 1-saddles at $(\pm(\frac{1}{2r^2} + 1)^{1/2}, 0, 0)$, and two 2-saddles at $(0, \pm(\frac{1}{r^2} + 1)^{1/2}, 0)$. Let $r^2 = 0.5$. We take $u_r = (0, 0, 0), u_p = (\pm 3, 0, 0)$ since $J(0, 0, 0) = -0.5 > J(\pm 3, 0, 0) = -23$.

Finding 1-saddles: Let v_0 be an initial point and $P(0, s(0))$ be the local maximum of J along an initial curve $P(0, s)$ connecting u_r, v_0, u_p. If we take the advantage of knowing the local maxima at $B = (0, 0, 2)$, $C = (0, 0, -2)$, and directly set $v_0 = P(0, s(0)) = B$ or C, then LMM will be stuck at B or C. Thus we follow Remark 2.2.1 (2) and use the eigenvector corresponding to the second eigenvalue of $J''(B)$ or $J''(C)$ to stay away from B or C. LMM will continue and find two 1-saddles $u_{s_1^1}, u_{s_1^2}$ shown in Table 2.3.

Finding 2-saddles: Once 1-saddles $u_{s_1^1}, u_{s_1^2}$ are found, we process to find 2-saddles. Let u_s be one of the 1-saddles. Choose an initial guess v_0 and construct an initial surface $P(t, s)$ connecting u_r, u_p, u_s, v_0. Again we may take the advantage of knowing the local maxima at $B = (0, 0, (\frac{3}{2r^2} + 1)^{1/2})$, $C = (0, 0, -(\frac{3}{2r^2} + 1)^{1/2})$ and directly set $P(0, s(0)) = B$ or C. Then LMM will be stuck at B or C. Thus we follow Remark 2.2.1 (2) and use the eigenvector corresponding to the third eigenvalue of $J''(B)$ or $J''(C)$ to stay away from B or C. LMM will continue and find two 2-saddles $u_{s_2^1}, u_{s_2^2}$ shown in Table 2.3.

In all the above numerical examples, if LMM with $\varepsilon = 10^{-4}$ is followed by a Newton

	Numerical Solution	$\|J'(\cdot)\|$	N_{It}
1-Saddle 1	(1.41421356,0,-0.000000146)	5.84614e-07	18
1-Saddle 2	(-1.41421356,0,-0.000000172)	6.90673e-07	21
2-Saddle 1	(0.0000000076,1.73205081,0)	1.19898e-07	6
2-Saddle 2	(0.0000000076,-1.73205081,0)	1.19898e-07	6

Table 2.3: Numerical data of saddles of (2.24) by LMM with $\varepsilon = 10^{-6}$.

method for one iteration, we will get $\|J'(\cdot)\| < 10^{-8}$.

2.6.2 Solving infinite-dimensional W/M-type problems

When we solve the model problem (1.6), the steps are the same as those in the algorithm description except a significant difference in evaluating the gradient $\nabla J(\cdot)$. If H is finite-dimensional, e.g., $H = \mathbb{R}^n$, we simply take a partial derivative with respect to each variable of J to get $\nabla J(x) = J'(x) = (J'_{x_1}(x), ..., J'_{x_n}(x)) \in \mathbb{R}^n$. However, if H is infinite-dimensional, e.g., $H = W^{1,2}(\Omega)$, since $J : W_0^{1,2}(\Omega) \to \mathbb{R}$,

$$J'(u) = -\Delta u(x) - \lambda u(x) + \kappa|x|^r|u(x)|^{p-1}u(x) \in W^{-1,2}(\Omega).$$

It cannot be used as a search direction in $W^{1,2}(\Omega)$. Thus we use the Riesz representation theorem to find its canonical dual $d = \nabla J(u) \in W_0^{1,2}(\Omega)$ of $J'(u)$ by solving

$$-\Delta d(x) + d(x) = J'(u), \tag{2.25}$$

a linear elliptic PDE. It can be solved by many numerical solvers, such as using a finite-difference method (FDM), a finite-element method (FEM) or a boundary element method (BEM), etc. Since the main effort in this research is to develop a new algorithm, its mathematical justification and implementation in an infinite-dimensional space, when numerical solvers are available for solving a linear sub-problem, we simply apply those solvers hand-

ily available without deliberating their CPU time or other computation cost here. In the following examples, we choose $p = 3$ and $\Omega = (-1, 1)^2$ wherein 82944 triangle elements are generated by the Matlab subroutine "initmesh" and (2.25) is solved by calling the Matlab subroutine "assempde". However, in order to clearly see the mesh grids and contours of a solution in one figure, a coarse mesh is used to redraw the profile and its contours. If interested, one may also zoom-in the upper portion of each figure below to find more numerical data on each solution.

In our numerical computation, we can also use the Newton's method to accelerate the local convergence if needed [26], so we can first use LMM until $\epsilon < 10^{-2}$, then follow it by the Newton's method. The reason we use LMM to decrease the error to a low level is that the Newton's method strongly relies on the initial guess even though the convergence is very fast. Actually the Newton's method does not assume any variational structure [27] and it can not recognize the order of saddles. When the initial guess is not sufficiently close to the target solution, the Newton's method could fail to converge and is likely to produce an unexpected solution. In addition, the invariance of the Newton's method to symmetry is insensitive to numerical errors [21, 26]. Thus we first use LMM to get closer to the target solution slowly, once the error is fairly small, we stop the LMM and switch to the Newton's method in order to speed up the convergence. In this way, we could find the target critical point with high accuracy (error is usually less than 10^{-6}). Further details related to symmetry invariance and some expressive numerical examples of the Newton's method can be found in [28].

When an initial direction v_0 is selected, we use an initial guess $u_0 = sv_0$ where the scalar s is chosen so that $\langle J'(sv_0), v_0\rangle = 0$ or otherwise as indicated.

For the W-type problem. We assume $0 < \lambda_k < \lambda < \lambda_{k+1}$, then 0 is a k-saddle of J and all other saddles u^* will have $J(u^*) < J(0) = 0$. In the first place, we use a negative gradient method to find a local minimum u_r where the initial guess is the first eigenfunction e_1 of

$-\Delta$. Computing the eigenfunctions of $-\Delta$ can be easily done by hand when the domain is a square/disk or by a numerical solver otherwise. Since the following implementations are conducted on the square $\Omega = (-1,1)^2$, we simply present the detailed computation of eigenfunctions in the end of this section. When the domain is symmetric about the origin, the problem is even-symmetric. Thus we simply take $u_p = -u_r$, another local minimum. Then the first step of our algorithm leads to $u_0 = P(0, s(0))$ a saddle. However, $J'(u_0) = 0 \Rightarrow d_0 = \nabla J(u_0) = 0$, so the algorithm gets stuck. Thus we follow Remark 2.2.1 (2) and check the eigenvalue of the linear operator $J''(0) = (-\Delta - \lambda I)$. If $J''(0)$ has only one negative eigenvalue, i.e., $\lambda_1 < \lambda \leq \lambda_2$, then 0 is a 1-saddle. The algorithm terminates. Otherwise, i.e., $\lambda > \lambda_2$, $J''(0)$ has at least two negative eigenvalues and the second one is doubled. The first one actually corresponds to the first eigenfunction e_1 and it is useless since it has the same direction as $u_p - u_r$. To solve the two 1-saddles, we replace d_0, respectively, by the two linearly independent eigenfunctions e_2^1 and e_2^2 corresponding to the second double eigenvalue λ_2, which are orthogonal to the direction $u_p - u_r$. Then we obtain $u_0(t') = -t'd_0/C_k$ and construct the curve $P(t', s)$ connecting u_r, u_p and $u_0(t')$ and the rest of the algorithm follows the steps stated in Section 2.2. In this way, the algorithm produces two 1-saddles.

After we solve the two 1-saddles u_{s_1} and u_{s_2}, we can pick either of them, which is denoted by u_s, to construct a new preferred surface to find the 2-saddle. For $u_0(t')$, the eigenfunction corresponding to the third eigenvalue of $-\Delta$ is used. The method of finding a local maximum of J on P is similar to what we did in finding the 1-saddles.

Case 1. In (1.6), we set $p = 3$, $\kappa = 1$, $\lambda = 20$, $r = 0, 1, 4$ respectively, and the domain $\Omega = (-1,1)^2$. Since $\lambda_3 < \lambda < \lambda_4$, where $\lambda_3 = 2\pi^2$ and $\lambda_4 = \frac{5}{2}\pi^2$ are the 3rd and 4th Dirichlet eigenvalue in $H_0^1(\Omega)$,we only have saddles with MI < 3. A local minimum, two 1-saddles and a 2-saddle are found and shown in Table 2.4 and Figure 2.4.

Case 2. In (1.6), we set $p = 3$, $\kappa = 1$, $\lambda(x) = 20e^{|x|^2}$, $r = 0, 1, 4$ respectively, and the

domain $\Omega = (-1,1)^2$. A local minimum, two 1-saddles and a 2-saddle are found and shown in Table 2.5 and Figure 2.5.

Remark 2.6.2. We consider the eigenfunctions of $-\Delta$ in the space $H = H_0^1(\Omega)$ where $\Omega = (-1,1)^2$, so the equation we are going to solve is a homogeneous Helmholtz Equation:

$$\Delta v + \lambda v = 0 \tag{2.26}$$

in $H_0^1(\Omega)$.

Separation of variables yields us the eigenfunctions:

$$e_{mn}(x,y) = \sin\left(\frac{m\pi(x+1)}{2}\right)\sin\left(\frac{n\pi(y+1)}{2}\right) \quad \text{for } m,n \in \mathbb{N}^+, \tag{2.27}$$

which have the corresponding eigenvalues

$$\lambda_{mn} = \left(\frac{m\pi}{2}\right)^2 + \left(\frac{n\pi}{2}\right)^2 \quad \text{for } m,n \in \mathbb{N}^+, \tag{2.28}$$

where $\mathbb{N}^+$ is the set of positive integers. Note that m and n can be any integers theoretically but we could only get 0 if at least one of m and n is zero and negative m or n will just produce the eigenfunctions with the same or the opposite sign as the sine function is an odd function.

In the implementation, we firstly let $m = n = 1$ and obtain the first eigenfunction $e_1 = e_{11} = \sin\left(\frac{\pi(x+1)}{2}\right)\sin\left(\frac{\pi(y+1)}{2}\right)$ and the first eigenvalue $\lambda_1 = \frac{\pi^2}{2}$. We set the initial guess to be e_1 in the negative gradient method in order to find the local minimum in the W-type problems. Then we let $m = 2, n = 1$ to get one of the eigenfunctions e_2^1 corresponding to the second eigenvalue $\lambda_2 = \frac{5}{4}\pi^2$. Another eigenfunction of λ_2 can be easily obtained if we let $m = 1$, $n = 2$, but it makes no difference since this eigenfunction is just a rotation of e_2^1 on a square domain. In the numerical implementation, we can obtain

a new eigenfunction $e_2^2 = e_{21} + e_{12}$ of λ_2, and e_2^2 has a different geometric symmetry with e_2^1 and is also orthogonal to e_1. Using e_2^1 and e_2^2 respectively, we can solve two 1-saddles in the W-type problems. If we continue to solve the saddles with higher MI, the initial guess $u_0(t')$ could be e_{22}, e_{31} or other eigenfunctions defined in (2.27) with increased m and n.

		LMM					Newton ($\|d\|$ <1e-6)		Refer
	r	$\|d\|$	ε	$\|J'(\cdot)\|_\infty$	J	N_{It}	$\|J'(\cdot)\|_\infty$	N_{It}	Fig. 2.4
A 0-saddle	0	2.9211e-4	3e-4	0.0010	-125.7119	39	1.7290e-6	6	(a)
1-saddle 1	0	4.9457e-4	5e-4	0.0055	-28.5317	22	4.8296e-6	7	(b)
1-saddle 2	0	8.7338e-4	1e-3	0.0111	-24.3412	24	9.7744e-6	7	(c)
A 2-saddle	0	1.6851e-4	2e-4	0.0018	-0.0303	8	4.3677e-6	6	(d)
A 0-saddle	1	4.6356e-4	5e-4	0.0079	-295.4949	24	6.9170e-6	7	(e)
1-saddle 1	1	1.7927e-4	2e-4	0.0024	-48.7268	25	5.7109e-6	6	(f)
1-saddle 2	1	3.6374e-4	4e-4	0.0032	-41.9067	26	7.8076e-6	6	(g)
A 2-saddle	1	2.5209e-4	3e-4	0.0024	-0.0420	9	5.7883e-6	6	(h)
A 0-saddle	4	0.0010	2e-3	0.0286	-4016.9	175	2.2333e-5	8	(i)
1-saddle 1	4	8.0420e-4	9e-4	0.0115	-203.9178	41	1.0105e-5	7	(j)
1-saddle 2	4	6.5449e-4	7e-4	0.0064	-180.1026	58	5.6744e-6	7	(k)
A 2-saddle	4	6.7800e-4	7e-4	0.0048	-0.0904	12	4.2186e-6	7	(l)

Table 2.4: Numerical data of Case 1 using quadratic curves/surfaces.

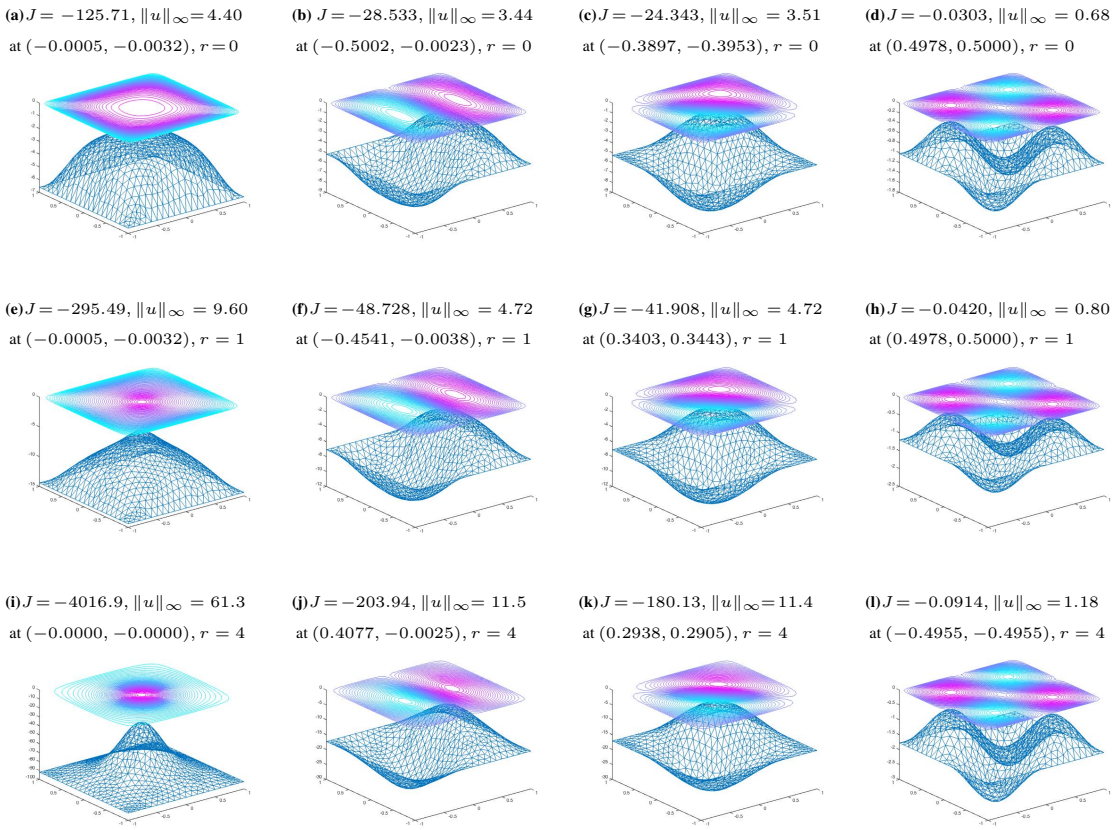

Figure 2.4: Saddles of (1.7) in W-type Case 1 presented in Table 2.4.

		LMM					Newton ($\|d\|$ <1e-6)		Refer
	r	$\|d\|$	ε	$\|J'(\cdot)\|_\infty$	J	N_{It}	$\|J'(\cdot)\|_\infty$	N_{It}	Fig. 2.5
A 0-saddle	0	7.9501e-5	8e-5	0.0042	-505.8232	91	4.5026e-5	5	(a)
1-saddle 1	0	3.9487e-4	4e-4	0.0176	-318.1268	73	4.2338e-5	6	(b)
1-saddle 2	0	0.0662	7e-2	0.9063	-230.4368	59	7.5605e-6	12	(c)
A 2-saddle	0	0.0225	3e-2	0.6271	-198.2357	67	9.2134e-6	10	(d)
A 0-saddle	1	2.4181e-4	3e-4	0.0114	-847.5466	75	2.7377e-5	6	(e)
1-saddle 1	1	7.3727e-4	8e-4	0.0379	-432.6320	65	3.3335e-5	7	(f)
1-saddle 2	1	0.0618	7e-2	0.8864	-329.5703	56	1.9102e-5	11	(g)
A 2-saddle	1	0.0384	4e-2	0.5264	-238.7583	58	5.3654e-6	10	(h)
A 0-saddle	4	0.0019	2e-3	0.0521	-6753.9	180	1.6776e-5	8	(i)
1-saddle 1	4	0.0579	6e-2	0.7365	-1219.4	63	1.1637e-5	11	(j)
1-saddle 2	4	0.0187	2e-2	0.2899	-1051.9	71	1.2514e-5	10	(k)
A 2-saddle	4	0.0763	8e-2	1.2755	-421.113	52	5.3671e-5	13	(l)

Table 2.5: Numerical data of Case 2 using quadratic curves/surfaces.

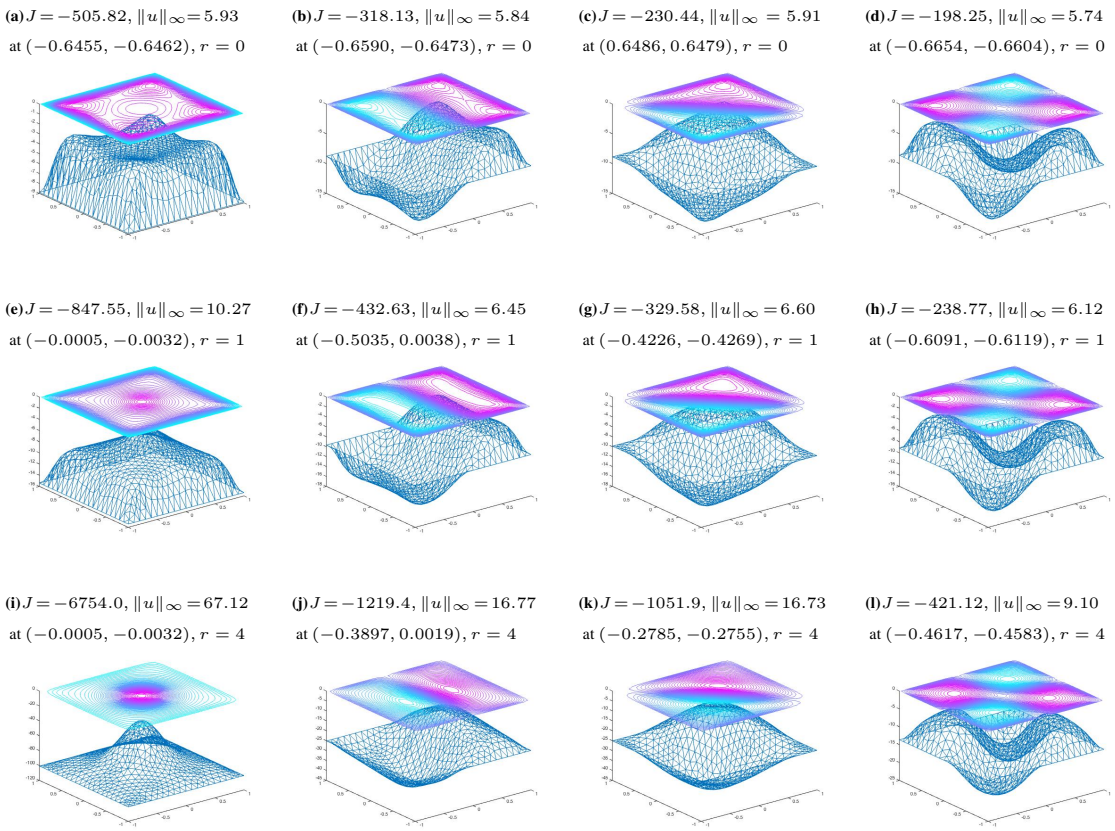

Figure 2.5: Saddles of (1.7) in W-type Case 2 presented in Table 2.5.

For the M-type problem. We set $\kappa = -1$ and $\lambda < \lambda_1$ in model problem (1.6), then it is obvious that $u_r = 0$ is the only local minimum and u_{p_t} can be easily selected as (1) a moving point along each direction with $J(u_{p_t}) < J(0) = 0$, or (2) a fixed point u_p with $J(u_p) < J(0) = 0$, or (3) mixing (1) and (2), i.e., in LMM, we fix u_{p_t} for several steps and then change it for the next several steps. For (1), the first few saddles can be found by using lines and planes, etc. as described in Section 2.5.1. While for (3), we present here numerical 1-saddles and 2-saddles found surprisingly by LMM using quadratic curves and surfaces as described in Section 2.5.2. First an initial guess $u_0 \in H_0^1(\Omega)$ can be easily selected by solving

$$-\Delta u_0(x) = c(x), \tag{2.29}$$

where $c(x) = -1, 0, 1$, respectively, are used to control the concavity of u_0 at x and consequently its peak(s) or symmetry. For example, in Case 3 and Case 4, we only need one peak location $(\tilde{x}_1, \tilde{x}_2)$ when searching for the 1-saddle. Thus we set $c(x_1, x_2) = -1$ if $|(x_1, x_2) - (\tilde{x}_1, \tilde{x}_2)| \leq r_{peak}$ and $c(x_1, x_2) = 0$ otherwise, where r_{peak} is used to control the shape of the peak. The peak looks flat when r_{peak} is large and sharp when r_{peak} is small. Then we set $u_p = t_0 u_0$ where $t_0 > 0$ is selected s.t. $J(u_p) < J(0) = 0$. The initial curve $P(0, s) = u_r + s u_p$ is actually a straight line and $P(0, s(0)) = s_0 u_p$ where $s_0 > 0$ can be easily computed by $\langle J'(s_0 u_p), u_p \rangle = 0$.

Once a 1-saddle u_s is found, to find a 2-saddle, we need a direction $u_0 \perp u_s$. This can be obtained by solving (2.29) and following a normalization. For Case 3 and Case 4 below, we should control the right-hand side $c(x)$ of (2.29) and generate the initial guess u_0 with two peak locations $(\tilde{x}_1, \tilde{x}_2)$ and $(\tilde{x'}_1\, \tilde{x'}_2)$. Thus we set $c(x_1, x_2) = -1$ if $|(x_1, x_2) - (\tilde{x}_1, \tilde{x}_2)| \leq r_{peak}$, $c(x_1, x_2) = 1$ if $|(x_1, x_2) - (\tilde{x'}_1\, \tilde{x'}_2)| \leq r_{peak}$ and $c(x_1, x_2) = 0$ otherwise.

Note that the term $|x|^r$ plays a significant role in the property of the solution and r is

usually called a bifurcation parameter. In detail, when r is not greater than certain value, the ground state solution is positive, symmetric and has one peak centered at the origin. Bifurcation occurs when r goes beyond certain value. Then the ground state solution bifurcates to multiple asymmetric positive solutions and the peak moves further away from the origin as r increases if λ is a constant. When λ is not a constant, such as $\lambda(x) = -e^{|x|^2}$ in Case 4, we can observe a combined effect of λ and r on the symmetry and shape of the solution. For the reason above, the peak location of the initial guess will be chosen depending on λ and r, e.g., when we find 1-saddles in the implementation, the single peak of the initial guess is placed further away from the origin as r increases. The detailed setting will be presented in Remark 2.6.3 when we do the implementation.

Case 3. In (1.6), we set $p = 3$, $\kappa = -1$, $\lambda = -1$, $r = 0, 1, 4$ respectively, and the domain $\Omega = (-1, 1)^2$. We could use lines and planes as in the original LMM [14]. Here we use the new LMM using quadratic curves and surfaces. A 1-saddle and two 2-saddles are found by LMM and shown in Table 2.6 and Figure 2.6.

Case 4. In (1.6), we set $p = 3$, $\kappa = -1$, $\lambda = -e^{|x|^2}$, $r = 0, 1, 4$ respectively, and the domain $\Omega = (-1, 1)^2$. A 1-saddle and two 2-saddles are found by LMM and shown in Table 2.7 and Figure 2.7.

Remark 2.6.3. To solve the problem, we firstly need an initial guess. Since the initial guess depends on the peak location(s) and r_{peak}, it is necessary to choose them appropriately in order to make the search faster and more accurately.

For finding 1-saddles in Case 3 and Case 4, when $r = 0$, there is no bifurcation, so we set $(\tilde{x}_1, \tilde{x}_2) = (0, 0)$. It is known that the bifurcation takes place when $r > 0.5$. The peak needs to be placed further away from the origin as r increases. Thus we set $(\tilde{x}_1, \tilde{x}_2) = (0.4, 0.4)$ for $r = 1$ and $(\tilde{x}_1, \tilde{x}_2) = (0.7, 0.7)$ for $r = 4$ respectively. Since 2-saddle 1 is expected to be odd symmetric to the line $y = -x$, we need one positive

peak and one negative peak. The initial guess should possess the same symmetry and the two peaks of it will be further away from the origin as r increases. For $r = 0$, we could set $(\tilde{x}_1, \tilde{x}_2) = (0.4, 0.4)$ and $(\tilde{x'}_1\, \tilde{x'}_2) = (-0.4, -0.4)$. If $r = 1$, we could set $(\tilde{x}_1, \tilde{x}_2) = (0.5, 0.5)$ and $(\tilde{x'}_1\, \tilde{x'}_2) = (-0.5, -0.5)$. When r increases to 4 we could move the centers of the two peaks to $(0.7, 0.7)$ and $(-0.7, -0.7)$ respectively. For the second 2-saddle, which is expected to be odd symmetric to the y-axis (it can also be odd symmetric to x-axis but the result would be equivalent due to symmetry of the space as we discussed), we need an initial guess with one positive peak and one negative peak which possesses the same symmetry. For $r = 0$, there is no bifurcation, we let the two peaks stay on the x-axis such that the initial guess is also even symmetric to the x-axis, so $(\tilde{x}_1, \tilde{x}_2) = (0.4, 0)$ and $(\tilde{x'}_1\, \tilde{x'}_2) = (-0.4, 0)$. For $r = 1$ or $r = 4$, the bifurcation occurs, so we move the peaks near the corner but still guarantee the initial guess possesses the odd symmetry about the y-axis. Thus we set $(\tilde{x}_1, \tilde{x}_2) = (0.5, 0.5)$ and $(\tilde{x'}_1\, \tilde{x'}_2) = (-0.5, 0.5)$ for $r = 1$, and $(\tilde{x}_1, \tilde{x}_2) = (0.7, 0.7)$ and $(\tilde{x'}_1\, \tilde{x'}_2) = (-0.7, 0.7)$ for $r = 4$.

In terms of r_{peak}, we expect the peaks of the solutions in Case 4 would be less flatter, so we set it to be 0.3 and 0.1 for Case 3 and Case 4 respectively.

		LMM					Newton ($\|d\|$ <1e-6)		Refer
	r	$\|d\|$	ε	$\|J'(\cdot)\|_\infty$	J	N_{It}	$\|J'(\cdot)\|_\infty$	N_{It}	Fig. 2.6
A 1-Saddle	0	9.7252e-6	1e-5	1.0660e-4	13.2090	93	3.5382e-9	1	(a)
2-Saddle 1	0	9.8132e-6	1e-5	2.0675e-4	56.1941	193	8.4482e-9	1	(b)
2-Saddle 2	0	0.0048	5e-3	0.0895	61.3218	89	9.1912e-8	2	(c)
A 1-Saddle	1	9.7564e-7	1e-6	3.3929e-5	36.0202	123		0	(d)
2-Saddle 1	1	9.7928e-6	1e-5	2.7780e-4	88.2231	137	1.5337e-9	1	(e)
2-Saddle 2	1	9.7972e-6	1e-5	2.9769e-4	97.8379	238	1.9698e-8	1	(f)
A 1-Saddle	4	5.7653e-6	6e-6	5.7845e-4	68.6985	103	1.9634e-9	1	(g)
2-Saddle 1	4	9.8790e-6	1e-5	7.1571e-4	139.9717	107	6.3743e-9	1	(h)
2-Saddle 2	4	1.9687e-5	2e-5	0.0011	142.8282	137	3.3462e-8	1	(i)

Table 2.6: Numerical data of Case 3 using quadratic curves/surfaces.

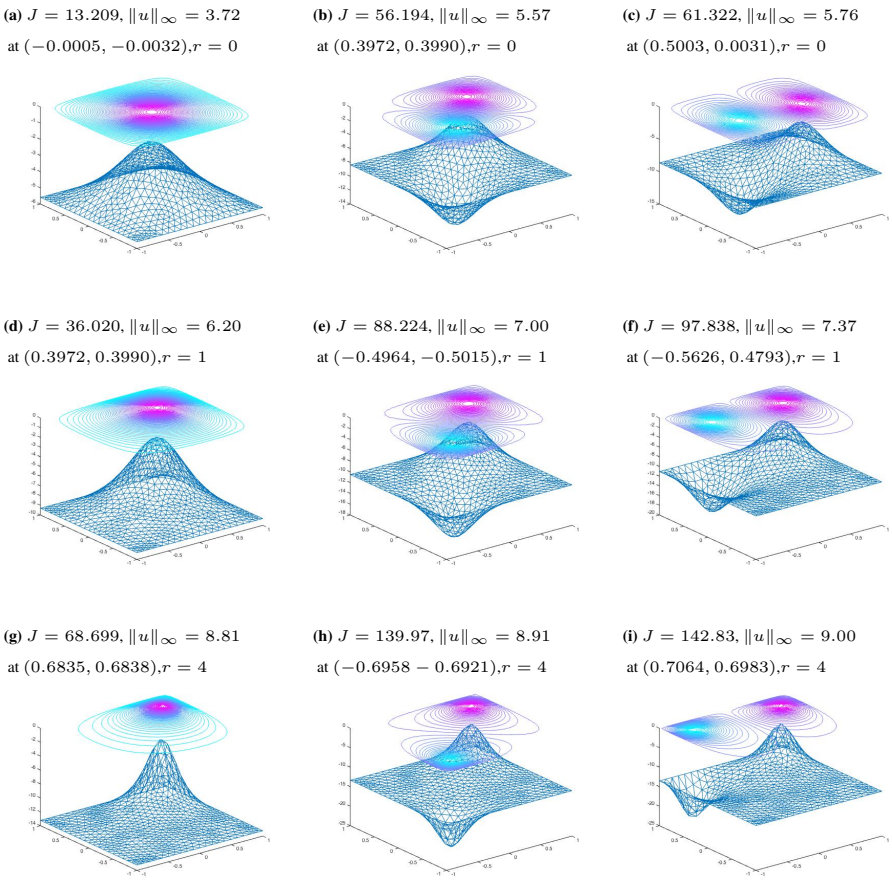

Figure 2.6: Saddles of (1.7) in M-type Case 3 presented in Table 2.6.

		LMM					Newton ($\|d\|$ <1e-6)		Refer
	r	$\|d\|$	ε	$\|J'(\cdot)\|_\infty$	J	N_{It}	$\|J'(\cdot)\|_\infty$	N_{It}	Fig. 2.7
A 1-Saddle	0	1.8566e-5	2e-5	2.1878e-4	14.1291	87	1.2554e-8	1	(a)
2-Saddle 1	0	9.6554e-6	1e-5	2.1932e-4	60.0645	286	4.8347e-6	1	(b)
2-Saddle 2	0	0.0021	3e-3	0.0363	64.6885	116	1.2222e-5	8	(c)
A 1-Saddle	1	1.9405e-5	2e-5	4.9654e-4	39.4887	149	1.2125e-8	1	(d)
2-Saddle 1	1	5.6344e-5	6e-5	8.7060e-4	96.0489	143	2.0887e-5	5	(e)
2-Saddle 2	1	4.9929e-5	5e-5	7.4802e-4	106.097	256	1.3427e-5	5	(f)
A 1-Saddle	4	9.3046e-6	1e-5	9.6464e-4	75.577	129	9.0770e-9	1	(g)
2-Saddle 1	4	9.6804e-5	1e-4	0.0096	153.4179	203	6.3072e-5	5	(h)
2-Saddle 2	4	4.7882e-5	5e-5	0.0033	156.0568	271	5.9592e-5	4	(i)

Table 2.7: Numerical data of Case 4 using quadratic curves/surfaces.

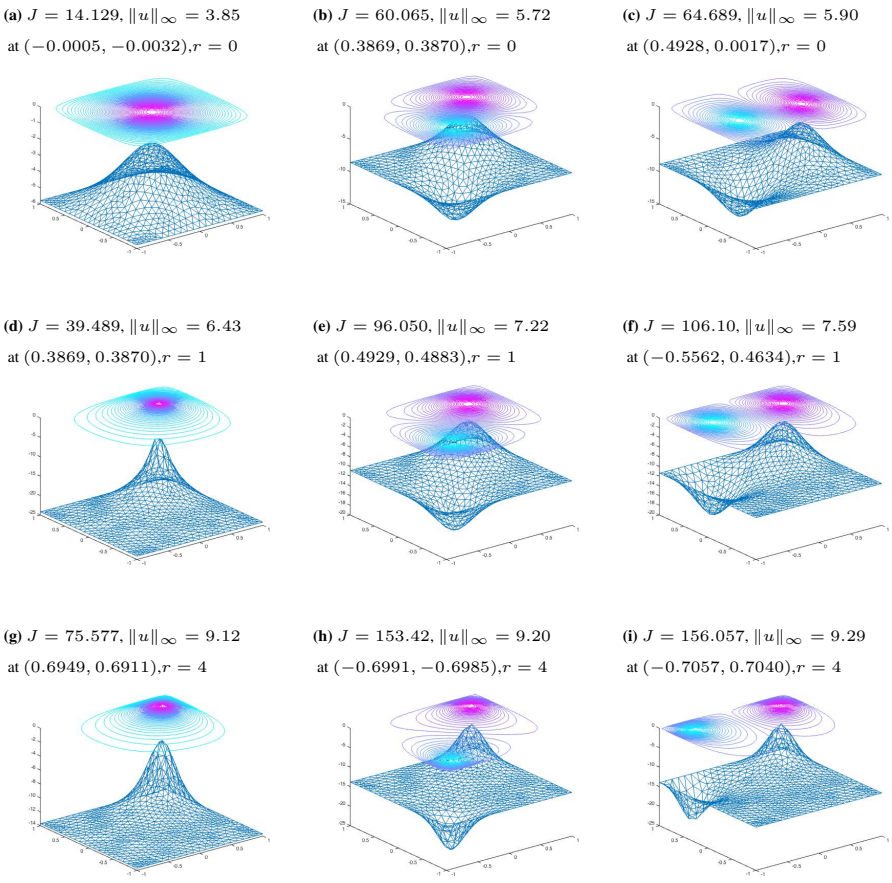

Figure 2.7: Saddles of (1.7) in M-type Case 4 presented in Table 2.7.

3. FINDING SADDLES WITH THE NEHARI MANIFOLD

3.1 Abstract Setting of the Nehari Manifold

Let us list some assumptions of λ in the main problem (1.3). For M-type problems, we assume $\lambda < \lambda_1$. Under this assumption, 0 is a local minimum and all the nontrivial saddles have MI ≥ 1. They are called definite problems in the literature. For W-type problems, we assume $\lambda_k < \lambda < \lambda_{k+1}$, where we usually let k be at least greater than 3 in our numerical examples since all the nontrivial saddles have MI $< k$ and such a k will enable us to test our algorithm for finding multiple solutions.

As we discussed in the last section, the geometric objects $P(t, s)$ are virtual and we do not have to know their expressions. This advantage gives us a great flexibility to choose preferred geometric objects for different purposes. To further explore such an advantage, let us observe the definitions of the quadratic curves (2.13)-(2.16) and quadratic surfaces (2.17)-(2.20) closely, we can see that those geometric objects are defined by the intersections of two types of geometric objects, where (2.13)/(2.17) defines a 2D-plane/3D-space passing through certain required points, while (2.14)/(2.18) can be viewed as certain constrained manifolds on which those points stay. Thus to find the point $P(t, s(t))$, it is not necessary to find an explicit expression (2.15)/(2.19), we can simply do 2D/3D-maximization on (2.13)/(2.17) subject to the constraint (2.14)/(2.18). It is quite natural to think about if a special type of geometric objects can be used to speed up algorithm convergence. Since all nonzero critical points are on the Nehari manifold $\mathcal{N}$, it actually puts no extra constraints to the problem, and we hope it helps us find the solutions faster. In addition, the PS condition stated in Definition 2.3.1 is guaranteed on the Nehari manifold, as we will discuss in Section 4. Thus we use $\mathcal{N}$ to replace (2.14)/(2.18) as an auxiliary constraint to define geometric objects whose explicit expressions are not available.

The definition of the Nehari manifold is motivated by the work of Zeev Nehari [29, 30]

$$\mathcal{N} = \{t_v v : t_v > 0, \|v\| = 1, \langle J'(t_v v), v\rangle = 0\}. \tag{3.1}$$

For the main problem (1.3),

$$\langle J'(t_v v), v\rangle = \int_\Omega \left[t_v |\nabla v(x)|^2 - t_v \lambda v^2(x) + \kappa f(x, t_v v) v(x)\right] dx, \tag{3.2}$$

and for the model problem (1.6),

$$\langle J'(t_v v), v\rangle = \int_\Omega \left[t_v |\nabla v(x)|^2 - t_v \lambda v^2(x) + \kappa |x|^r t_v^p |v(x)|^{p+1}\right] dx, \tag{3.3}$$

where t_v can actually be solved.

In the implementation, the Nehari manifold is defined in the following equivalent way:

$$\mathcal{N} = \{u \in H \backslash \{0\} \mid \langle J'(u), u\rangle = 0\}, \tag{3.4}$$

where by the Green's identity, we have

$$\begin{aligned}\langle J'(u), u\rangle &= \int_\Omega \left[|\nabla u(x)|^2 - \lambda u^2(x) + \kappa f(x, u) u(x)\right] dx \\ &= \int_\Omega \left[-u(x)\Delta u(x) - \lambda u^2(x) + \kappa f(x, u) u(x)\right] dx,\end{aligned} \tag{3.5}$$

and the expression in the last line above is used in our implementation. By doing so, we can avoid computing ∇u in the implementation.

For the model problem (1.6), we have

$$\langle J'(u), u\rangle = \int_\Omega \left[-u(x)\Delta u(x) - \lambda u^2(x) + \kappa |x|^r |u(x)|^{p+1}\right] dx. \tag{3.6}$$

Then in Step 3 of the algorithm, we let

$$P(t_k + t', s) = L(t_k, t', s) \cap \mathcal{N}, \tag{3.7}$$

where $L(t_k, t', s)$ is defined in (2.13)/(2.17) and can be easily expanded to form a (k+1)D-space, while $\mathcal{N}$ remains the same as in (3.4). A local maximum of J on $P = L \cap \mathcal{N}$ can be found by low-dimensional equality constrained optimization methods, such as the Matlab subroutine "fmincon" in L subject to $\mathcal{N}$. Other steps in the algorithm remain the same. Thus a k-saddle can be found by this method. We can also easily extend this method for finding saddles with higher MI since we do not need to acquire the complicated explicit expression of $P(t, s)$ and $\mathcal{N}$ does not change for computing different saddles.

3.2 Numerical Implementation and Examples

For the W-type problem. It is the same as in Section 2.6.2, except that we use the constraint $\mathcal{N}$ to replace the equation (2.14)/(2.18) in Step 3 of the algorithm, i.e., we let $u_{p_k,t'} = u_p = -u_r$ and

$$P(t_k + t', s) = L(t_k, t', s_1, s_2) \cap \mathcal{N}, \tag{3.8}$$

be the implicit expression of the curve where

$$L(t_k, t', s_1, s_2) = u_r + s_1(u_k(t') - u_r) + s_2(u_{p_k,t'} - u_r). \tag{3.9}$$

A local maximum of J on P is found by the Matlab subroutine "fmincon" through min $-J$ on L over $s = (s_1, s_2)$ subject to the constraint $\mathcal{N}$. After we find the two 1-saddles u_{s_1}

and u_{s_2}, we can pick either one of them, denoted by u_s, to compute a 2-saddle, i.e., we let

$$P(t_k + t', s) = L(t_k, t', s_1, s_2, s_3) \cap \mathcal{N}, \tag{3.10}$$

be the implicit expression of the surface where

$$L(t_k, t', s_1, s_2, s_3) = u_r + s_1(u_k(t') - u_r) + s_2(u_{pk,t'} - u_r) + s_3(u_s - u_r). \tag{3.11}$$

A local maximum of J on P can be found by the Matlab subroutine "fmincon" through min $-J$ on L over $s = (s_1, s_2, s_3)$ subject to the constraint $\mathcal{N}$. This method can be easily extended to find saddles with higher MI if exist. We re-do the Cases 1 and 2 in this way and document their numerical data in Tables 3.1 and 3.2 for computation speed comparison. Note that we do not list the figures of solutions again here since they can be found through the column "Refer" in Tables 3.1 and 3.2.

	r	$\|d\|$	ϵ	$\|J'(\cdot)\|_\infty$	J	N_{It}	Refer
A Local Min	0	8.3234e-05	1e-4	1.5439e-03	-125.7122	13	Fig. 2.4(a)
1-saddle 1	0	0.0009	1e-3	0.0063	-28.5326	14	Fig. 2.4(b)
1-saddle 2	0	0.0019	2e-3	0.0162	-24.3429	14	Fig. 2.4(c)
2-saddle	0	8.0899e-05	1e-4	0.0011	-0.0303	6	Fig. 2.4(d)
A Local Min	1	3.8283e-04	4e-4	2.7002e-02	-295.4945	10	Fig. 2.4(e)
1-saddle 1	1	4.8885e-04	5e-4	3.7831e-03	-48.7282	12	Fig. 2.4(f)
1-saddle 2	1	3.1071e-04	4e-4	2.8164e-03	-41.9083	19	Fig. 2.4(g)
2-saddle	1	2.2167e-04	3e-4	2.0852e-03	-0.0420	9	Fig. 2.4(h)
A Local Min	4	7.2575e-04	1e-3	1.6138e-02	-4016.9000	19	Fig. 2.4(i)
1-saddle 1	4	6.0710e-04	8e-4	1.2526e-02	-203.9375	32	Fig. 2.4(j)
1-saddle 2	4	6.1039e-04	7e-4	1.1783e-02	-180.1284	35	Fig. 2.4(k)
2-saddle	4	3.6015e-04	5e-4	2.8650e-03	-0.0914	12	Fig. 2.4(l)

Table 3.1: Numerical data of Case 1 using geometric objects on $\mathcal{N}$.

	r	$\|d\|$	ϵ	$\|J'(\cdot)\|_\infty$	J	N_{It}	Refer
A Local Min	0	0.0004	1e-3	0.0147	-505.8239	18	Fig. 2.5(a)
1-saddle 1	0	1.9806e-4	2e-4	0.0107	-318.1348	34	Fig. 2.5(b)
1-saddle 2	0	0.0031	5e-3	0.0647	-230.4429	41	Fig. 2.5(c)
2-saddle	0	0.0175	2e-2	0.2287	-198.2465	32	Fig. 2.5(d)
A Local Min	1	1.8581e-04	2e-4	1.0533e-02	-847.5476	25	Fig. 2.5(e)
1-saddle 1	1	4.4257e-04	5e-4	1.8674e-02	-432.6319	53	Fig. 2.5(f)
1-saddle 2	1	0.0083	1e-2	0.1218	-329.5795	44	Fig. 2.5(g)
2-saddle	1	0.0303	0.05	0.3451	-238.7703	32	Fig. 2.5(h)
A Local Min	4	0.0008	1e-3	0.0315	-6753.9851	26	Fig. 2.5(i)
1-saddle 1	4	0.0097	0.01	0.1252	-1219.4057	40	Fig. 2.5(j)
1-saddle 2	4	0.0536	0.06	1.4855	-1051.9000	56	Fig. 2.5(k)
2-saddle	4	0.0197	0.06	0.8036	-421.1175	20	Fig. 2.5(l)

Table 3.2: Numerical data of Case 2 using geometric objects on $\mathcal{N}$.

For the M-type problem. Since 0 is the only local minimum of J but not on the Nehari manifold $\mathcal{N}$, it cannot be used. Thus this part is different from the corresponding part in Section 2.6.2. A preprocessing is required to use the Nehari manifold $\mathcal{N}$. We first use the Matlab subroutine "fmincon" to minimize J subject to the constraint $\mathcal{N}$ to find a solution u_r which is actually a 1-saddle of J. By the symmetry of the problem, $u_{p_k,t'} = u_p = -u_r$ is another 1-saddle of J or another local minimum of J on $\mathcal{N}$.

To find a 2-saddle, an initial direction u_0 is constructed as the same as in Section 2.6.2, by solving (2.29). We use three point u_r, u_p and u_0 to construct an initial space

$$L(0, 0, s_1, s_2) = u_r + s_1(u_0 - u_r) + s_2(u_p - u_r),$$

which is obviously a 2D-space. Taking an intersection of this space and the Nehari manifold will define the initial implicit curve, i.e., $P(0, s) = L(0, 0, s_1, s_2) \cap \mathcal{N}$. The Matlab subroutine "fmincon" can be used to minimize $-J$ on L over $s = (s_1, s_2)$ subject to the constraint defined in $\mathcal{N}$ so that the initial local maximum point $P(0, s(0))$ can be

found. Then the LMM starts to run. The curve in Step 3 of our algorithm is defined by $P(t_k + t', s) = L(t_k, t', s_1, s_2) \cap \mathcal{N}$, where the space

$$L(t_k, t', s_1, s_2) = u_r + s_1(u_k(t') - u_r) + s_2(u_p - u_r).$$

Note that we have already preprocessed $u_k(t')$ by multiplying it with a scalar such that it is on $\mathcal{N}$. Then the local maximum point $u_{k+1} = P(t_{k+1}, s_{k+1})$ can be computed by the Matlab subroutine "fmincon" to minimize $-J$ on L over $s = (s_1, s_2)$ subject to the constraint $\mathcal{N}$. The rest parts of the algorithm are the same. Finally LMM can find two 2-saddles $u^2_{s_1}$ and $u^2_{s_2}$, where the superscripts indicate the MI, with two different initial guesses u_0.

After we find two 2-saddles $u^2_{s_1}$ and $u^2_{s_2}$, we can use one of them, denoted by u^2_s, to find a 3-saddle. The initial guess u_0 is obtained in the same way as we did for finding 2-saddles, by solving (2.29). Then the four points u_r, u_p, u^2_s and u_0 are used to construct an initial 3D-space

$$L(0, 0, s_1, s_2, s_3) = u_r + s_1(u_0 - u_r) + s_2(u_p - u_r) + s_3(u^2_s - u_r),$$

and an initial curve $P(0, s) = L(0, 0, s_1, s_2, s_3) \cap \mathcal{N}$. Then the initial maximum point $P(0, s(0))$ can be found by the Matlab subroutine "fmincon" to minimize $-J$ on the space L over $s = (s_1, s_2, s_3)$ subject to the constraint $\mathcal{N}$. Then LMM starts to run. In Step 3, through the four points u_r, u_p, u_s and $u_k(t')$, we construct a 3D-space

$$L(t_k, t', s_1, s_2, s_3) = u_r + s_1(u_k(t') - u_r) + s_2(u_p - u_r) + s_3(u^2_s - u_r)$$

where the point $u_k(t')$ has been multiplied by a scalar so that it is on $\mathcal{N}$ and the surface is implicitly defined by $P(t_k + t', s) = L(t_k, t', s_1, s_2, s_3) \cap \mathcal{N}$. The point $u_{k+1} =$

$P(t_{k+1}, s(t_{k+1}))$ can be computed by the Matlab subroutine "fmincon" to minimize $-J$ on L over $s = (s_1, s_2, s_3)$ subject to the constraint $\mathcal{N}$. Other steps are the same. The method can be easily extended to find more saddles. It is significant to note that finding saddles with high MI might be complicated. Some problems do not have 3-saddles or too difficult to compute numerically, e.g. the 3-saddle with $r = 1$ in Case 3 and Case 4 below. For finding a 4-saddle, we need 2 previous solutions chosen from 2-saddles and 3-saddles to construct the space in our implementation. We do not have a general pattern of choosing the previous solutions, so we can only use our experience and even do the numerical experiment in a way of trial and error.

Note that u_0 and $u_k(t')$ are preprocessed in each iteration by multiplying it with a scalar because the geometric object is required to be on $\mathcal{N}$ so all the points connecting this geometric object should also be on $\mathcal{N}$, including u_0 and $u_k(t')$.

We re-do Cases 3 and 4, and document their numerical data in Tables 3.3 and 3.4 for convergence speed comparison. It is obvious that the Nehari manifold is advantageous in computation speed. Note that we only list figures of 3-saddles and 4-saddles in Figure 3.1 and 3.2 to show the method's capability of computing saddles with higher MI, while the figures of 1-saddles and 2-saddles can be found through the column "Refer" in Tables 3.3 and 3.4.

	r	$\|d\|$	ε	$\|J'(\cdot)\|_\infty$	J	N_{It}	Refer
A 1-saddle	0	4.1321e-06	1e-5	1.4708e-04	13.2091	16	Fig. 2.6(a)
2-saddle 1	0	9.8800e-06	1e-5	2.0394e-04	56.1944	92	Fig. 2.6(b)
2-saddle 2	0	1.6885e-03	2e-3	5.4989e-02	61.3222	45	Fig. 2.6(c)
A 3-saddle	0	2.5059e-03	3e-3	1.4332e-01	189.3313	60	Fig. 3.1(j)
A 4-saddle	0	9.5865e-05	1e-4	2.2767e-03	165.5144	61	Fig. 3.1(l)
A 1-saddle	1	6.1166e-07	1e-6	4.9142e-04	36.0204	31	Fig. 2.6(d)
2-saddle 1	1	9.6298e-06	1e-5	2.9491e-04	88.2238	114	Fig. 2.6(e)
2-saddle 2	1	9.6702e-06	1e-5	2.6417e-04	97.8384	183	Fig. 2.6(f)
4-saddle	1	9.7850e-05	1e-4	2.8846e-03	218.6623	165	Fig. 3.1(m)
A 1-saddle	4	4.5127e-06	5e-6	4.5167e-04	68.6989	20	Fig. 2.6(g)
2-saddle 1	4	9.7707e-06	1e-5	6.3297e-04	139.9730	108	Fig. 2.6(h)
2-saddle 2	4	9.4499e-06	1e-5	7.9035e-04	142.8290	106	Fig. 2.6(i)
A 3-saddle	4	9.4652e-04	1e-3	5.0519e-02	207.8980	133	Fig. 3.1(k)
A 4-saddle	4	9.7361e-05	1e-4	5.1396e-03	291.0134	133	Fig. 3.1(n)

Table 3.3: Numerical data of Case 3 using geometric objects on $\mathcal{N}$.

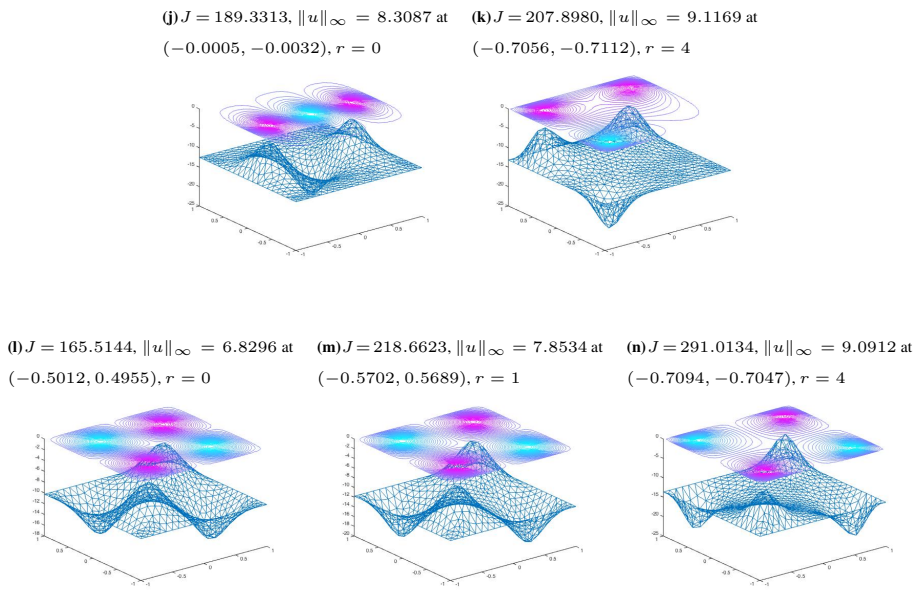

Figure 3.1: Saddles (j)-(n) in Case 3 presented in Table 3.3.

	r	$\|d\|$	ε	$\|J'(\cdot)\|_\infty$	J	N_{It}	Refer
A 1-saddle	0	9.5946e-06	1e-5	3.5777e-04	14.1293	14	Fig. 2.7(a)
2-saddle 1	0	9.5560e-06	1e-5	1.8326e-04	60.0649	77	Fig. 2.7(b)
2-saddle 2	0	8.6285e-04	1e-3	3.2653e-02	64.6892	38	Fig. 2.7(c)
A 3-saddle	0	1.6977e-03	2e-3	1.1597e-01	194.6572	62	Fig. 3.2(j)
A 4-saddle	0	9.9318e-05	1e-4	2.4290e-03	176.8576	103	Fig. 3.2(l)
A 1-saddle	1	8.6822e-06	1e-5	1.2469e-03	39.4887	26	Fig. 2.7(d)
2-saddle 1	1	4.9282e-05	5e-5	1.5380e-03	96.0497	124	Fig. 2.7(e)
2-saddle 2	1	4.8666e-05	5e-5	1.6039e-03	106.0977	213	Fig. 2.7(f)
A 4-saddle	1	9.8955e-05	1e-4	3.1237e-03	236.6930	178	Fig. 3.2(m)
A 1-saddle	4	2.5312e-06	5e-6	4.0241e-04	75.5768	21	Fig. 2.7(g)
2-saddle 1	4	4.9550e-05	5e-5	3.8147e-03	153.4184	84	Fig. 2.7(h)
2-saddle 2	4	4.7336e-05	5e-5	3.4085e-03	156.0572	102	Fig. 2.7(i)
A 3-saddle	4	9.5584e-04	1e-3	5.3110e-02	228.3316	101	Fig. 3.2(k)
A 4-saddle	4	9.4778e-05	1e-4	5.7656e-03	317.0536	107	Fig. 3.2(n)

Table 3.4: Numerical data of Case 4 using geometric objects on $\mathcal{N}$.

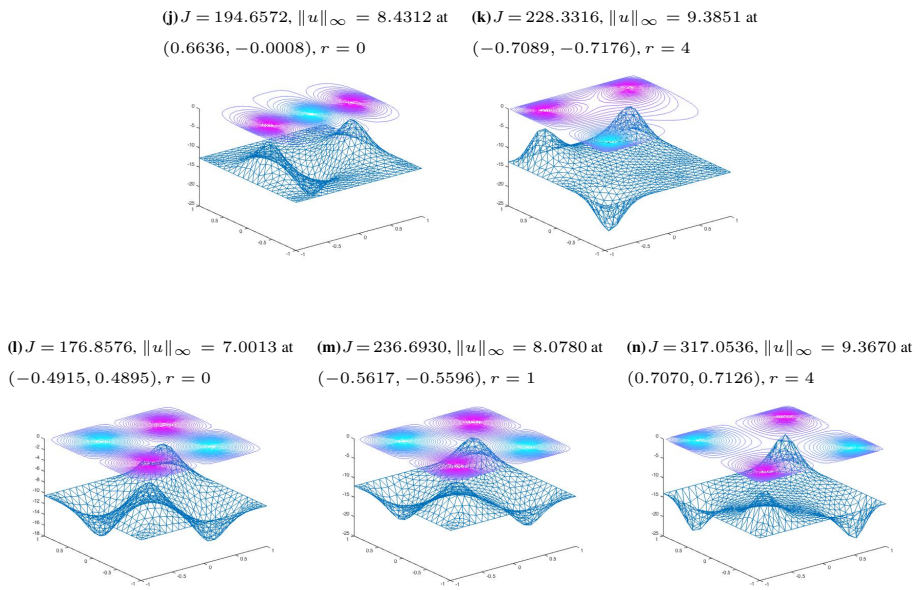

Figure 3.2: Saddles (j)-(n) in Case 4 presented in Table 3.4.

3.3 Extension for the Mixed M and W Type Problems

We are concerned with the following concave-convex elliptic problem

$$-\Delta u - \lambda(x)u - a(x)\left|u(x)\right|^{q-1}u(x) - b(x)\left|u(x)\right|^{p-1}u(x) = 0, \tag{3.12}$$

where $u \in H = H_0^1(\Omega)$, $0 < q < 1 < p < 2^*$, λ, a, and b are non-negative functions in Ω. Its energy functional is

$$J(u) = \int_\Omega \left[\frac{1}{2}\left|\nabla u(x)\right|^2 - \frac{1}{2}\lambda(x)u^2(x) - \frac{a(x)}{q+1}\left|u(x)\right|^{q+1} - \frac{b(x)}{p+1}\left|u(x)\right|^{p+1}\right] dx. \tag{3.13}$$

This problem has a combined effect of concave and convex nonlinearities [31], and it has various applications in mathematical physics and population dynamics [32]. The sublinear and superlinear terms together make problem (3.12) be a combination of the focusing and defocusing problems. The function profile is given in Figure 3.3, and it is clear that both the locally W-type and M-type profiles can be found in it. The previous methods, including the local minimax method [14] and the local min-max-min method [33] could not handle this case.

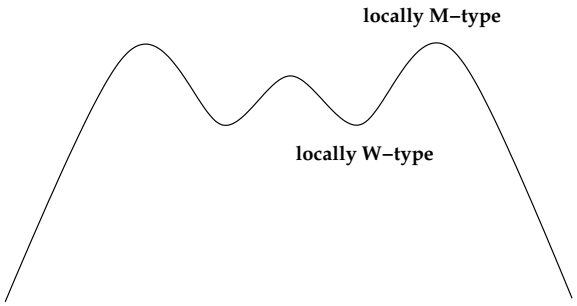

Figure 3.3: Function profile of the mixed M and W type problem.

3.3.1 Numerical implementation and example

For the mixed M and W type problem (3.12), it is difficult to implement LMM in the same way as we find saddles for the typical M or W problem by the Nehari manifold since the Nehari manifold for this problem consists of two layers and the saddle point may jump between these two layers. Thus we need a small modification of our original method based on the Nehari manifold. From the function profile, we know $J < 0$ on the inner Nehari manifold and $J > 0$ on the outer Nehari manifold, so these two constraints can be added to the local maximum search respectively when we solve the locally W-type and locally M-type problems. This is feasible in programming as the Matlab subroutine "fmincon" gives us a great flexibility to manipulate such constraints.

As a numerical example, we set $\lambda(x) = 0$, $a(x) = 1.4$, $b(x) = 1$, $p = 4$, $q = 0.05$, and the domain $\Omega = (-1, 1)^2$ in (3.12).

Saddles on the inner Nehari manifold ($J < 0$)

We run the code then generate Table 3.5 and Figure 3.4.

	$\|d\|$	ϵ	$\|J'(\cdot)\|_\infty$	J	$\mathrm{N_{It}}$
A Local Min	6.7713e-05	1e-4	1.8550e-03	-0.4314	2
1-saddle 1	6.0396e-05	1e-4	4.5517e-03	-0.1589	12
1-saddle 2	1.4349e-03	2e-3	1.7296	-0.1445	10
2-saddle 1	6.4994e-04	1e-3	1.8041	-0.0930	2
2-saddle 2	3.8810e-04	1e-3	1.6591	-0.0671	2
3-saddle 1	3.1093e-04	1e-3	1.7061	-0.0756	3
3-saddle 2	9.7327e-04	1e-3	1.8123	-0.0732	5

Table 3.5: Numerical data for the locally W-type saddles using the Nehari manifold.

$J = -0.4314$, $\|u\|_\infty = 0.3896$ at $(-0.0005, -0.0032)$

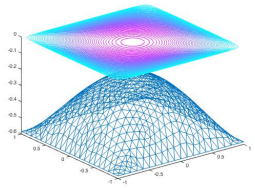

(a) A local min

$J = -0.1589$, $\|u\|_\infty = 0.1425$ at $(0.5002, -0.0001)$

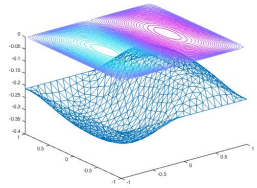

(b) 1-saddle 1

$J = -0.1445$, $\|u\|_\infty = 0.1478$ at $(0.3944, 0.3906)$

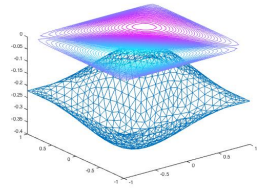

(c) 1-saddle 2

$J = -0.0930$, $\|u\|_\infty = 0.0900$ at $(0.5000, -0.5015)$

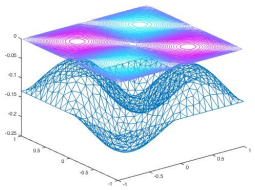

(d) 2-saddle 1

$J = -0.0671$, $\|u\|_\infty = 0.0713$ at $(0.0018, -0.6103)$

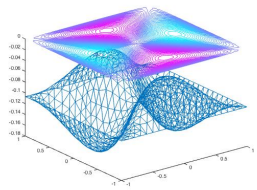

(e) 2-saddle 2

$J = -0.0756$, $\|u\|_\infty = 0.0659$ at $(-0.6659, -0.0042)$

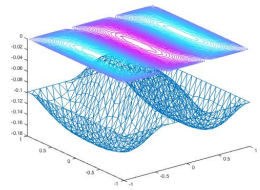

(f) 3-saddle 1

$J = -0.0732$, $\|u\|_\infty = 0.1026$ at $(-0.0001, -0.0005)$

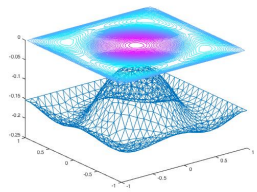

(g) 3-saddle 2

Figure 3.4: Saddles on the inner Nehari manifold with $J < 0$.

Saddles on the outer Nehari manifold ($J > 0$)

We run the code then generate Table 3.6 and Figure 3.5.

	$\|d\|$	ϵ	$\|J'(\cdot)\|_\infty$	J	$\mathrm{N_{It}}$
1-saddle	7.1195e-05	1e-4	2.5866e-03	2.1680	8
2-saddle 1	1.9724e-03	2e-3	1.7803	18.0417	33
2-saddle 2	8.0313e-04	1e-3	4.9448e-02	19.5636	31
3-saddle	2.9454e-03	3e-3	1.7360	56.6545	44
4-saddle 1	9.7078e-04	1e-3	1.4056	53.2726	39
4-saddle 2	2.8994e-03	3e-3	1.6513	65.1720	45
5-saddle	0.0045	5e-3	0.9794	76.8336	204

Table 3.6: Numerical data for the locally M-type saddles using the Nehari manifold.

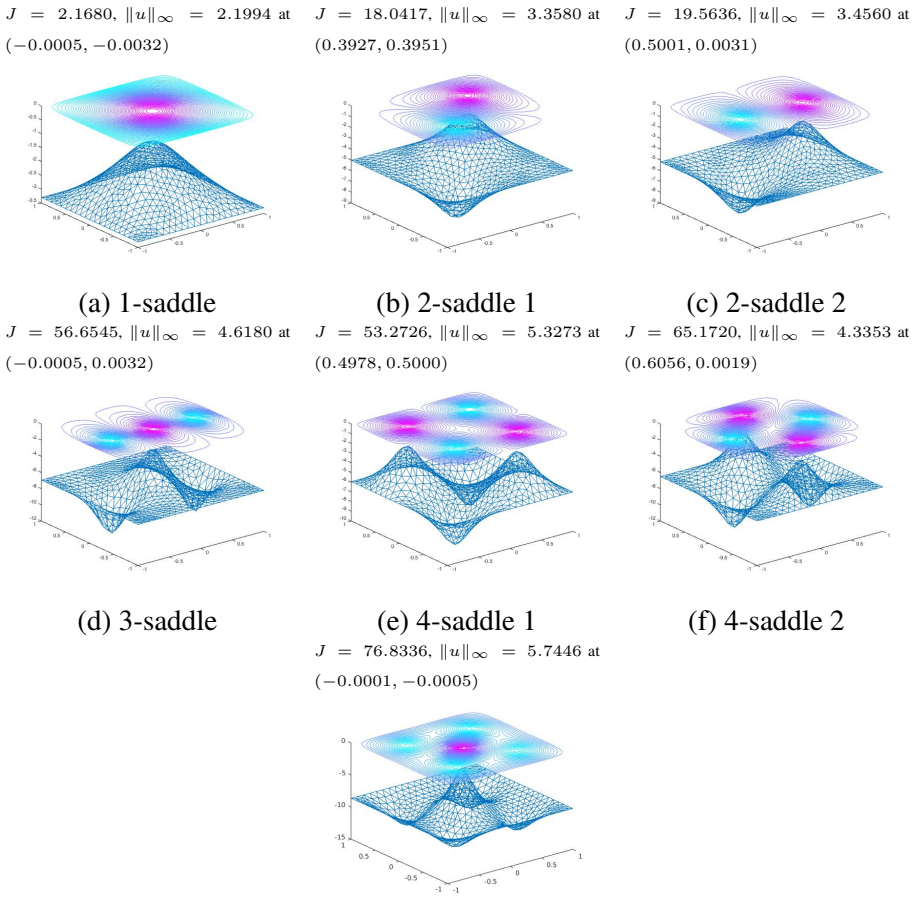

(a) 1-saddle (b) 2-saddle 1 (c) 2-saddle 2

(d) 3-saddle (e) 4-saddle 1 (f) 4-saddle 2

(g) 5-saddle

Figure 3.5: Saddles on the outer Nehari manifold with $J > 0$.

4. THE METHOD OF THE GENERALIZED NEHARI MANIFOLD

4.1 Introduction of the Generalized Nehari Manifold

Let us return to the main problem which is a non-autonomous nonlinear elliptic PDE:

$$-\Delta u - \lambda u + \kappa f(x, u(x)) = 0, \tag{4.1}$$

where f satisfies the assumptions **AS** defined in Section 1 and $\kappa < 0$ such that it is an M-type problem. We also assume that λ is greater than λ_1. Under this assumption, 0 is a saddle instead of a local minimum. The problem is called indefinite in the literature.

The Palais-Smale (PS) condition defined in Definition 2.3.1 is a crucial condition in the literature to prove the existence of solutions to nonlinear elliptic PDEs and also a basic assumption to establish the convergence results for the previously developed LMM type algorithms. However, it is also known that many nonlinear elliptic PDEs do not satisfy the PS condition and others satisfy the condition only on certain manifold rather than in the whole space. Thus for the success of numerical computation of the multiple solutions, an algorithm must be carried out on that manifold. So far the literature does not provide any such numerical algorithms. However, LMM with virtual geometric objects developed in Section 2 provides us with such possibilities. In this section we will further explore such techniques.

In the following certain manifold will be introduced that all the non-trivial solutions of the indefinite problem (4.1) are on it and the PS condition can be verified only on it [20, 34], called the generalized Nehari manifold defined in (4.7). Our purpose is to apply the LMM with virtual geometric objects where those objects will be defined only on the generalized Nehari manifold. However, a correction technique must be carried out in order

to keep all the numerical computations on the generalized Nehari manifold. It changes the convergence behavior of the original method. Thus the correction must be well-understood and a proper modification has to be developed. After our analysis on the correction, see Lemma 4.2.3, the original algorithm is generalized accordingly so that its convergence will be guaranteed with such a type of corrections.

Let $E = H_0^1(\Omega)$ and $E = E^+ \oplus E^0 \oplus E^-$ be the orthogonal spectral decomposition of $-\Delta - \lambda$ with respect to the positive, zero, and negative part of the spectrum. We may assume $\lambda_k < \lambda = \lambda_{k+1} = \cdots = \lambda_m < \lambda_{m+1}$, where $1 \leq k < m$, then the spectral decomposition provides us

$$E^- = \text{span}\{e_1, \ldots, e_k\} \text{ and } E^0 = \text{span}\{e_{k+1}, \ldots, e_m\}. \tag{4.2}$$

It is easy to see that the definite M-type problems we have solved are special cases in which $E^- = \{0\}$ and $E^0 = \{0\}$. For any $u \in E$, we can decompose it as $u = u^+ + u^0 + u^- \in E^+ \oplus E^0 \oplus E^- = E$, so it is natural to introduce an equivalent norm $\|\cdot\|_E$:

$$\begin{aligned}
\|u\|_E^2 &= -\int_\Omega (|\nabla u(x)|^2 - \lambda u^2(x))dx \quad \text{for } u \in E^-, \\
\|u\|_E^2 &= \int_\Omega (|\nabla u(x)|^2 - \lambda u^2(x))dx \quad \text{for } u \in E^+, \\
\|u\|_E^2 &= 0 \quad \text{for } u \in E^0.
\end{aligned}$$

Thus for $u \in E$, we have

$$\int_\Omega (|\nabla u(x)|^2 - \lambda u^2(x))dx = \|u^+\|_E^2 - \|u^-\|_E^2. \tag{4.3}$$

In this way, the energy functional $J(u)$ can be expressed by

$$J(u) = \frac{1}{2}\|u^+\|_E^2 - \frac{1}{2}\|u^-\|_E^2 + \kappa I(u), \tag{4.4}$$

where

$$I(u) = \int_\Omega F(x,u)dx. \tag{4.5}$$

For model problem (1.6), we have

$$I(u) = \int_\Omega \frac{1}{p+1}\,|x|^r\,|u(x)|^{p+1}\,dx. \tag{4.6}$$

Let $V = E^0 \oplus E^-$, the following generalized Nehari manifold was proposed by Pankov [18]:

$$\mathcal{M} = \{u \in E\backslash V : \langle J'(u), u\rangle = 0 \text{ and } \langle J'(u), v\rangle = 0 \text{ for all } v \in V\}, \tag{4.7}$$

which contains all the non-trivial critical points of functional J. Zhou [35] gave a very general definition of the solution manifold in the perspective of orthogonal mapping and the support set formed by previously found critical points which is a general closed subspace. Inspired by his definition, the solution manifold is constructed by using the spectral decomposition above in our research. Let

$$c := \inf_{u\in\mathcal{M}} J(u). \tag{4.8}$$

Szulkin and Weth [17] showed that $c > 0$ is attained and if $u_0 \in \mathcal{M}$ such that $J(u_0) = c$, then u_0 is a critical point and hence it must be a ground state solution for $J'(u) = 0$, i.e. c is the lowest level for J where there are nontrivial solutions of the main problem (4.1).

Let us introduce the minimax characterization of the least energy value c in the perspective of the generalized Nehari manifold before applying it to our algorithm based on

virtual curves and surfaces. For $u \in E\backslash V$, the following two subspaces are defined:

$$E(u) := V \oplus \mathbb{R}u = V \oplus \mathbb{R}u^+ \text{ and } \hat{E}(u) := V \oplus \mathbb{R}^+u = V \oplus \mathbb{R}^+u^+, \tag{4.9}$$

where $\mathbb{R}^+$ is the nonnegative real number set and $u^+ \in E^+$. The unit sphere set on E^+ is also defined:

$$S^+ := S \cap E^+ = \{u \in E^+ : \|u\|_E = 1\}, \tag{4.10}$$

where S is the unit sphere in E.

The following theorem was proven in [17] and shows that the intersection of $\hat{E}(u)$ and $\mathcal{M}$ actually is a point which is the unique global maximum point of J on $\hat{E}(u)$. A minimax characterization could be deduced from this theorem. Besides, our correction technique which keeps all the numerical computations on $\mathcal{M}$ is based on it. The correction technique will be discussed in detail when we introduce the algorithm.

Theorem 4.1.1. *(Szulkin and Weth) For any $u \in E\backslash V$, $\hat{E}(u) \cap \mathcal{M}$ consists of precisely one point which is the unique global maximum of J on $\hat{E}(u)$.*

As a consequence of Theorem 4.1.1, the minimax characterization of the ground state solution was proposed in [17]:

$$c = \inf_{v \in E^+\backslash\{0\}} \max_{u \in \hat{E}(v)} J(u). \tag{4.11}$$

Moreover, if $f(x, u)$ is odd with respect to u, for an instance, the model problem (1.6) with odd p, then the minimax characterization reduces to the following:

$$c = \inf_{v \in E^+\backslash\{0\}} \max_{u \in E(v)} J(u). \tag{4.12}$$

Note that the infima and the maxima are taken in a global sense in (4.11) and (4.12), and

they are only for existence issue in mathematical analysis. Thus it is impossible to implement them numerically. In [14], Li and Zhou developed a new minimax method. In their algorithm, peak selection was used to take the local maximum and the local minimizer was approximated by a gradient descent search. Their new local minimax method is able to find not only the ground state solution but also saddle points with higher MI, which was very challenging at that time. Besides, they provided a solid convergence analysis in a subsequent paper [15].

The following lemma proven by Szulkin and Weth in [17] shows that $\mathcal{M}$ is bounded away from zero and V.

Lemma 4.1.2. *(Szulkin and Weth)*

- *Define* $S_R := \{u \in E^+ : \|u\|_E = R\}$*, there exists* $\alpha > 0$ *such that* $c = \inf_{\mathcal{M}} J \geq \inf_{S_\alpha} J > 0$.
- *For any* $u \in \mathcal{M}$*, there exists a constant* $\delta > 0$ *such that* $\|u^+\|_E \geq \delta$.

Theorem 4.1.1 actually defines a map $\hat{m} : E\backslash V \mapsto \mathcal{M}$, $\hat{m}(u) = \hat{E}(u) \cap \mathcal{M}$. This map will be used to carry out the correction in our algorithm. In the next lemma, it was shown by Szulkin and Weth [17] that $\hat{m}$ is continuous if it is restricted on $E^+\backslash\{0\}$.

Lemma 4.1.3. *(Szulkin and Weth)* $\hat{m}$ *is continuous on* $E^+\backslash\{0\}$.

Next the inverse map $\check{m}$ of $\hat{m}$ on S^+ is considered in [17]:

$$\check{m} : \mathcal{M} \mapsto S^+, \quad \check{m}(u) = \frac{u^+}{\|u^+\|_E}. \tag{4.13}$$

Lemma 4.1.4. *(Szulkin and Weth) The map* $\check{m}$ *defined in (4.13) is Lipschitz continuous.*

Consider the map $\hat{m}$ restricted on S^+. For any $u \in \mathcal{M}$, we can always find a point $\check{m}(u) \in S^+$ since $u^+ \neq 0$ by Lemma 4.1.2. Thus the map $\hat{m}$ restricted on $E^+\backslash\{0\}$ is

onto. It can also be easily shown that the map is one-to-one, so it is a bijection. Thus it is a homeomorphism from S^+ to $\mathcal{M}$ by Lemma 4.1.3 and Lemma 4.1.4, then $\mathcal{M}$ is path connected since S^+ has this property. Furthermore, Pankov[36] proved that $\mathcal{M}$ is a $\mathcal{C}^1$ manifold, then any two distinct points on $\mathcal{M}$ can be connected by a smooth path.

4.2 A Local Minimax Characterization of 1-saddles Based on Curves on $\mathcal{M}$

For simplicity, in our local minimax characterization, we assume $k = 1$ and $m = k$, i.e., $\lambda_1 < \lambda < \lambda_2$, then $V = E^- = \{e_1\}$ and 0 is the only 1-saddle in E, so all the non-trivial saddles have MI > 1, i.e., we only have 2-saddles and saddles with higher MI in E. Since we are seeking critical points on $\mathcal{M}$, it is convenient and reasonable that we call the local minimum on $\mathcal{M}$ be a 0-saddle on $\mathcal{M}$, which is actually a 2-saddle in E. In this way, the index of a saddle on $\mathcal{M}$ is the dimension of the subspace contained on $\mathcal{M}$ where J attains its local maximum at this point, so the 3-saddle in E is a 1-saddle on $\mathcal{M}$ and the 4-saddle in E is a 2-saddle on $\mathcal{M}$. Same to the previous notations, let u_r be a local minimum of J on $\mathcal{M}$ and $u_{p_t} \in \mathcal{M}$ be another local minimum or a fixed or a moving point such that $J(u_{p_t}) \leq J(u_r)$ and $\|u_r - u_{p_t}\| > \delta > 0$. Since $\mathcal{M}$ is a connected $\mathcal{C}^1$ manifold, for each $t \geq 0$, there exists a smooth curve $P(t, s)$ connecting u_r and u_{p_t} in the variable s on $\mathcal{M}$. We may assume $0 \leq s \leq 1$ with $P(t, 0) = u_r$ and $P(t, 1) = u_{p_t}$. For each $t \geq 0$, let $s(t) \in (0, 1)$ be the first local maximum of $J(P(t, s))$ in s. Such an $s(t)$ always exists with $0 < \delta < s(t) < 1$ for some $\delta > 0$ and nondegenerate u_r since u_r is a local minimum of $J(P(t, s))$ in s and $J(u_{p_t}) \leq J(u_r)$. Then we have

$$\frac{dJ(P(t,s))}{ds}|_{s=s(t)} = J'(P(t, s(t)))P'_s(t, s(t)) = 0. \tag{4.14}$$

Once the value $s(t)$ and the direction $P'_s(t, s(t))$ are specified as in (4.14), for the t-parametrized family of curves $P(t, s)$ to evolve in t in a regular way or to avoid a sliding, we need to assign a moving direction. We know that $P'_t(t, s(t))$ defines the di-

rection of the t-parametrized family of curves $P(t,s)$ moving away locally from the point $P(t,s(t))$. It is significant to note that in our research we are actually going to propose a system which is a dynamics of t-parametrized points $P(t,s(t))$ starting from an initial point $P(0,s(0))$, rather than a dynamics of t-parametrized family of smooth curves $P(t,s)$. When the t-parametrized family of smooth curves $P(t,s)$ evolves in t, we need to move $P(t,s(t)) \in \mathcal{M}$ to a new point which is also on $\mathcal{M}$ and construct a new smooth curve joined by this new point, u_r and u_{p_t}. In Section 2, since we expect that the value of $J(P(t,s(t)))$ will be strictly decreasing or obey the energy dissipation law, the moving direction was set to be along certain negative gradient flow and it was given by $P_t'(t,s(t)) = -J'(P(t,s(t)))/C_t \in H_t$. However, we can not repeat what we did in Section 2 because only moving $P(t,s(t))$ along the negative flow will not necessarily give us a new point on $\mathcal{M}$. Since the negative gradient flow is a descent direction, we could firstly move $P(t,s(t))$ along the negative gradient flow to a point P_1, and carry out a small correction in order to move the point P_1 to $P_2 \in \mathcal{M}$. It is obvious to see the direction from $P(t,s(t))$ to P_1 is just along the negative gradient flow, but $P_t'(t,s(t))$, which represents the direction from $P(t,s(t))$ to P_2, is not easy to get directly because of the small correction which moves P_1 to P_2 in order to make sure the new point P_2 is also on $\mathcal{M}$.

By the idea above, we propose the following 1-saddle search system:

$$\langle J'(P(t,s(t))), P_s'(t,s(t))\rangle = 0, \tag{4.15}$$

$$\langle J'(P(t,s(t))), P_t'(t,s(t))\rangle = -\|J'(P(t,s(t)))\|^2/C_t \tag{4.16}$$

starting from an initial point $P(0,s(0))$ on $\mathcal{M}$ on a given initial smooth curve $P(t,s)$ on $\mathcal{M}$ which connects u_r, $P(0,s(0))$ and u_{p_0}. The dynamic system (4.15) - (4.16) is a generalization of the system (2.2) - (2.3) we proposed for finding 1-saddles with virtual curves. (4.15) is the same as (2.2) and it is achieved by taking a local maximum of $J(P(t,s))$

in s, while (4.16) includes (2.3), i.e., (2.3) is a special case of (4.16). Actually (4.16) gives us infinitely many choices of the direction of moving point $P(t, s(t))$. The negative gradient flow is an ideal choice since the functional J is strictly decreasing on it, but itself alone could not guarantee the point $P(t, s(t))$ always stays on $\mathcal{M}$, thus we need another descent direction satisfying this requirement. Note that this direction from (4.16) may not be an explicit one. (4.16) implies that we could move the point $P(t, s(t))$ along the negative gradient flow and do a small correction forcing the point back on $\mathcal{M}$, i.e., $P(t + t', s(t)) = \hat{m}(u - t'J'(P(t, s(t)))/C_t)$. In the following we will show that such an implementation satisfies the generalized dynamic system (4.15) - (4.16).

Lemma 4.2.1. *For a fixed $u \in E$, define the symmetric bilinear form $B_2 : E \times E \mapsto \mathbb{R}$ which is given by $B_2(v_1, v_2) = \int_{\Omega_1} f'_u(x, u)v_1v_2dx - \int_{\Omega_1} u^{-1}f(x, u)v_1v_2dx$, where $\Omega_1 \subset \Omega$ s.t. $u \neq 0$ on Ω_1, then it satisfies the Cauchy-Schwarz inequality, i.e., $B_2^2(v_1, v_2) \leq B_2(v_1, v_1)B_2(v_2, v_2)$.*

Proof. By the assumption (**AS.6**), there exists $\theta \in (0, 1)$ s.t. $0 < u^{-1}f(x, u(x)) \leq \theta f'_u(x, u(x))$ for every $x \in \Omega_1$, then we have

$$B_2(v, v) \geq (1 - \theta) \int_{\Omega_1} f'_u(x, u)v^2dx \geq 0, \tag{4.17}$$

$$B_2(v, v) \geq (\frac{1}{\theta} - 1) \int_{\Omega_1} u^{-1}f(x, u)v^2dx \geq 0. \tag{4.18}$$

Without loss of generality, suppose $B_2(v_1, v_1) = 0$, then it is easy to see that

$$\int_{\Omega_1} f'_u(x, u)v_1^2dx = 0 \text{ and } \int_{\Omega_1} u^{-1}f(x, u)v_1^2dx = 0$$

from (4.17) and (4.18). Since $f'_u(x, u)$ and $u^{-1}f(x, u)$ are positive by the assumption

(**AS.6**),

$$\int_{\Omega_1} f'_u(x,u)v_1v_2dx = 0 \text{ and } \int_{\Omega_1} u^{-1}f(x,u)v_1v_2dx = 0,$$

then $B_2(v_1, v_2) = 0$. We have the equality immediately.

If $B_2(v_1, v_1) \neq 0$ and $B_2(v_2, v_2) \neq 0$, let $v = v_1 - \dfrac{B_2(v_1, v_2)}{B_2(v_2, v_2)}v_2$, then

$$B_2(v, v_2) = B_2\left(v_1 - \frac{B_2(v_1, v_2)}{B_2(v_2, v_2)}v_2, v_2\right) = B_2(v_1, v_2) - \frac{B_2(v_1, v_2)}{B_2(v_2, v_2)}B_2(v_2, v_2) = 0.$$

We have

$$\begin{aligned}
B_2(v_1, v_1) &= B_2(v + \frac{B_2(v_1, v_2)}{B_2(v_2, v_2)}v_2, v + \frac{B_2(v_1, v_2)}{B_2(v_2, v_2)}v_2) \\
&= B_2(v, v) + 2B_2(v, \frac{B_2(v_1, v_2)}{B_2(v_2, v_2)}v_2) + B_2(\frac{B_2(v_1, v_2)}{B_2(v_2, v_2)}v_2, \frac{B_2(v_1, v_2)}{B_2(v_2, v_2)}v_2) \\
&= B_2(v, v) + 2\frac{B_2(v_1, v_2)}{B_2(v_2, v_2)}B_2(v, v_2) + \left(\frac{B_2(v_1, v_2)}{B_2(v_2, v_2)}\right)^2 B_2(v_2, v_2) \\
&= B_2(v, v) + \frac{B_2^2(v_1, v_2)}{B_2(v_2, v_2)} \\
&\geq \frac{B_2^2(v_1, v_2)}{B_2(v_2, v_2)},
\end{aligned}$$

so we can get the inequality immediately after the multiplication by $B_2(v_2, v_2)$. □

For a given point $u_0 \in \mathcal{M}$, define a map

$$\tilde{m}_{u_0} : \mathbb{R}^+ \mapsto \mathbb{R}^+ \times \mathbb{R}, \quad \tilde{m}_{u_0}(t) = (C_1, C_2) \text{ s.t. } C_1(u_0 - tv_0) + C_2e_1 \in \mathcal{M}, \tag{4.19}$$

where $v_0 = J'(u_0)/C_{u_0}$ and $C_{u_0} = \max\{\|J'(u_0)\|, 1\}$.

Lemma 4.2.2. *For any given point $u \in \mathcal{M}$, the corresponding map $\tilde{m}_u$ is $\mathcal{C}^1$ in a right neighborhood of zero (the intersection of a neighborhood of zero and the domain $\mathbb{R}^+$).*

Proof. Consider a map $M : \mathbb{R}^+ \times \mathbb{R}^+ \times \mathbb{R} \mapsto \mathbb{R}^2$ defined by

$$\begin{aligned} M(t, C_1, C_2) &= (M_1(t, C_1, C_2), M_2(t, C_1, C_2)) \\ &= (\langle J'(C_1(u - tv) + C_2 e_1), (C_1(u - tv) + C_2 e_1)\rangle, \\ &\quad \langle J'(C_1(u - tv) + C_2 e_1), e_1\rangle), \end{aligned}$$

where $v = J'(u)/C_u$, and M_1 and M_2 map $\mathbb{R}^+ \times \mathbb{R}^+ \times \mathbb{R}$ to $\mathbb{R}$.

Since $u \in \mathcal{M}$, $M(0, 1, 0) = (0, 0)$, then we consider the Jacobian matrix $J_{M,y}(0, 1, 0)$, where $y = (C_1, C_2)$ and $J_{M,y}$ is with the form:

$$J_{M,y} = \begin{bmatrix} \dfrac{\partial M_1}{\partial C_1} & \dfrac{\partial M_1}{\partial C_2} \\ \dfrac{\partial M_2}{\partial C_1} & \dfrac{\partial M_2}{\partial C_2} \end{bmatrix}$$

Denote the $(i, j)^{th}$ element in $J_{M,y}(0, 1, 0)$ by $J_{i,j}$, then we obtain

$$\begin{aligned} J_{1,1} &= \frac{\partial M_1}{\partial C_1}(0, 1, 0) = 2B(u, u) + \kappa[\int_\Omega f(x, u)u dx + \int_\Omega f'_u(x, u)u^2 dx], \\ J_{1,2} &= \frac{\partial M_1}{\partial C_2}(0, 1, 0) = 2B(u, e_1) + \kappa[\int_\Omega f(x, u)e_1 dx + \int_\Omega f'_u(x, u)ue_1 dx], \\ J_{2,1} &= \frac{\partial M_2}{\partial C_1}(0, 1, 0) = B(u, e_1) + \kappa \int_\Omega f'_u(x, u)ue_1 dx, \\ J_{2,2} &= \frac{\partial M_2}{\partial C_2}(0, 1, 0) = B(e_1, e_1) + \kappa \int_\Omega f'_u(x, u)e_1^2 dx, \end{aligned}$$

where $B : E \times E \mapsto \mathbb{R}$ is a symmetric bilinear form given by

$$B(v_1, v_2) := \int_\Omega (\nabla v_1 \cdot \nabla v_1 - \lambda v_1 v_2) dx, \text{ where } v_1, v_2 \in E. \tag{4.20}$$

Since $u \in \mathcal{M}$, by the definition of the generalized Nahari manifold, we have

$$\langle J'(u), u\rangle = B(u,u) + \kappa \int_\Omega f(x,u)u dx = 0, \tag{4.21}$$

$$\langle J'(u), e_1\rangle = B(u,e_1) + \kappa \int_\Omega f(x,u)e_1 dx = 0. \tag{4.22}$$

Let $\Omega_1 \subset \Omega$ such that $u \neq 0$ on Ω_1, we know that Ω_1 can not be empty since $u \in \mathcal{M}$. Besides, $f(x,u) = 0$ on $\Omega\backslash\Omega_1$ by the assumption (**AS.2**). Then the 4 elements of the Jacobian matrix can be rewritten as

$$\begin{aligned}
J_{1,1} &= \kappa[\int_\Omega f'_u(x,u)u^2 dx - \int_\Omega f(x,u)u dx] \\
&= \kappa[\int_{\Omega_1} f'_u(x,u)u^2 dx - \int_{\Omega_1} u^{-1}f(x,u)u^2 dx] = \kappa B_2(u,u), \\
J_{1,2} &= \kappa[\int_\Omega f'_u(x,u)ue_1 dx - \int_\Omega f(x,u)e_1 dx] \\
&= \kappa[\int_{\Omega_1} f'_u(x,u)ue_1 dx - \int_{\Omega_1} u^{-1}f(x,u)ue_1 dx] = \kappa B_2(u,e_1), \\
J_{2,1} &= \kappa[\int_\Omega f'_u(x,u)ue_1 dx - \int_\Omega f(x,u)e_1 dx] \\
&= \kappa[\int_{\Omega_1} f'_u(x,u)ue_1 dx - \int_{\Omega_1} u^{-1}f(x,u)ue_1 dx] = \kappa B_2(u,e_1), \\
J_{2,2} &= B(e_1,e_1) + \kappa \int_\Omega f'_u(x,u)e_1^2 dx \\
&= B(e_1,e_1) + \kappa \int_{\Omega\backslash\Omega_1} f'_u(x,u)e_1^2 dx + \kappa \int_{\Omega_1} f'_u(x,u)e_1^2 dx \\
&= B(e_1,e_1) + \kappa \int_{\Omega\backslash\Omega_1} f'_u(x,u)e_1^2 dx + \kappa \int_{\Omega_1} u^{-1}f(x,u)e_1^2 dx + \kappa B_2(e_1,e_1),
\end{aligned}$$

where $B_2(\cdot,\cdot)$ is defined in Lemma 4.2.1. Thus the determinant of the Jacobian matrix is

$$\begin{aligned}
|J_{M,y}(0,1,0)| &= J_{1,1}J_{2,2} - J_{1,2}J_{2,1} \\
&= \kappa B_2(u,u)B(e_1,e_1) + \kappa^2 B_2(u,u)\int_{\Omega\setminus\Omega_1} f'_u(x,u)e_1^2 dx \\
&+ \kappa^2 B_2(u,u)\int_{\Omega_1} u^{-1}f(x,u)e_1^2 dx + \kappa^2\left[B_2(u,u)B_2(e_1,e_1) - B_2^2(u,e_1)\right] \\
&\geq \kappa B_2(u,u)B(e_1,e_1) + \kappa^2\left[B_2(u,u)B_2(e_1,e_1) - B_2^2(u,e_1)\right] \\
&> \kappa^2\left[B_2(u,u)B_2(e_1,e_1) - B_2^2(u,e_1)\right] \\
&\geq 0.
\end{aligned} \tag{4.23}$$

We would like to give more details for the three inequalities above. It is not difficult to obtain that $\Omega_1 \neq \emptyset$ and $B_2(u,u) \geq (1-\theta)\int_{\Omega_1} f'_u(x,u)u^2 dx > 0$. Besides, by the assumption (**AS.6**), $f'_u(x,u)$ is continuous in u and $f'_u(x,u) > 0$ for $u(x) \neq 0$, then we have $f'_u(x,u) \geq 0$ for all $u(x) \in \mathbb{R}$, so the first inequality holds since the two integrals are non-negative, the second inequality holds since $B(e_1,e_1)$ is negative, and the last inequality is directly from Lemma 4.2.1. Finally the implicit function theorem applies and leads to the conclusion. □

It is convenient that the 1st and 2nd elements of $\tilde{m}_u(t)$ are denoted by $\tilde{m}_u^1(t)$ and $\tilde{m}_u^2(t)$ respectively. Now we claim that (4.16) implies the implementation with the correction we mentioned, so the generalized dynamic system (4.15) - (4.16) is satisfied.

Lemma 4.2.3. *(4.16) is satisfied when the correction step ($P(t+t',s(t)) = \hat{m}(u - t'J'(P(t,s(t)))/C_t)$) is taken.*

Proof. Consider the moving direction at $u = P(t, s(t))$:

$$\begin{aligned}
P_t^{'}(t, s(t)) &= \lim_{t' \to 0} \frac{P(t + t', s(t)) - P(t, s(t))}{t'} \\
&= \lim_{t' \to 0} \frac{\hat{m}(u - t' J'(P(t, s(t)))/C_t) - u}{t'} \\
&= \lim_{t' \to 0} \frac{\tilde{m}_u^1(t')(u - t' J'(P(t, s(t)))/C_t) + \tilde{m}_u^2(t') e_1 - u}{t'} \\
&= \lim_{t' \to 0} \frac{(\tilde{m}_u^1(t') - 1)u + \tilde{m}_u^2(t') e_1 - \tilde{m}_u^1(t') t' J'(P(t, s(t)))/C_t}{t'} \\
&= \lim_{t' \to 0} \big[\frac{(\tilde{m}_u^1(t') - \tilde{m}_u^1(0))u + (\tilde{m}_u^2(t') - \tilde{m}_u^2(0)) e_1}{t'} \\
&\quad - \frac{\tilde{m}_u^1(t') t' J'(P(t, s(t)))/C_t}{t'} \big] \\
&= \lim_{t' \to 0} \big[\frac{(\tilde{m'}_u^1(0) t' + o(t'))u + (\tilde{m'}_u^2(0) t' + o(t')) e_1}{t'} \\
&\quad - \frac{(1 + O(t')) t' J'(P(t, s(t)))/C_t}{t'} \big] \\
&= \tilde{m'}_u^1(0) u + \tilde{m'}_u^2(0) e_1 - J'(P(t, s(t)))/C_t \\
&= \tilde{m'}_u(0) [u, e_1]^T - J'(P(t, s(t)))/C_t,
\end{aligned} \tag{4.24}$$

where $\tilde{m'}_u^1$ and $\tilde{m'}_u^2$ are the 1st and 2nd element of $\tilde{m'}_u$ respectively. Note that $\tilde{m}_u$ is locally $\mathcal{C}^1$ at zero by Lemma 4.2.2, so $\tilde{m'}_u(0)$ is bounded for a given u. Thus it is easy to see

$$\begin{aligned}
\langle J'(P(t, s(t))), P_t'(t, s(t)) \rangle &= \langle J'(P(t, s(t))), \tilde{m'}_u^1(0) u + \tilde{m'}_u^2(0) e_1 - J'(P(t, s(t)))/C_t \rangle \\
&= \tilde{m'}_u^1(0) \langle J'(P(t, s(t))), u \rangle + \tilde{m'}_u^2(0) \langle J'(P(t, s(t))), e_1 \rangle \\
&\quad - \langle J'(P(t, s(t))), J'(P(t, s(t)))/C_t \rangle \\
&= -\| J'(P(t, s(t))) \|^2 / C_t,
\end{aligned} \tag{4.25}$$

where the first two terms in the second equality above vanish since $\langle J'(P(t, s(t))), u \rangle = 0$ and $\langle J'(P(t, s(t))), e_1 \rangle = 0$ according to the definition of $\mathcal{M}$. Hence (4.16) is satisfied when the correction is taken in the implementation. □

It is important to note that for the definite problem a small correction is also taken by multiplying the point with a scalar such that it is on the Nehari manifold after moving it along the negative gradient flow. We did not prove the dynamic system same as (4.15) - (4.16) is satisfied when the method was introduced in Section 3. However, it is not difficult to see that our proof for Lemma 4.2.3 covers the similar result of the method of the Nehari manifold.

From the 1-saddle search system defined above, we note that we do not need to know the explicit expressions of the curves $P(t,s)$ on $\mathcal{M}$ as long as the points $P(t,s(t))$ can be found on $\mathcal{M}$, so we call those curves virtual. This distinctive feature will be clearer in the algorithm. It reduces the complexity of the problem, speeds up the convergence of algorithm and enables us to easily extend the method to find saddles with higher MI. In addition, we assume that the scalar function $0 < s(t) < 1$ is locally Lipschitz continuous. Since for each $t \geq 0$, the equation (4.15) can be used to solve $s(t)$, a local maximum of $J(P(t,s)))$ in s, by using the implicit function theorem, a condition can always be proposed such that s is locally $\mathcal{C}^1$.

It looks like we are finding equality constrained saddles in our model problem even though the constraints from the definition of the generalized Nehari manifold are actually natural. However, it is significant to note that our dynamic system is different from the Constrained Local Minimax Method (CLMM) proposed in [37], which actually evolves the point $P(t,s(t))$ in just one step with an orthogonal projection. In [37], Li and Zhou used the gradient of constraints G to construct an orthogonal projection operator $\mathbb{P}_T(u)$ at u by the classical projection theorem, where $u = P(t,s(t))$ is on the constrained manifold. Then they applied the operator to the negative gradient flow $-J'(P(t,s(t)))$ to obtain the direction of the t-parametrized family of smooth curves $P(t,s)$ moving along the constrained manifold in t away locally from the point $P(t,s(t))$ which is exactly $P'_t(t,s(t))$. In our research, the explicit expression of the constraints from the generalized Nehari

manifold is complicated, so the gradient of these constraints is difficult to compute numerically. Besides, the constraints from the generalized Nehari manifold are not extra and all the non-trivial critical points should be on it theoretically. In addition, in our two-step point evolution, the point $P(t, s(t))$ is moved along the negative gradient flow just a little bit, and it is still very close to $\mathcal{M}$, so the correction actually is not very large, especially when error is sufficiently small, i.e., P_1 and P_2 are very close for small gradient of J. Thus we prefer LMM followed by an additional small correction since it not only generally follows a regular non-slid search direction and obeys the energy dissipation law, but also has a big advantage to implement numerically.

In the 1-saddle search system, (4.15) is achieved by taking a local maximum of J along the curve $P(t, s) \subset \mathcal{M}$ in s, while (4.16) indicates that this system follows a negative gradient flow and the evolution of points $P(t, s(t))$ is done on $\mathcal{M}$ so it leads to a local minimum of $J(P(t, s(t)))$ in t. Thus the system (4.15)-(4.16) is a new local minimax principle for a 1-saddle. Modifications of the system (4.15)-(4.16) can be developed for other purposes. Also different discrete realizations of this system in t may lead to different numerical algorithms for finding a 1-saddle of different types of functionals. When a discretization is used along t, since a 1-saddle is an unstable solution, we do not want to go too fast to lose algorithm stability in the search process. It is known that the energy dissipation law is important for algorithm stability, but it alone is not enough for an algorithm to converge when a numerical approximation of the dynamics is involved. We need to set up a stepsize rule, a stronger version of the energy dissipation law.

Lemma 4.2.4. *(Stepsize Rule) If $P(t_0, s(t_0))$ is not a critical point, then there exists $s_0 > 0$ s.t. when $0 < t' < s_0$, we have a stepsize rule*

$$J(P(t_0 + t', s(t_0 + t'))) - J(P(t_0, s(t_0))) < \frac{-t'}{4} \|J'(P(t_0, s(t_0)))\|^2 / C_{t_0}.$$

Furthermore, if $P(t_k, s(t_k)) \to P(t_0, s(t_0))$ *as* $t_k \to t_0$*, then there exists* $N > 0$ *s.t. when* $0 < t' < s_0/2, k > N$*, we have a uniform stepsize rule*

$$J(P(t_k + t', s(t_k + t'))) - J(P(t_k, s(t_k))) < \frac{-t'}{4}\|J'(P(t_k, s(t_k)))\|^2/C_{t_k}.$$

Proof. We first note that

$$\begin{aligned} &P(t_0 + t', s(t_0 + t')) - P(t_0, s(t_0)) \\ =&P'_t(t_0, s(t_0))t' + P'_s(t_0, s(t_0))(s(t_0 + t') - s(t_0)) + o(t' + |s(t_0 + t') - s(t_0)|). \end{aligned} \tag{4.26}$$

Then we assume that $s(t)$ is locally Lipschitz continuous, i.e., $|s(t_0 + t') - s(t_0)| \leq \ell_0 t'$. Since $P(t_0, s(t_0))$ is on the smooth curve $P(t, s)$, it is bounded and we point out that $P'_t(t_0, s(t_0))$ is bounded for bounded point $P(t_0, s(t_0))$, which is shown in convergence analysis below. It follows that $o(\|P(t_0 + t', s(t_0 + t')) - P(t_0, s(t_0))\|) = o(|t'|)$ and we have

$$\begin{aligned} &J(P(t_0 + t', s(t_0 + t'))) - J(P(t_0, s(t_0))) \\ =&\langle J'(P(t_0, s(t_0))), P(t_0 + t', s(t_0 + t')) - P(t_0, s(t_0))\rangle \\ &+ o(\|P(t_0 + t', s(t_0 + t')) - P(t_0, s(t_0))\|) \\ =&\langle J'(P(t_0, s(t_0))), P'_t(t_0, s(t_0))t' + P'_s(t_0, s(t_0))(s(t_0 + t') - s(t_0))\rangle + o(|t'|) \\ =&-t'\|J'(p(t_0, s(t_0)))\|^2/C_{t_0} + o(|t'|) \text{ (by (4.15) and (4.16)).} \end{aligned} \tag{4.27}$$

Then it is easy to see there exist $s_0 > 0$ such that when $0 < t' < s_0$,

$$J(P(t_0 + t', s(t_0 + t'))) - J(P(t_0, s(t_0))) < \frac{-t'}{4}\|J'(P(t_0, s(t_0)))\|^2/C_{t_0}. \tag{4.28}$$

Since J and J' both are continuous, the second conclusion follows directly from

$P(t_k, s(t_k)) \to P(t_0, s(t_0))$ as $t_k \to t_0$ and the stepsize rule in the first part. □

Theorem 4.2.5. *(Local Minimax Characterization) If* $t_0 = \arg\text{loc-}\min_{t>0} J(P(t, s(t)))$. *Then* $P(t_0, s(t_0))$ *is a saddle point.*

Proof. Arguing by contradiction, suppose $P(t_0, s(t_0))$ is not a saddle point, since it is a local maximum of J along the smooth curve $P(t_0, s)$ in s, it cannot be a local minimum of J either. Then by Lemma 4.2.4, there exists $s_0 > 0$ s.t. when $0 < t' < s_0$, we have

$$J(P(t_0 + t', s(t_0 + t'))) - J(P(t_0, s(t_0))) < \frac{-t'}{4} \|J'(P(t_0, s(t_0)))\|^2 / C_{t_0}, \tag{4.29}$$

which yields a contradiction to $t_0 = \arg\text{loc-}\min_{t>0} J(P(t, s(t)))$. □

Remark 4.2.1. This local minimax characterization implies a two-level optimization. In the inner local maximum level, the local maximum is taken along the smooth curve connecting u_r and a flexible point u_{p_t}. In programming, this can be done by some subroutines. For the outer local minimum level, the local minimum can be obtained by the gradient descent method. We present the following new algorithm.

4.3 A Local Minimax Method on $\mathcal{M}$

Assume that u_r is a local minimum of J and u_{p_0} is either another fixed local minimum of J or any point on $\mathcal{M}$ with $J(u_{p_0}) \leq J(u_r)$. We can use the negative gradient method to find the local minimum point u_r on $\mathcal{M}$. Given $\lambda, \varepsilon, \tau_k > 0$ with $\tau_k \to 0$ as $k \to \infty$, $\sum_{k=0}^{\infty} \tau_k = +\infty$, and an initial guess u_0 on $\mathcal{M}$, the following steps serve as a flow chart of our algorithm.

Step 1: Let $P(0, s)$ be a smooth curve on $\mathcal{M}$ connecting u_r, u_0 and u_{p_0} such that $P(0, 0) = u_r, P(0, 1) = u_{p_0}$ and $s(0)$ be the first local maximum of $J(P(0, s))$ on $\mathcal{M}$, namely, $s(0) = \arg\max_{s>0} J(P(0, s))$, s.t. $P(0, s)$ is on $\mathcal{M}$. Set $k = 0, t_0 = 0$, and $u_k = P(t_k, s(t_k))$;

Step 2: Evaluate $d_k = J'(u_k)$. If $\|d_k\| < \varepsilon$, then output u_k and stop, otherwise continue.

Step 3: For $t' = \frac{\lambda}{2^m}, m = 1, 2, ...$, let $u_k(t') = P(t_k, s(t_k)) - t' d_k / C_{t_k}$. Let $u_{p_k,t'} \in \mathcal{M}$ be a local minimum of J or chosen in a continuous way in t' s.t. $J(u_{p_k,t'}) \leq J(u_r)$. Construct a smooth curve $P(t_k + t', s) \subset \mathcal{M}$ passing through $u_r, \hat{m}(u_k(t')), u_{p_k,t'}$. Use $s(t_k)$ as an initial guess to solve for $s(t_k + t') = \arg\max_{s>0} J(P(t_k + t', s))$ s.t. $P(t_k + t', s)$ is on $\mathcal{M}$. Denote

$$t'_k = \max\{t' = \frac{\lambda}{2^m} \leq \tau_k | m \in \mathbb{N}^+, \\ J(P(t_k + t', s(t_k + t'))) - J(u_k) \leq -\frac{t'}{4}\|d_k\|^2 / C_{t_k}\},$$

$t_{k+1} = t_k + t'_k$ and $u_{k+1} = P(t_{k+1}, s(t_{k+1})) \in \mathcal{M}$;

Step 4: Set $k = k + 1$ and go to Step 2.

Remark 4.3.1. Some remarks regarding the algorithm are given to make it clearer.

(1) We do not set limit to the total length of stepsizes, so $\sum_{k=0}^{\infty} \tau_k = +\infty$;

(2) In the numerical implementation, the construction of the smooth curve connecting three points on $\mathcal{M}$ is actually done by taking the intersection of the space formed by the three points and the generalized Nehari manifold. As we know, the dimension of the geometric object would be one which is just a curve since the co-dimension of $\mathcal{M}$ is two while the space formed by the three points is 3-D;

(3) When we take local maximum of J on s, there can be multiple selections along the smooth curve. Each one is called a peak selection. It is significant to avoid the oscillation among different peak selections since we need to guarantee the continuity of P in s. Using the previous value $s(t_k)$ could help us to avoid such an unnecessary oscillation. On the other hand, in Step 1, by starting with a small $s > 0$, we intend to choose the peak selection which is closest to the local minimum u_r;

(4) Note that the smooth curve passes through $\hat{m}(u_k(t')) \in \mathcal{M}$. Here the domain of $\hat{m}$ is $E\backslash V$ instead of $E^+\backslash\{0\}$, so $\hat{m}$ indicates a small correction to $u_k(t')$ to force it back to $\mathcal{M}$.

We will give more details about the algorithm in the numerical implementation section.

4.4 Convergence Analysis

Before doing the convergence analysis, it is crucial to point out the fact that J is coercive on $\mathcal{M}$ as this property will be used in the proof of convergence.

Lemma 4.4.1. *(Szulkin and Weth) J is coercive on $\mathcal{M}$, i.e., $J(u) \to \infty$ as $\|u\|_E \to \infty$, $u \in \mathcal{M}$.*

Using the notation in the new algorithm, we have the following convergence result.

Theorem 4.4.2. *Let $t_{k+1} = t_k + t'_k$ where $0 < t'_k \leq \tau_k, \tau_k \to 0, \sum_{k=0}^{\infty} \tau_k = +\infty$ and $u_k = P(t_k, s(t_k))$ be the sequence generated by the algorithm with $\varepsilon = 0$. Then*

*(**a**) $\lim_{k\to\infty} t'_k J'(u_k)/C_{t_k} = 0$;*

*(**b**) there is a subsequence $u_{k_j} \to u^*$ a saddle of J;*

Denote $K = \{u \in H : J'(u) = 0, J(u) = J(u^*)\}$, then

*(**c**) any convergent subsequence of $\{u_k\}$ converges to a point of K;*

*(**d**) Let $\overline{\{u_k\}}$ be all the limiting points of $\{u_k\}$. If furthermore $\|P'_s(t_k, s(t_k))\|$ is bounded and the scalar function $s(t)$ is Lipschitz continuous, then $\overline{\{u_k\}} \cap K \neq \emptyset$ is connected and dis$(u_k, K) \to 0$ as $k \to \infty$.*

Proof. Since $J(u_r) < J(u_{k+1}) < J(u_k)$ by the stepsize rule, $\lim_{k\to\infty} J(u_k)$ exists and

$$J(u_r)-J(u_0) \leq \lim_{k\to\infty} J(u_k)-J(u_0) = \sum_{k=0}^{\infty}(J(u_{k+1})-J(u_k)) < -\frac{1}{4}\sum_{k=0}^{\infty} t'_k\|J'(u_k)\|^2/C_{t_k},$$

where $C_{t_k} = \max\{1, \|J'(u_k)\|\}$. Thus $t'_k\|J'(u_k)\|^2/C_{t_k} \to 0$. Then we get

$t'_k J'(u_k)/C_{t_k} \to 0$ if $\|J'(u_k)\| > 1$ or $\|J'(u_k)\| \leq 1$ and $0 < t'_k < \tau_k \to 0$. So (a) is verified.

To prove (b), there are totally only two Cases for $\{u_k\}$, (1) there is $\eta > 0$ s.t. $\|J'(u_k)\| > \eta, k = 1, 2, ...,$ or (2) there is a subsequence $J'(u_{k_i}) \to 0$.

If Case (1) holds, we may assume $\eta < \frac{1}{2}$. Thus $-\|J'(u_k)\| < -\eta < -\eta^2$ and

$$J(u_r) - J(u_0) < -\frac{1}{4}\sum_{k=0}^{\infty} t'_k \|J'(u_k)\|^2/C_{t_k} \leq -\frac{\eta^2}{4}\sum_{k=0}^{\infty} t'_k = -\frac{\eta^2}{4}\sum_{k=0}^{\infty} |t_{k+1} - t_k|. \quad (4.30)$$

That is, $\{t_k\}$ is a Cauchy sequence. We obtain $t_k \to t^*$. By the continuity, we have $u_k = P(t_k, s(t_k)) \to u^* = P(t^*, s(t^*))$ and $\|J'(P(t^*, s(t^*)))\| \geq \eta$, i.e., u^* is not a critical point. Then Lemma 4.2.4 states that there exist $s_0 > 0, N > 0$ s.t. when $k > N$, we have $\frac{s_0}{2} \leq t'_k < \tau_k \to 0$, a contradiction. Thus Case (2) must hold true. Since $\{J(u_k)\}$ is bounded and $J'(u_{k_j}) \to 0$, by the PS condition, (b) is proven.

To establish (c), let $\{u_{k_j}\} \subset \{u_k\}$ be any convergent subsequence with $u_{k_j} \to u'$. If $J'(u') \neq 0$, we can pass to a subsequence if necessary, then $t'_k J'(u_k)/C_{t_k} \to 0$ and $\|J'(u_{k_j})\| > \eta > 0$ lead to $t'_{k_j} \to 0$, a contradiction to Lemma 4.2.4 under $u_{k_j} \to u'$. Thus $J'(u') = 0$ must hold. Since $\lim_{k\to\infty} J(u_k)$ exists, we have $J(u') = J(u^*)$, i.e., $u' \in K$.

To prove (d), we have

$$\begin{aligned} u_{k+1} - u_k &= P(t_{k+1}, s(t_{k+1})) - P(t_k, s(t_k)) \\ &= P'_t(t_k, s(t_k))t'_k + P'_s(t_k, s(t_k))(s(t_{k+1}) - s(t_k)) \\ &\quad + o(|t'_k| + |s(t_{k+1}) - s(t_k)|). \end{aligned}$$

Since $\{J(u_k)\}$ is bounded and J is coercive on $\mathcal{M}$ by Lemma 4.4.1, then $\{u_k\}$ must be bounded as well. Then there exists a constant number $R > 0$ such that $\|\tilde{m}'_{u_k}(0)\| \leq R$

since $\tilde{m}_{u_k}$ is locally $\mathcal{C}^1$ at zero. By (4.24), we have

$$\|P_t'(t_k, s(t_k))\| \leq \max(\|u_k\|, \|e_1\|)R + 1 \leq M_1,$$

where $M_1 > 0$ is a constant number. The scalar function $s(t)$ is Lipschitz continuous, as $k \to \infty$ we have $0 < t_k' \leq \tau_k \to 0$, then $\|P_s'(t_k, s(t_k))\| \leq M_2,\ |s(t_{k+1}) - s(t_k))| \leq \ell(t_k') \to 0$. Thus there is an $\ell_1 > 0$ s.t.

$$\|u_{k+1} - u_k\| = \|P(t_{k+1}, s(t_{k+1})) - P(t_k, s(t_k))\| \leq \ell_1(t_k') \to 0 \ \text{ as } \ k \to \infty. \quad (4.31)$$

From (b), we have $\overline{\{u_k\}} \cap K \neq \emptyset$. Let $I \subset \mathbb{N}^+ = \{1, 2, ...\}$ and call $\sum_{i\in I} \|u_{i+1} - u_i\|$ the total distance traveled by the subsequence $\{u_i\}_{i\in I}$. For any given $\eta > 0$, let $i \in I \subset \mathbb{N}^+$ denote the whole index set in $\mathbb{N}^+$ with $\|J'(u_i)\| > \eta$. Since $J(u_r) < J(u_{k+1}) < J(u_k)$, similar to (4.30), we have

$$\begin{aligned} -\infty < J(u_r) - J(u_0) &\leq \sum_{k=1}^{\infty}[J(u_{k+1}) - J(u_k)] \leq \sum_{i\in I}[J(u_{i+1}) - J(u_i)] \\ &< -\frac{1}{4}\sum_{i\in I} t_i'\|J'(u_i)\|^2/C_{t_i} \leq -\frac{\eta^2}{4}\sum_{i\in I} t_i'. \end{aligned} \quad (4.32)$$

By (4.31), it leads to

$$\sum_{i\in I} \|u_{i+1} - u_i\| \leq \ell_1 \sum_{i\in I} t_i' < +\infty, \quad (4.33)$$

i.e., the total distance traveled by $\{u_i\}_{i\in I}$ is finite.

Suppose there is $\delta_3 > 0$ s.t. there are infinitely many points u in $\{u_k\}$ with $\|u - u^*\| > \delta_3$. By the inequality (4.31), for any $0 < \delta_1 < \delta_2 < \delta_3$, there is $M > 0$ s.t. when $k > M$, $\|u_{k+1} - u_k\| < \frac{1}{4}(\delta_2 - \delta_1)$, i.e., two consecutive points u_k, u_{k+1} cannot jump over the region $\mathcal{R} = \{u \in H : \delta_1 < \|u - u^*\| < \delta_2\}$. Since u^* is a limit point and there are infinitely many points u in $\{u_k\}$ such that $\|u - u^*\| > \delta_3$, there must exist infinitely many

points $\{u_{k_i}\} \subset \{u_k\}$ in the region $\mathcal{R}$. However, each time the sequence entered this region $\mathcal{R}$, it has to travel at least $\frac{1}{2}(\delta_2 - \delta_1)$ distance before it pass the region into another region. Thus the total distance traveled by u_{k_i} is infinite, which contradicts with (4.33). Thus there must be a subsequence $\{u_{k_{i'}}\} \subset \{u_{k_i}\}$ s.t. $J'(u_{k_{i'}}) \to 0$ and $J(u_{k_{i'}}) \to J(u^*)$. By the PS condition, there is a subsequence, denoted by $\{u_{k_{i'}}\}$ again, s.t. $u_{k_{i'}} \to u'$ with $J'(u') = 0$ and $J(u') = J(u^*)$. Thus $u' \in K \cap \mathcal{R}$. It leads to a contradiction since $0 < \delta_1 < \delta_2 < \delta_3$ can be any numbers and u^* can be any limit point of $\{u_k\}$. Thus for any $\delta_3 > 0$, there are at most a finite number of points $u \in \{u_k\}$ s.t. dis$(u, K) > \delta_3$, i.e., dis$(u_k, K) \to 0$ and also, $\overline{\{u_k\}} \cap K$ must be connected. Finally (d) is verified. □

Remark 4.4.1. (1) To obtain a sequence convergence (d) from a subsequence convergence (b) in Theorem 4.4.2, it is crucial to assume the bounded scalar function $s(t)$ to be locally Lipschitz continuous. Observe that if $s(t) \in (0, 1)$ is only continuous with unbounded $|s'(t_k)|$, it must oscillate infinitely many times. Then there could be subsequences of $\{s(t_k)\}$ converging to different points in $[0, 1]$. Consequently we can have only the subsequence convergence (b) but not the sequence convergence (d). The boundedness of $\|P'_s(t_k, s(t_k))\|$ will also be checked below. Conclusion (d) implies $u_k \to u^*$ if u^* is isolated. It is clear that this convergent result can be easily extended for k-saddles and actually covers several different variational methods since the algorithm framework is general.

(2) The curves $P(t_k, s)$ are a family of smooth curves passing through u_r, u_{p_t} and u_k, so $\|P'_s(t_k, s(t_k))\|$ is bounded if and only if $\{u_k\} = \{P(t_k, s(t_k))\}$ is bounded. Since $J(u_r) < J(u_k) < J(u_0)$ and J is coercive on $\mathcal{M}$ by Lemma 4.4.1, $\{u_k\}$ is bounded then $\|P'_s(t_k, s(t_k))\|$ is bounded as well.

4.5 Finding 2-saddles on $\mathcal{M}$

Once LMM on the generalized Nehari manifold for finding 1-saddles is established and justified mathematically, it can be easily extended for finding 2-saddles on $\mathcal{M}$. It is interesting to note that we do not need to acquire the complicated expression of surfaces as ours are just virtual.

Let $P(t, s_1, s_2)$ be a t-parametrized family of smooth 2D-surfaces on $\mathcal{M}$ in variables s_1, s_2 connecting u_r, u_{p_t}, u_s where u_r, u_{p_t} are the same as before and u_s is a previously found proper 1-saddle of J which is not a local maximum of J on $P(t, s_1, s_2)$. We may assume $s_i \in [0, 1]$ for $i = 1, 2$ with $P(t, 0, 0) = u_r, P(t, 1, 0) = u_{p_t}, P(t, 0, 1) = u_s$. Denote $s = (s_1, s_2)$ and $P(t, s(t)) = P(t, s_1(t), s_2(t))$ where $s(t) = (s_1(t), s_2(t))$ is a local maximum point of J on the surface $P(t, s) \subset \mathcal{M}$ closest to u_s. By the chain rule, we have

$$J'(P(t, s_1(t), s_2(t)))P'_{s_1}(t, s(t)) = 0,\ J'(P(t, s_1(t), s_2(t)))P'_{s_2}(t, s(t)) = 0. \tag{4.34}$$

Since $P'_t(t, s(t))$ is the direction of this t-parametrized family of surfaces moving away locally from the point $P(t, s(t))$ and we want this evolution to be nonsliding and also to follow a negative gradient flow. As we pointed out when finding 1-saddles, the dynamic system we will propose is not a dynamics of t-parametrized family of smooth surfaces $P(t, s)$, instead it is a dynamics of t-parametrized points $P(t, s(t))$ starting from an initial point $P(0, s(0))$. If we focus on the evolution of points $P(t, s(t))$, we know the idea of finding 1-saddles can be applied on finding 2-saddles again, which is moving $P(t, s(t))$ to a point P_1 along the negative gradient flow and then doing a small correction to move P_1 to $P_2 \in \mathcal{M}$. The correction of P_1 to P_2 makes sure that all points connecting the new

surface are on $\mathcal{M}$. Then the 2-saddle search system is as follows:

$$\langle J'(P(t,s(t))), P'_{s_1}(t,s(t))\rangle = 0, \langle J'(P(t,s(t))), P'_{s_2}(t,s(t))\rangle = 0, \tag{4.35}$$

$$\langle J'(P(t,s(t))), P'_t(t,s(t))\rangle = -\|J'(P(t,s(t)))\|^2/C_t \tag{4.36}$$

starting from an initial point $P(0,s(0))$ on an initial surface $P(0,s)$. (4.35) is the result of chain rule, while (4.36) implies a combination of moving point along the negative gradient flow and a small correction forcing the point back on $\mathcal{M}$. Such a claim can be proven in a similar way as we did for 1-saddle search system (4.15) - (4.16). There are infinitely many surfaces satisfying the system and we do not have to know their expressions so we call these surfaces virtual. This feature helps us avoid acquiring complex expressions of geometric objects. Since all the non-trivial critical points are on $\mathcal{M}$, our method is natural and speeds up the numerical computation. We denote $P'_s(t,s(t)) = (P'_{s_1}(t,s(t)), P'_{s_2}(t,s(t)))$ and assume $s(t)$ to be locally Lipschitz continuous in t, since for each $t \geq 0$, the equations in (4.35) can be used to solve for $s(t)$. Conditions can always be proposed so that $s(t)$ is locally $\mathcal{C}^1$ by the implicit function theorem. The stepsize rule and 2-saddle characterization can be proven in a similar way as we do for 1-saddles, thus we only list them but omit the detailed proof below.

Lemma 4.5.1. *(Stepsize Rule) If $P(t_0,s(t_0))$ is not a critical point of J, then there exists $s_0 > 0$ s.t. when $0 < t' < s_0$, we have*

$$J(P(t_0+t', s(t_0+t'))) - J(P(t_0,s(t_0))) < \frac{-t'}{4}\|J'(P(t_0,s(t_0)))\|^2/C_{t_0}.$$

Furthermore, if $P(t_k,s(t_k)) \to P(t_0,s(t_0))$, then there exists $s_0 > 0$ and $N > 0$ s.t. when

$0 < t' < s_0, k > N$, *we have the uniform stepsize rule*

$$J(P(t_k + t', s(t_k + t'_k))) - J(P(t_k, s(t_k))) < \frac{-t'}{4} \|J'(P(t_k, s(t_k)))\|^2 / C_{t_k}.$$

Proof. Similar to that of Lemma 4.2.4. □

Theorem 4.5.2. *(Index-2 Saddle Characterization). Let* $t_0 = \arg \text{loc-}\min_{t \geq 0} J(P(t, s(t)))$. *Then* $P(t_0, s(t_0))$ *is a saddle point.*

Proof. By Lemma 4.5.1 and follow a proof similar to that of Theorem 4.2.5. □

A convergence result similar to Theorem 4.4.2 can be proven.

LMM for finding 2-saddles. We basically follow the description of LMM for finding 1-saddles and we note the changes by the order of steps in LMM. Denote the previously found 1-saddle we are using by u_s.

In Step 1, let $P(0, s) \subset \mathcal{M}$ where $s = (s_1, s_2)$, be a preferred initial smooth surface connecting u_r, u_{p_0}, u_s and u_0 s.t. $P(0, (0, 0)) = u_r, P(0, (0, 1)) = u_{p_0}, P(0, (1, 0)) = u_s$, where u_r and u_{p_0} remain the same and $u_0 \in \mathcal{M}$ is an initial guess obtained from an eigenfunction. Then we find a local maximum $P(0, s(0)) \in \mathcal{M}$ of J on $P(t, s)$ closest to u_s.

We do not make any changes in Step 2.

In Step 3, $u_k(t')$ and $\hat{m}(u_k(t'))$ are the same but the smooth surface $P(t_k + t', s) \subset \mathcal{M}$ passes through u_r, $\hat{m}(u_k(t'))$, $u_{p_k,t'}$ and u_s instead of just 3 points u_r, $\hat{m}(u_k(t'))$ and $u_{p_k,t'}$. Then use $s(t_k)$ as an initial guess to solve for $s(t_k + t') \ldots$.

Other parts in LMM remain the same. By using different previous critical point u_s and proper initial guess u_0, we could find different 2-saddles.

In a similar way, LMM can be further modified to find saddles with higher MI if necessary. The only difference is the geometric object is joined by more previously found

critical points.

4.6 Numerical Implementation

4.6.1 Using curves for finding 1-saddles on $\mathcal{M}$

From Remark 2.6.2 we can get the 1st Dirichlet eigenfunction e_1 and the 1st eigenvalue λ_1 on $H_0^1(\Omega)$:

$$e_1 = \sin\left(\frac{\pi(x+1)}{2}\right)\sin\left(\frac{\pi(y+1)}{2}\right) \quad \text{and} \quad \lambda_1 = \frac{\pi^2}{2},$$

where $\Omega = (-1,1)^2$ in our most numerical examples. Since we assume $\lambda_1 < \lambda < \lambda_2$, then $V = \{e_1\}$, thus for every u in $\mathcal{M}$, we have two Nehari constraints $\langle J'(u), u\rangle = 0$ and $\langle J'(u), e_1\rangle = 0$. Firstly we have to use the eigenfunctions corresponding to the second eigenvalue to find the local minima on $\mathcal{M}$, which are the 2-saddles in E. From our numerical experience, the second eigenvalue λ_2 is doubled, i.e., there are two sets of eigenfunctions e_2^1 and e_2^2 corresponding to λ_2, and they are different in terms of geometric symmetry. Let us list the second eigenfunctions and eigenvalue of $-\Delta$ for $\Omega = (-1,1)^2$ here:

$$\begin{aligned} e_2^1 &= -\sin(\pi(x+1))\sin\left(\frac{\pi(y+1)}{2}\right) - \sin\left(\frac{\pi(x+1)}{2}\right)\sin(\pi(y+1)), \\ e_2^2 &= -\sin(\pi(x+1))\sin\left(\frac{\pi(y+1)}{2}\right) \quad \text{and} \quad \lambda_2 = \frac{5\pi^2}{4}. \end{aligned}$$

In the numerical implementation, we set e_2^1 and e_2^2 as the initial guess u_0 respectively and find the intersection point of $\hat{E}(u_0) \cap \mathcal{M}$. Technically we just solve $s_1 \in \mathbb{R}^+$ and $s_2 \in \mathbb{R}$ such that $s_1u_0 + s_2e_1$ meets the two Nehari constraints, namely, $\langle J'(s_1u_0 + s_2e_1), u_0\rangle = 0$ and $\langle J'(s_1u_0 + s_2e_1), e_1\rangle = 0$. Then we use a negative gradient method to locate the local minimum. As a result, we get two different local minima on $\mathcal{M}$ with different geometric

symmetry and denote them by u_r and u_p, where $J(u_p) < J(u_r)$.

To find the 1-saddles on $\mathcal{M}$, we need the eigenfunctions corresponding to the next few eigenvalues. Note that there might be multiple 1-saddles corresponding to the different choices of initial guesses which are different eigenfunctions with different eigenvalues, e.g., in some of our implementations with $\Omega = (-1,1)^2$, some of the eigenfunctions corresponding to $\lambda_3 = 2\pi^2$ and $\lambda_4 = \frac{5\pi^2}{2}$ can both be chosen as proper initial guesses to find 1-saddles. Denote the initial guess we are taking by e_3. Apparently e_3 is not necessarily on $\mathcal{M}$, so we seek a point $u_0 = \hat{E}(e_3) \cap \mathcal{M}$. According to Theorem 4.1.1, this is done by finding the maximum point on $\hat{E}(e_3)$. This step is crucial in our algorithm as we require the smooth curve to be always on $\mathcal{M}$ then all the points on the curve should also be on $\mathcal{M}$. After we obtain u_0, we consider the local maximum point on the smooth curve connecting u_r, u_p and u_0. As we discussed in Remark 4.3.1, the curve actually is virtual and it comes from an intersection of a space formed by these three points above and $\mathcal{M}$. In detail, for the inner maximum level, we actually use the Matlab subroutine "fmincon" to find a local maximum point of $J(s_1u_r + s_2u_p + s_3u_0)$ over $s = (s_1, s_2, s_3)$ subject to the two orthogonal constraints from the definition of the generalized Nehari manifold. Then we find the gradient of J on this maximum point u_1 and check if the norm of the gradient is smaller than the criteria ϵ we set earlier. If yes, we stop the iteration and output u_1 otherwise we move u_1 along the direction of the negative gradient, so we have $u_1(t') = u_1 - t'J'(u_1)/C_{t_1}$, where t' is controlled by the stepsize rule. Since $u_1(t')$ is not necessarily on $\mathcal{M}$ as well, we repeat the step that we process e_3, to seek $\hat{m}(u_1(t')) = E(u_1(t')) \cap \mathcal{M}$. Then the new curve on $\mathcal{M}$ passes through u_r, u_p and $\hat{m}(u_1(t'))$, and LMM starts to run. In Step 3 of the algorithm in Section 4.3, we actually find the local maximum point $u_{k+1} = P(t_{k+1}, s(t_{k+1}))$ by Matlab subroutine "fmincon" to minimize $-J(s_1u_r + s_2u_p + s_3\hat{m}(u_k(t')))$ over $s = (s_1, s_2, s_3)$ subject to the Nehari constraints. Other steps are the same, we can continue the iteration until the gradient of J is less than the criteria ϵ. Note

that for the subroutine "fmincon" in Matlab, we need to assign a starting point for searching $s = (s_1, s_2, s_3)$. To avoid oscillation among different peak selections which would destroy the continuity of $P(t, s(t))$ in t, it is significant to use $\hat{m}(u_k(t'))$ as the start point of search to consistently track a peak selection. In our numerical computation, we actually let the "fmincon" subroutine search the maximum point starting from $(s_1, s_2, s_3) = (0, 0, 1)$.

4.6.2 Using surfaces for finding 2-saddles on $\mathcal{M}$

Once 1-saddles on $\mathcal{M}$ are found, we can use one of them, denoted by u_s, with the initial guess u_0, which is obtained in a similar way as what we do for the initial guess of 1-saddle, to construct a surface on $\mathcal{M}$ by taking the intersection of $\mathcal{M}$ and the space formed by u_r, u_p, u_0, and u_s. We have multiple previously found 1-saddles, and different choices of u_s could lead to different 2-saddles, so we should choose a proper 1-saddle to be u_s based on which eigenfunction we take to obtain the initial guess u_0. It is hard to conclude a pattern of the selection of u_s, so it is chosen based on our numerical experience in the implementation. The dimension of the geometric object is two since the co-dimension of $\mathcal{M}$ is two and four points are used to form the space, then it is a surface. The maximum point of $J(s_1u_r + s_2u_p + s_3u_s + s_4u_0)$ over $s = (s_1, s_2, s_3, s_4)$ subject to the constraints $\mathcal{M}$ is found by using the Matlab subroutine "fmincon". Then LMM starts to run. In Step 3, we use the Matlab subroutine "fmincon" to minimize $J(s_1u_r + s_2u_p + s_3u_s + s_4\hat{m}(u_k(t')))$ over $s = (s_1, s_2, s_3, s_4)$ subject to the constraints $\mathcal{M}$ to find the maximum point $u_{k+1} = P(t_{k+1}, s(t_{k+1}))$. The rest parts are the same. 2-saddles can be found by doing the similar minimax iteration as we do for 1-saddles. Note that $(0, 0, 0, 1)$ serves as the starting point for "fmincon" search in order to consistently trace the local maximum and avoid unnecessary oscillation.

Remark 4.6.1. (1) An interesting observation in our numerical computation is: the correction of moving the point $u_k(t')$ to $\hat{m}(u_k(t')) \in \mathcal{M}$ actually decreases the gradient of J,

i.e., $\|J'(\hat{m}(u_k(t')))\| \leq \|J'(u_k(t'))\|$. This is nice as it does a little help on the numerical computation speed;

(2) Let us clarify the reason that we let $s_1 \in \mathbb{R}^+$ when computing the local minima on $\mathcal{M}$. p is an odd number in most of our numerical examples, then J is even to u, so we could theoretically just find the intersection point $E(u) \cap \mathcal{M}$, i.e., $s_1 \in \mathbb{R}$. However, the profile of the solution looks flipped as the coefficient s_1 may oscillate between positive and negative number. To make sure the solution we have in the current iteration has a continuity with the one from the last iteration, s_1 is limited to be non-negative;

(3) We call the curves or surfaces virtual since we do not know their explicit expressions and here we only use the intersection of the space formed by some points and the generalized Nehari manifold. As we pointed out before, there are infinitely many ways to implement LMM since the geometric object are virtual. Some geometric objects with explicit expressions were used, such as quadratic ones in Section 2 and [38], but the expression becomes more and more complicated when finding saddles with higher MI. After consideration, we think we only need some geometric object passing through the given points and it is not necessary to have an explicit expression. It is quite natural to think about if there exists a special type of geometric objects can be used to speed up the numerical computation. Since all the non-trivial critical points stay on $\mathcal{M}$, it actually puts no extra constraints to the problem, i.e., all the constraints in our algorithm are necessary and natural. Hence, compared with using explicit geometric objects, our method could accurately locate the critical points and it is easier to extend to seek saddles with higher MI since we do not need to acquire the complicated expressions.

4.7 Numerical Example

Case 5. In the model problem (1.6), we set $p = 3$, $\kappa = -1$, $\lambda = 9$, and $r = 0$, and the domain $\Omega = (-1, 1)^2$. The first and second Dirichlet eigenvalue are 4.9348 and 12.3370

respectively, so all non-trivial saddles have MI > 1, i.e., we only have 2-saddles and saddles with higher Morse indices. Then $V = \{e_1\}$ and we have two orthogonal constraints from $\mathcal{M}$. It is easy to know we will not have the solution with 1 peak, so the 2-saddles start from 2-peak solutions.

We run the code then generate Table 4.1 and Figure 4.1.

	$\|d\|$	ϵ	$\|J'(\cdot)\|_\infty$	J	$\mathrm{N_{It}}$
2-saddle 1	0.0003	1e-3	0.0045	4.0664	7
2-saddle 2	0.0009	1e-3	0.0100	4.6964	5
3-saddle 1	0.0008	1e-3	0.0297	47.8666	8
3-saddle 2	0.0036	5e-3	0.0863	83.6811	20
3-saddle 3	0.0018	2e-3	0.0375	84.3115	13
4-saddle	0.0009	1e-3	0.0345	93.7847	32

Table 4.1: Numerical data of Case 5 using the generalized Nehari manifold.

$J = 4.0664$, $\|u\|_\infty = 2.5284$ at $(0.3927, 0.3951)$

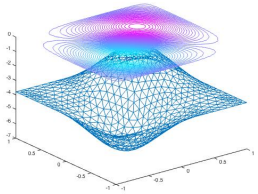

(a) 2-saddle 1

$J = 4.6964$, $\|u\|_\infty = 2.5387$ at $(0.5003, 0.0031)$

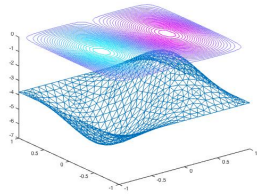

(b) 2-saddle 2

$J = 47.8666$, $\|u\|_\infty = 4.6244$ at $(-0.5012, 0.4955)$

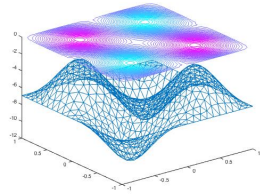

(c) 3-saddle 1

$J = 83.6811$, $\|u\|_\infty = 6.1552$ at $(-0.0005, -0.0032)$

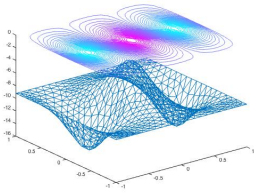

(d) 3-saddle 2

$J = 84.3115$, $\|u\|_\infty = 5.7194$ at $(-0.6056, 0.0019)$

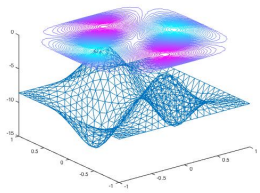

(e) 3-saddle 3

$J = 93.7847$, $\|u\|_\infty = 8.0711$ at $(-0.0005, -0.0032)$

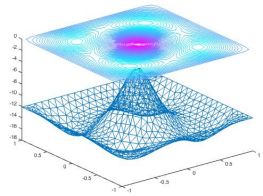

(f) 4-saddle

Figure 4.1: Saddles of Case 5 using the generalized Nehari manifold.

5. NUMERICAL INVESTIGATION OF THE INDEFINITE BIFURCATION PROBLEMS

5.1 Introduction

Let us return to the M-type model problem:

$$-\Delta u - \lambda u + \kappa |x|^r |u(x)|^{p-1} u(x) = 0, \tag{5.1}$$

where $u \in E = H_0^1(\Omega)$, $\kappa < 0$, $p \in (1, 2^*)$ and r is a prescribed parameter. We assume that $0 \in \Omega$.

The factor $|x|^r$ gives a different weight to the nonlinear term $\kappa |u(x)|^{p-1} u(x)$ in (5.1) depending on the distance between the point and the origin. As r increases, the term $|x|^r$ pulls the peak of the ground state solution away from the origin, so the symmetry of the solution will be broken if it has. In this section, we also assume that Ω is convex and symmetric about the origin in order to observe not only the bifurcation, but also the symmetry breaking phenomena.

"Symmetries exist in many natural phenomena, such as in crystals, elementary particle physics, symmetry of the Schrödinger equation for the atomic nucleus and the electron shell w.r.t. permutations and rotations, energy conservation law for systems which are invariant w.r.t. time translation, etc." [21, 26, 39] Several researchers studied symmetry characterized with compact group actions, which was used to prove the existence of multiple solutions in the Ljusternik-Schnirelman theory [40–42]. Because of the nonlinear term with non-zero r in (5.1), the system is non-autonomous, then the well-known Gidas-Ni-Nirenberg theorem on symmetry proven in [43] is not applicable to the M-type problems in our research. As the numerical examples presented in Section 2, for the definite M-type

problems, i.e., $\lambda < \lambda_1$, when r is less than certain value, the ground state solution has only one peak, which is positive and possesses all the symmetry properties that Ω has. Some of the symmetric properties are broken when r goes beyond certain value. The single ground state solution bifurcates to multiple solutions with peak away from the origin. Thus these ground state solutions do not preserve all the symmetric properties possessed by the original one.

Since the indefinite problems are much more complicated, so far such bifurcation and symmetry breaking phenomena have not been observed, even numerically. It is interesting to know whether the indefinite problems have similar bifurcation phenomena with the definite problems, as the solutions and the critical bifurcation value could not be found in the literature. With the numerical algorithm developed in the previous sections, we are ready to do some numerical investigations.

Due to the unstable nature of some critical points with high MI, certain symmetry of the expected solution has to be used to capture the specific critical point. In [13], odd symmetry is used and the initial guess was restricted in a particular symmetry subspace to capture sign-changing solutions by a minimization on the Nehari manifold. Even rotational symmetry is also enforced in [44], and the high-linking theorem is adopted to obtain the sign-changing solutions. The reason that we should enforce certain symmetry in a negative gradient-type minimax algorithm is the algorithm itself can only inherit the symmetry, thus it is unstable. $\nabla J(u)$ is used in every numerical iteration and it can inherit the symmetry. However, it is obtained by some numerical PDE solver and the computation error is inevitable. When the norm of the gradient is small, the asymmetric part of the computation error will dominate and break the symmetry of $\nabla J(u)$, then the symmetry of the sequence collapses and the minimization search finds a slider away from the expected saddle point. Finally the search leads to an unexpected solution.

It is proven that the local minimax method (LMM) is invariant to the symmetry [39].

Our method is a new LMM with the small correction introduced in Section 4. It is known that the correction is a linear combination of the point itself and $V = E^0 \oplus E^-$. All the points in V should possess all the symmetries that the non-trivial critical points do, since these non-trivial critical points are in the form of linear combinations of E^+ and V. Thus our new LMM is also invariant to the symmetry. As long as the initial guess possesses certain type of symmetry, the sequence will also have such type of symmetry. However, such an invariance is sensitive to the numerical error from the computation of $\nabla J(u)$. To deal with this issue, the Haar projection has been used to enforce the symmetry in [39] such that $\nabla J(u)$ does not lose it. In our research, we will study the indefinite bifurcation problems with the Haar projection in a similar way as [39], i.e., the asymmetric part of $\nabla J(u)$ will be removed by the Haar projection. In detail, the Haar operator $\mathcal{H}$, used as an projection from E onto E_G in the literature, will be applied on $\nabla J(u)$ in our research, where $E_G = \{u \in E : gu = u, \forall g \in G\}$ is called the invariant subspace of E under a compact group of linear isomorphisms G of E. Different types of symmetry will be described by G in our implementation. This method has a great advantage as the efficiency and stability of LMM are enhanced. When certain symmetry is enforced, we can solve the problem in a symmetry invariant subspace in order to reduce the dimension of the virtual geometric objects used for finding saddles possessing the symmetry. To cooperate with the Haar projection, a symmetric mesh will be generated and used, which will be discussed in detail when we do the numerical investigation. In this research, we will mainly focus on the numerical investigation of bifurcation and symmetry breaking phenomena of the indefinite M-type problems and the dependency of solutions on the parameter r in (5.1) since the nature of bifurcation for such problems is still to be discovered. The objective is to provide numerical evidence for PDE analysts for future study.

5.2 Numerical Investigation

Since we will enforce different types of symmetry by the corresponding Haar projection for finding different saddles, developing a symmetric mesh grids on Ω is crucial. This mesh should possess all types of symmetry we will enforce.

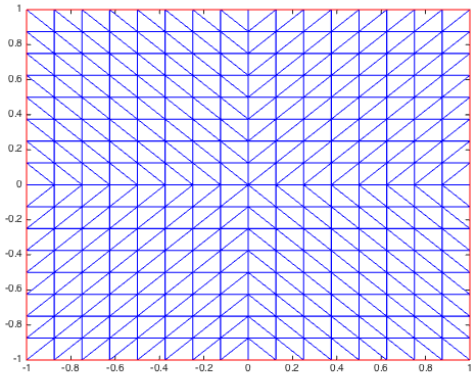

Figure 5.1: A sample symmetric mesh on $\Omega = (-1, 1)^2$.

Figure 5.1 is a coarse version of a sample symmetric mesh on the square domain $\Omega = (-1, 1)^2$. It is symmetric with respect to the x-axis, the y-axis, the line $y = x$, the line $y = -x$ and etc., so our requirement for the symmetry can be satisfied by this mesh.

Let $p = 3, \kappa = -1, \lambda = 9$, and the domain $\Omega = (-1, 1)^2$ in the model problem (1.6), then we investigate the bifurcation phenomena when r changes. When $r = 0$, it is autonomous, so the Gidas-Ni-Nirenberg theorem is applicable. The problem is just Case 5 in Section 4, so the solutions without bifurcation can be found in Figure 4.1. In the next several subsections, various solutions with different r will be discovered. Although some solutions have the similar profiles shown in Figure 4.1, their MI actually have increased since there is another branch with lower MI. Some other solutions with higher MI, which

are hard to be computed by the usual LMM, are easily found by using the symmetry on the other hand.

5.2.1 Solutions with even reflection about the line $y = x$

When $r = 0$, the problem is autonomous, so there is no bifurcation, and the solution can be found in Figure 4.1 (a). We list the solutions with other r in Figure 5.2.

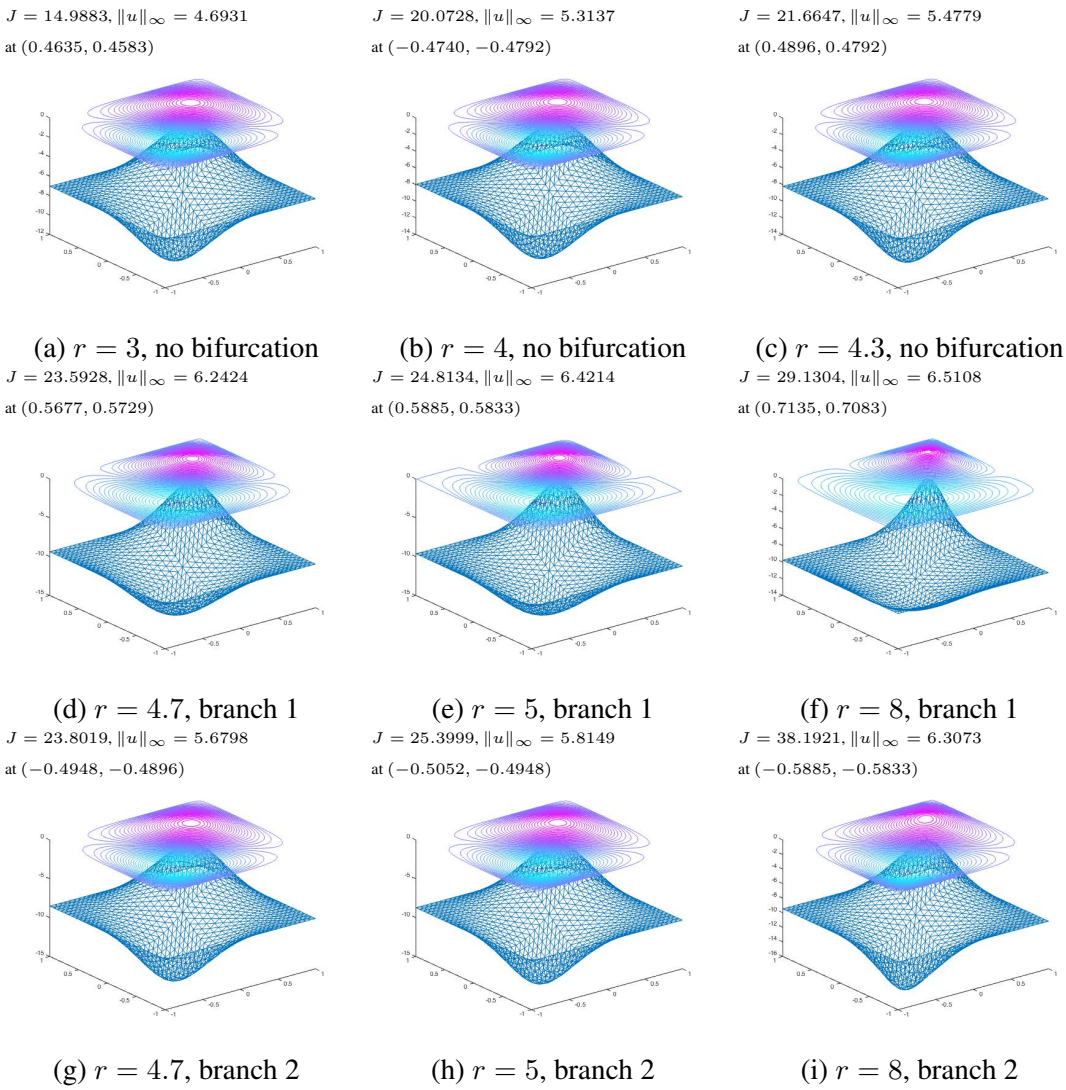

(a) $r = 3$, no bifurcation (b) $r = 4$, no bifurcation (c) $r = 4.3$, no bifurcation

(d) $r = 4.7$, branch 1 (e) $r = 5$, branch 1 (f) $r = 8$, branch 1

(g) $r = 4.7$, branch 2 (h) $r = 5$, branch 2 (i) $r = 8$, branch 2

Figure 5.2: Solutions with even reflection about the line $y = x$.

When $r > 4.5$, the solutions bifurcate to two branches. The first branches are shown in Figure 5.2 (d) - (f). Compared to the solutions without bifurcation shown in Figure 5.2 (a) - (c), the first branches are still even symmetric about the line $y = x$, but lose the odd symmetry about the line $y = -x$. Note that the first branches are still sign-changing solutions, as the indefinite M-type problems could not have positive solutions. When the bifurcation takes place, the solutions easily slide to the first branches, so the Morse indices of the solutions with odd reflection about the line $y = -x$ increase by one. We have two ways to obtain these solutions, namely, the second branches. If we only use LMM in an usual way discussed before, we have to compute the first branch beforehand, then construct a geometric object passing through it and the initial guess to solve the expected solution. However, it can be observed that the first branch does not possess all the symmetries that the second branch possesses, so we can reduce the dimension of the space dramatically by using the symmetry. To compute the solution in an efficient and stable way, the Haar projection $(\mathcal{H}u)(x, y) = \frac{1}{2}(u(x, y) - u(-y, -x))$ is used to enforce the odd reflection symmetry about the line $y = -x$. For the second branches shown in Figure 5.2 (g) - (i), we could observe that the energy levels are higher than those of the first branches respectively. In addition, the peak and valley move further away from the origin as r increases.

5.2.2 Solutions with odd reflection about the y-axis

When $r = 0$, there is no bifurcation, so the solution can be found in Figure 4.1 (b). We list the solutions with other r in Figure 5.3.

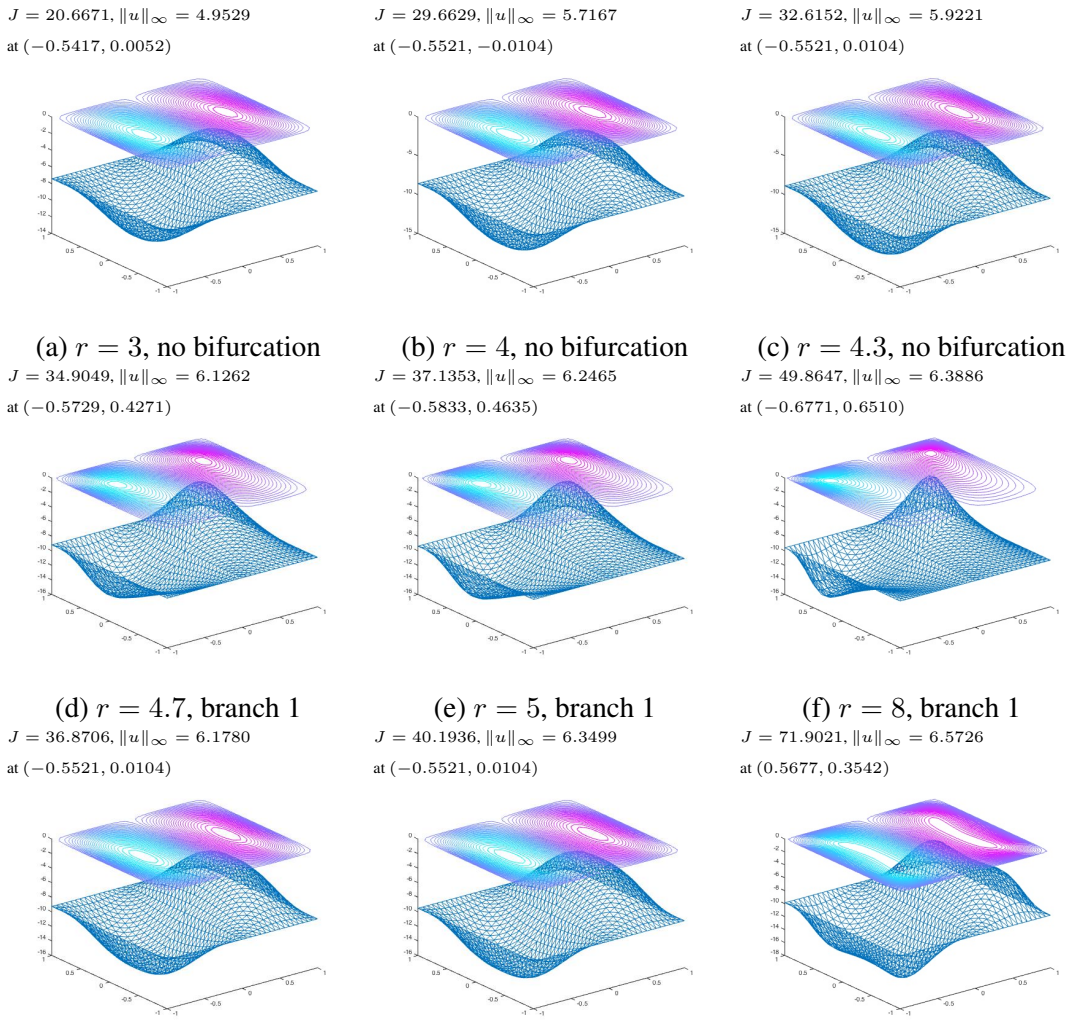

(a) $r = 3$, no bifurcation (b) $r = 4$, no bifurcation (c) $r = 4.3$, no bifurcation

(d) $r = 4.7$, branch 1 (e) $r = 5$, branch 1 (f) $r = 8$, branch 1

(g) $r = 4.7$, branch 2 (h) $r = 5$, branch 2 (i) $r = 8$, branch 2

Figure 5.3: Solutions with odd reflection about the y-axis.

When $r > 4.5$, the solutions bifurcate to two branches. The first branches are shown in Figure 5.3 (d) - (f). Compared to the solutions without bifurcation shown in Figure 5.3 (a) - (c), the first branches are still odd symmetric about the y-axis, but lose the even symmetry about the x-axis. When the bifurcation takes place, the solutions easily slide to the first branches, so the Morse indices of the solutions with even reflection about the x-axis increase by one. We have two ways to obtain these solutions, namely, the second

branches. If we only use LMM in an usual way discussed before, we have to compute the first branch beforehand, then construct a geometric object passing through it and the initial guess to solve the expected solution. However, it can be observed that the first branch does not possess all the symmetries that the second branch possesses, so we can reduce the dimension of the space dramatically by using the symmetry. To compute the solution in an efficient and stable way, the Haar projection $(\mathcal{H}u)(x,y) = \frac{1}{2}(u(x,y) + u(x,-y))$ is used to enforce the even reflection symmetry about the x-axis. For the second branches shown in Figure 5.3 (g) - (i), we could observe that the energy levels are higher than those of the first branches respectively.

5.2.3 Solutions with even reflection about the y-axis

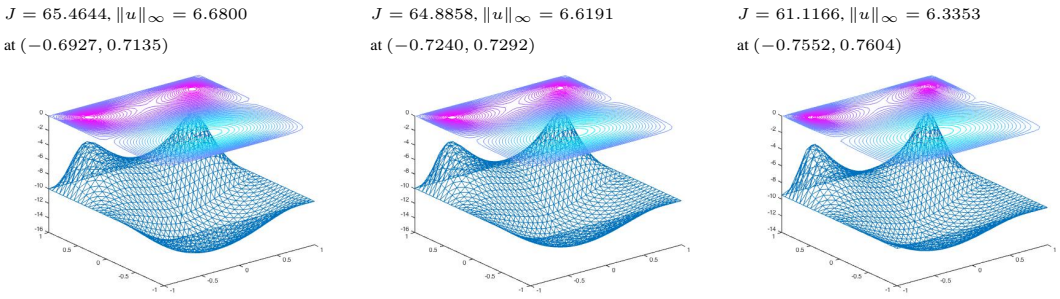

(a) $r = 7.5$ (b) $r = 8$ (c) $r = 9$

Figure 5.4: Solutions with even reflection about the y-axis.

The solution does not exist when $r < 7.5$. To compute the solutions shown in Figure 5.4 in an efficient and stable way, the Haar projection $(\mathcal{H}u)(x,y) = \frac{1}{2}(u(x,y)+u(-x,y))$ is used to enforce the even reflection symmetry about the y-axis. Note that these solutions are sign-changing ones, as the indefinite M-type problems could not have positive solutions.

5.2.4 Solutions with even reflection about the line $y = -x$

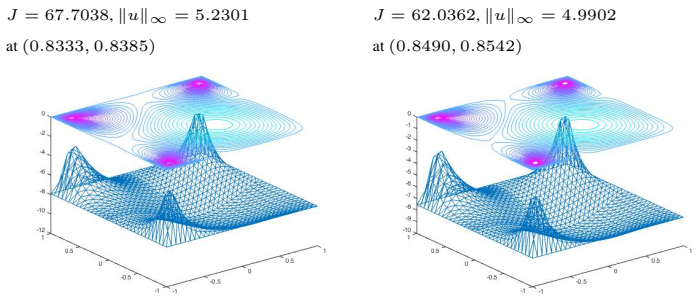

(a) $r = 12$ (b) $r = 12.5$

Figure 5.5: Solutions with even reflection about the line $y = -x$.

The solution does not exist when $r < 12$. To compute the solutions shown in Figure 5.5 in an efficient and stable way, the Haar projection $(\mathcal{H}u)(x, y) = \frac{1}{2}(u(x, y)+u(-y, -x)$ is used to enforce the even reflection symmetry about the line $y = -x$. Note that these solutions are sign-changing ones, as the indefinite M-type problems could not have positive solutions.

5.3 Summary

We have observed some more complicated bifurcation phenomena for the indefinite problems compared with the definite problems. From Case 3 and Case 4 studied in Section 2 and Section 3, as well as the numerical examples in [22], the bifurcation takes place after $r > 0.5$ for the definite M-type problems.

While for the indefinite problems, the critical bifurcation value increases from 0.5 to some larger number, e.g. in the case we just investigated, it is 4.5. The change of MI for solutions after bifurcation has also been observed. As r further increases beyond certain

values, more solutions with multiple positive peaks appear, which actually do not exist when r is small.

6. CONCLUSIONS

A local minimax method (LMM) using virtual geometric objects has been developed for finding saddles of the main problem (1.3). A dynamic saddle search system was proposed and it is a dynamics of points on virtual geometric objects such as curves, surfaces, etc. Our method covers several existing algorithms in the literature as the algorithm framework is general. Its mathematical validations, including the stepsize rule and convergence result, were established. The new algorithm was firstly implemented and tested on several benchmark problems. Then we implemented the LMM with quadratic curves and surfaces on some infinite-dimensional numerical examples and successfully found some critical points.

It was shown that those virtual geometric objects can be easily defined without knowing their explicit expressions and extended to find k-saddles so there is a great flexibility to choose preferred geometric objects for some purposes, such as convergence acceleration. Inspired by this feature, since all the non-trivial critical points stay on the Nehari manifold, it was used to accelerate the numerical computation. We also compared the computation speed between using the Nehari manifold and quadratic geometric objects to solve the same semilinear elliptic PDE, and it can be seen that using the Nehari manifold is advantageous in computation speed. A special problem, mixed M and W type problem was introduced. All the previous methods could not handle this case due to the combined effect of concave and convex nonlinearities. From our study, the Nehari manifold of this problem consists of two layers so we modified the LMM and computed the saddles in a locally M-type and locally W-type separately.

For the indefinite M-type problems, 0 is not a local minimum anymore, instead it is a saddle, so the Nehari manifold could not be used. The Palais-Smale (PS) condition is a

basic assumption to establish the convergence results for the previously developed LMM type algorithms. However, many nonlinear elliptic PDEs only satisfy the condition only on certain manifold. It is interesting to note that the generalized Nehari manifold is such a manifold that the PS condition can be verified on it. It was introduced in detail and a more general dynamic system of points with a correction technique on it was proposed. We proved that the generalized dynamic system is satisfied when the correction technique is carried out. The corresponding local minimax method was justified by establishing a strong energy dissipation law and showing the convergence of the algorithm. The new algorithm with the generalized Nehari manifold was then applied to solve an indefinite M-type case.

Note that the term $|x|^r$ in the model problem (1.6) plays a significant role in the property of the solution and r is usually called a bifurcation parameter. We observed the symmetry breaking phenomena of the solutions when r goes beyond certain value. The original solution bifurcates to multiple ones which lose some symmetries. The MI of the solution with the original symmetries increases. There are two ways to compute it. One is the usual LMM with computing the symmetry-losing solution beforehand. Another one is using the symmetry, which is efficient and stable. The Haar projection was used to enforce the symmetry and some numerical examples with profiles were given. Some solutions appearing when r goes beyond certain value were also given. We also discussed the difference of bifurcation between definite and indefinite problems. The objective is to provide numerical evidence for PDE analysts for future study.

REFERENCES

[1] Z. H. Musslimani, M. Segev, D. N. Christodoulides, and M. Soljačić, "Composite multihump vector solitons carrying topological charge," *Physical Review Letters*, vol. 84, no. 6, p. 1164, 2000.

[2] J. J. García-Ripoll, V. M. Pérez-García, E. A. Ostrovskaya, and Y. S. Kivshar, "Dipole-mode vector solitons," *Physical Review Letters*, vol. 85, no. 1, p. 82, 2000.

[3] J. J. García-Ripoll and V. M. Pérez-García, "Optimizing Schrödinger functionals using Sobolev gradients: applications to quantum mechanics and nonlinear optics," *SIAM Journal on Scientific Computing*, vol. 23, no. 4, pp. 1316–1334, 2001.

[4] J. Zhou, "Instability analysis of saddle points by a local minimax method," *Mathematics of Computation*, vol. 74, no. 251, pp. 1391–1411, 2005.

[5] C. J. Cerjan and W. H. Miller, "On finding transition states," *The Journal of Chemical Physics*, vol. 75, no. 6, pp. 2800–2806, 1981.

[6] E. Weinan, W. Ren, and E. Vanden-Eijnden, "Simplified and improved string method for computing the minimum energy paths in barrier-crossing events," *The Journal of Chemical Physics*, 2007.

[7] G. Henkelman and H. Jónsson, "A dimer method for finding saddle points on high dimensional potential surfaces using only first derivatives," *The Journal of Chemical Physics*, vol. 111, no. 15, pp. 7010–7022, 1999.

[8] L. Lin, X. Cheng, E. Weinan, A.-C. Shi, and P. Zhang, "A numerical method for the study of nucleation of ordered phases," *Journal of Computational Physics*, vol. 229, no. 5, pp. 1797–1809, 2010.

[9] R. Olsen, G. Kroes, G. Henkelman, A. Arnaldsson, and H. Jónsson, "Comparison of methods for finding saddle points without knowledge of the final states," *The Journal*

of Chemical Physics, vol. 121, no. 20, pp. 9776–9792, 2004.

[10] J. C. Palmer, F. Martelli, Y. Liu, R. Car, A. Z. Panagiotopoulos, and P. G. Debenedetti, "Metastable liquid-liquid transition in a molecular model of water," *Nature*, vol. 510, no. 7505, p. 385, 2014.

[11] E. Zeidler, *Nonlinear Functional Analysis and Its Applications I and III*. Springer, 1985.

[12] A. Ambrosetti and P. H. Rabinowitz, "Dual variational methods in critical point theory and applications," *Journal of Functional Analysis*, vol. 14, no. 4, pp. 349–381, 1973.

[13] Y. S. Choi and P. J. McKenna, "A mountain pass method for the numerical solution of semilinear elliptic problems," *Nonlinear Analysis: Theory, Methods & Applications*, vol. 20, no. 4, pp. 417–437, 1993.

[14] Y. Li and J. Zhou, "A minimax method for finding multiple critical points and its applications to semilinear PDEs," *SIAM Journal on Scientific Computing*, vol. 23, no. 3, pp. 840–865, 2001.

[15] Y. Li and J. Zhou, "Convergence results of a local minimax method for finding multiple critical points," *SIAM Journal on Scientific Computing*, vol. 24, no. 3, pp. 865–885, 2003.

[16] Z. Liu and Z.-Q. Wang, "On the Ambrosetti-Rabinowitz superlinear condition," *Advanced Nonlinear Studies*, vol. 4, no. 4, pp. 563–574, 2004.

[17] A. Szulkin and T. Weth, *Ground state solutions for some indefinite problems*. Department of Mathematics, Stockholm University, 2007.

[18] A. Pankov, "Periodic nonlinear Schrödinger equation with application to photonic crystals," *Milan Journal of Mathematics*, vol. 73, no. 1, pp. 259–287, 2005.

[19] M. Hénon, "Numerical experiments on the stability of spherical stellar systems," *Astronomy and Astrophysics*, vol. 24, p. 229, 1973.

[20] P. H. Rabinowitz *et al.*, *Minimax methods in critical point theory with applications to differential equations*. American Mathematical Soc., 1986.

[21] X. Chen and J. Zhou, "On homotopy continuation method for computing multiple solutions to the Hénon equation," *Numerical Methods for Partial Differential Equations*, vol. 24, no. 3, pp. 728–748, 2008.

[22] M. Li and J. Zhou, "Finding Gateaux-saddles by a local minimax method," *Numerical Functional Analysis and Optimization*, vol. 38, no. 2, pp. 205–223, 2017.

[23] J. Zhou, "Local characterizations of saddle points and their morse indices," *Control of Nonlinear Distributed Parameter Systems*, vol. 218, p. 233, 2001.

[24] J. Zhou, "Global sequence convergence of a local minimax method for finding multiple solutions in Banach spaces," *Numerical Functional Analysis and Optimization*, vol. 32, no. 12, pp. 1365–1380, 2011.

[25] K. Müller and L. D. Brown, "Location of saddle points and minimum energy paths by a constrained simplex optimization procedure," *Theoretica Chimica Acta*, vol. 53, no. 1, pp. 75–93, 1979.

[26] Z.-Q. Wang and J. Zhou, "A local minimax-newton method for finding multiple saddle points with symmetries," *SIAM Journal on Numerical Analysis*, vol. 42, no. 4, pp. 1745–1759, 2004.

[27] G. Chen, B. G. Englert, and J. Zhou, "Convergence analysis of an optimal scaling algorithm for semilinear elliptic boundary value problems," *Contemporary Mathematics*, vol. 357, pp. 69–84, 2004.

[28] J. Zhou, "Solving multiple solution problems: computational methods and theory revisited," *Communication on Applied Mathematics and Computation*, vol. 31, pp. 1–31, 2017.

[29] Z. Nehari, "On a class of nonlinear second-order differential equations," *Transactions of the American Mathematical Society*, vol. 95, no. 1, pp. 101–123, 1960.

[30] Z. Nehari, "Characteristic values associated with a class of nonlinear second-order differential equations," *Acta Mathematica*, vol. 105, no. 3, pp. 141–175, 1961.

[31] A. Ambrosetti, H. Brezis, and G. Cerami, "Combined effects of concave and convex nonlinearities in some elliptic problems," *Journal of Functional Analysis*, vol. 122, no. 2, pp. 519–543, 1994.

[32] K.-J. Chen, "Combined effects of concave and convex nonlinearities in elliptic equation on $\mathbb{R}^N$," *Journal of Mathematical Analysis and Applications*, vol. 355, no. 2, pp. 767–777, 2009.

[33] M. Li and J. Zhou, "A local minmaxmin method for defocusing nonlinear PDEs." in preparation.

[34] A. Szulkin and T. Weth, "The method of Nehari manifold," *Handbook of Nonconvex Analysis and Applications*, vol. 597632, 2010.

[35] J. Zhou, "A local min-orthogonal method for finding multiple saddle points," *Journal of Mathematical Analysis and Applications*, vol. 291, no. 1, pp. 66–81, 2004.

[36] A. Pankov, "Gap solitons in periodic discrete nonlinear Schrödinger equations," *Nonlinearity*, vol. 19, no. 1, p. 27, 2005.

[37] Z. Li and J. Zhou, "A local minimax method using virtual curves, surfaces, etc.: Part II—for finding equality constrained saddles." submitted.

[38] Z. Li, B. Ji, and J. Zhou, "A local minimax method using virtual geometric objects: Part I—for finding saddles." submitted.

[39] Z.-Q. Wang and J. Zhou, "An efficient and stable method for computing multiple saddle points with symmetries," *SIAM Journal on Numerical Analysis*, vol. 43, no. 2, pp. 891–907, 2005.

[40] F. Catrina and Z.-Q. Wang, "Nonlinear elliptic equations on expanding symmetric domains," *Journal of Differential Equations*, vol. 156, no. 1, pp. 153–181, 1999.

[41] Z. Liu and J. Sun, "Invariant sets of descending flow in critical point theory with

applications to nonlinear differential equations," *Journal of Differential Equations*, vol. 172, no. 2, pp. 257–299, 2001.

[42] S. Li and Z.-Q. Wang, "Ljusternik-Schnirelman theory in partially ordered Hilbert spaces," *Transactions of the American Mathematical Society*, vol. 354, no. 8, pp. 3207–3227, 2002.

[43] B. Gidas, W.-M. Ni, and L. Nirenberg, "Symmetry and related properties via the maximum principle," *Communications in Mathematical Physics*, vol. 68, no. 3, pp. 209–243, 1979.

[44] D. G. Costa, Z. Ding, and J. M. Neuberger, "A numerical investigation of sign-changing solutions to superlinear elliptic equations on symmetric domains," *Journal of Computational and Applied Mathematics*, vol. 131, no. 1, pp. 299–319, 2001.